Remote Sensing in Exploration Geology

Golden, Colorado to Washington, D.C.
June 30–July 8, 1989

Field Trip Guidebook T182

Leaders:
Keenan Lee, Editor; Daniel H. Knepper, Jr.,
Fred A. Kruse, Ronald W. Marrs and Nancy M. Milton

American Geophysical Union, Washington, D.C.

2000 Florida Ave., N.W., Washington, D.C. 20009

ISBN: 0-87590-564-1

Printed in the United States of America

COVER Southern Colorado Front Range.

CONTENTS

Leaders:

Keenan Lee
Department of Geology
Colorado School of Mines
Golden, CO 80401
and
U.S. Geological Survey
MS 964, Box 25046, DFC
Denver, CO 80225-0046

Daniel H. Knepper, Jr.
U.S. Geological Survey
MS 964, Box 25046, DFC
Denver, CO 80225-0046

Fred A. Kruse
Center for the Study of Earth from Space
CIRES, University of Colorado
Boulder, CO 80309

Ronald W. Marrs
Department of Geology and Geophysics
University of Wyoming
Laramie, WY 82070

Nancy M. Milton
U.S. Geological Survey
927 National Center
Reston, VA 22092

IGC FIELD TRIP T182:
REMOTE SENSING IN EXPLORATION GEOLOGY

HISTORY, GEOGRAPHY, AND GEOLOGY OF THE COLORADO FRONT RANGE

Keenan Lee
Colorado School of Mines, Golden, Colorado
U.S. Geological Survey, Denver, Colorado

HISTORY

The earliest people in the Front Range area left scant record. During the Pleistocene, the first migrations of Oriental people crossed the Bering land bridge and some eventually moved into Colorado. Cliff-dwelling Pueblo cultures developed in southwestern Colorado about 2000 years ago, with more nomadic tribes like the Ute and Apache arriving in Colorado about 700 years ago (Brown, 1985).

By the middle of the eighteenth century, the Pawnee had firm control of the South Platte River, with the Comanches to the south. Decimated by smallpox, the Pawnees moved northeast, and the dominant plains tribes became the Cheyenne and Arapahoe, who hunted from the Arkansas River to the North Platte River. Several tribes of Utes continued to inhabit the mountains.

One of the earliest known Europeans to arrive in the Front Range area was Juan Bautista de Anza. In 1779 he led troops north from Santa Fe and chased Chief Cuerno Verde and a band of his Comanches through Poncha Pass and onto the plains below Pikes Peak (Sprague, 1976).

President Thomas Jefferson doubled the size of the U.S. in 1803 by acquiring from Napoleon the Louisiana Purchase, comprising everything Napoleon owned west of the Mississippi River (a bargain at four cents an acre). The eastern part of what became Colorado was included in the Purchase, with the western half owned by Charles IV of Spain (later acquired from Mexico). The boundary was in dispute, being either the Arkansas River or the Red River.

In 1806 the Army sent 16 soldiers, led by Capt. Zebulon Montgomery Pike, to find out what Jefferson had bought, to explore the two rivers, and check on Spanish defenses. On 15 November 1806 the party sighted the Front Range from near Las Animas; they estimated the elevation of the highest peak at 4000 ft (1200 m) and the distance about a day's march away. Pike and his men arrived at the base of the mountains two weeks later, where they re-estimated Pikes Peak at 18,582 ft (5,664 m) (actually 14,110 ft; 4,301 m).

Pike's soldiers ascended the Arkansas River by Canon City, but when blocked by the sheer walls of the Royal Gorge, moved up Current Creek to South Park and on to Leadville. (Pike's troops eventually moved south to the Wet Mountains and the San Luis Valley, where they were captured by the Spanish and taken to Santa Fe).

In 1858, two unrelated events popularized Colorado. Placer gold was found in what is today downtown Denver, and stories were sent back east about fortunes to be had "at Pikes Peak", which came to be the recognizable landmark that referred to the Front Range from the Arkansas River to Wyoming. In August of 1858, Julia Holmes, at age 20 became the first woman to climb Pikes Peak. These two events made headlines back east, and soon the caravans were headed west, some fifty thousand people determined to make it to "Pikes Peak or Bust". (For those who made the 700 mile journey from the Missouri but who were not inclined to climb the peak, they could settle for the present town of Bust, at the base of Pikes Peak on the northeast side).

The Denver gold placer soon played out, but in January 1859, George A. Jackson, prospecting on Clear Creek above Golden, found rich placers at a hot spring, later to become Idaho Springs. Later that spring, John H. Gregory panned upstream from Golden, but when he reached the confluence of the north and south forks of Clear Creek, he followed the richer color he found in the north fork to locate the first gold lode deposit. This site eventually became Central City, a district that billed itself as the "Richest Square Mile on Earth".

In 1861 President Abraham Lincoln's proclamation originated the Colorado

Territory. Golden City (Golden after 1872) became the capitol city from 1862 through 1867, with Denver taking over permanently in 1867. The opportunity for statehood came in 1864, but was rejected by the Colorado voters.

In 1870, the Colorado Territorial Legislature appropriated funds for a building in Golden "for mining instruction" (Wagenbach and Thistlewood, 1987). In 1874 the Colorado School of Mines became a territorial institution, later continuing as a state university.

The Colorado Constitution was eventually ratified 1 July 1876, whereupon President Grant on 1 August 1876 declared Colorado, known as the Centennial State, the 38th state.

The second gold rush in Colorado's history took place in the 1890's when Cripple Creek was discovered. In 1878 Bob Womack, a cowboy tending cattle west of Pikes Peak, found gold-bearing float in Poverty Gulch. For twelve years he chased the float upstream, until he finally found an outcropping of the strange gray rock that held gold, and on 20 October 1890 he staked the standard 1500 ft by 300 ft (457 m by 91 m) lode claim and named it the El Paso lode (Sprague, 1953).

Although assay values on some of the samples were high, Womack's discovery was not an instant call of "Bonanza". There was very little free gold in the rocks at Cripple Creek (Penrose, 1895), despite the anomalous Globe Hill above Poverty Gulch, where "they prospected with plows, mined with roadscrapers, and actually shipped the scenery" (Anon., 1894). It was not until others, like Winfield Scott Stratton (who had studied at the Colorado School of Mines), recognized the main ore mineral as sylvanite, a dull gray gold-silver telluride, that the true gold rush was on. Stratton was to become Cripple Creek's first millionaire.

Cripple Creek became known as the "World's Greatest Gold Camp", and along with Victor, the "City of Mines", and several other outlying mining towns, reached a peak district population of about 50,000 in 1900. Gold production also peaked in 1900 at $18,199,736 (Sprague, 1953, table 1), with cumulative production by World War II of a little over $400,000,000 (not including high-graded ore). The mines were shut down during the war, and there has been little mining since.

GEOGRAPHY

The Front Range forms the initial rampart of the Southern Colorado Rocky Mountains, a major barrier to east-west travel. The mountains must be crossed by high passes, all above 9,000 ft (2,700 m) in altitude and some above 11,000 ft (3,350 m).

The eastern third of Colorado is part of the Great Plains physiographic province (fig. 1), sloping gently upward from about 3,500 ft (1,067 m) along the Kansas border to about 6,000 ft (1,829 m) at the foothills of the Front Range. The Front Range rises rapidly, in places precipitously, to an upland surface at about 9,000 ft (2,743 m), with occasional erosional remnants higher, the most notable being the 5,000 ft (1,524 m) monadnock of Pikes Peak, which dominates the Front Range at 14,110 ft (4,301 m).

The climate of the Front Range area is altitudinally zoned, with the warm, dry climate of Canon City changing rapidly to alpine conditions at Pikes Peak. With each thousand feet of altitude being the equivalent of about five degrees of latitude, one can drive in a few hours from Colorado Springs's Upper Sonoran climate (Sonora is a state in northern Mexico) to Pikes Peak's arctic climate similar to northern Alaska.

Vegetation is likewise altitudinally zoned, with five zones recognized in this area (Pesman, 1967) (fig. 2):

- Alpine zone (Arctic, north of 66°), >11,500 ft (timberline), grasses and herbs
- Subalpine zone (Hudsonian, 60°-66°), 10,000 to 11,500 ft, Engelmann spruce, limber pine
- Montane zone (Canadian, 50°-60°), 8,000 to 10,000 ft, spruce - fir forests and lodgepole pine
- Foothills zone (Transition, 40°-50°), 6,000 to 8,000 ft, Ponderosa pine on south slopes, Douglas fir on north
- Plains zone (Upper Sonoran, 30°-40°), 4,000 to 6,000 ft, Pinyon pine and juniper, Gambel oak

GEOLOGY

The mountains of the Front Range region are underlain primarily by Precambrian crystalline rocks, and the foothills and plains are underlain mostly by Phanerozoic sedimentary rocks. The contact between the two is a series of high-angle reverse faults along the Front Range from Golden to Colorado Springs. South of the Springs, however, the Precambrian rocks plunge under Paleozoic rocks in the Canon City structural embayment in a series of southeast-plunging folds (fig. 3). First-order structures are an anticline-syncline pair, with several second-order folds of the same orientation.

Superimposed on the Precambrian basement are two sets of high-angle faults. The northwest-trending faults frequently show Neogene offset (Taylor, 1975), whereas the northeast faults usually do not. The northeast faults are restricted to a northeast-trending zone more-or-less coincident with the offset of the Front Range (fig. 3).

Precambrian rocks are of three ages: 1.7 Ga migmatites at the Royal Gorge, augen gneisses at Cripple Creek, and mica schists in High Park and Cripple Creek are the oldest (fig. 4). 1.4 Ga quartz monzonites intrude the Boulder Creek metamorphic rocks at Cripple Creek, and these in turn are intruded by the Pikes Peak Granite (1.0 Ga) north and east of Cripple Creek.

Phanerozoic rocks of the area include sedimentary rocks and volcanic rocks. Lower Paleozoic rocks are shelf-type marine sedimentary rocks (fig. 4), with massive red arkoses of Pennsylvanian (Late Carboniferous) age. Mesozoic fluvial sequences give way to Cretaceous marine sedimentary rocks. Tertiary rocks consist of ash-flow tuffs and lahars, with occasional gravels preserved in down-faulted areas. Quaternary alpine glacial deposits occur in the high mountains, with pediment alluviums along the foothills.

A generalized geologic history is summarized in figure 5. Discounting perhaps multiple orogenies in the Precambrian, the Colorado Front Range region has seen four "Rocky Mountains" (with at least the last three in very much the same place), each separated from the next by almost complete removal of highland areas and the development of a regional erosion surface of very low relief. The Precambrian mountains are poorly documented, but the 1.0 Ga Pikes Peak plutonic rocks were exposed by erosion that required the removal of many thousands of feet of country rock before the Cambrian sea, in which the Sawatch Sandstone was deposited, transgressed over a featureless surface.

The Ancestral Rocky Mountains orogeny of Pennsylvanian age raised the ancestral Front Range along bounding faults that were very close in position to the bounding faults of the current mountains, as evidenced by the thick bajadas of arkose that are preserved as the Fountain Formation. This orogeny probably is related to the collision of North America with Africa and South America (Hamilton, 1987). The ancestral mountains were eroded during latest Paleozoic time, forming an erosion surface, probably by Triassic time, across which the Upper Jurassic Morrison Formation fluvial sediments were deposited by streams heading in western Colorado or Utah.

The Laramide orogeny of Cretaceous to Eocene age once again raised the Front Range, perhaps on the order of 6,000 m (Trimble, 1980). This crustal shortening is associated with uncommonly rapid subduction of oceanic lithosphere along the west coast of North America (Hamilton, 1987). Again, a widespread erosion surface of low relief developed by the end of the Eocene, sloping gently eastward, across which the Oligocene Wall Mountain Tuff (ash flow) flowed.

The present Rocky Mountains owe their elevation and relief to Oligocene and younger uplift and differential movement along high-angle faults. The Front Range has been raised about 2,000 m and fragmented, with much, if not most, of the movement occurring in Neogene and Quaternary times. In fact, there is evidence to suggest the current (unnamed) orogeny has not yet peaked; Scott's (1975) figures for Clear Creek near Golden show downcutting rates of about 13 m/my for Miocene, 42 m/my for Pliocene, and 75 m/my for the Quaternary.

REFERENCES

Anonymous, 1894, History and description of the Cripple Creek mining district. Mining and business directory, City of Cripple Creek and adjacent towns: Cripple Creek, Colorado, Hazeltine, 161 p.

Brown, R. L., 1985, The great Pikes Peak gold rush: Caldwell, Idaho, Caxton Printers, 124 p.

Hamilton, Warren, 1987, Plate-tectonic evolution of the western U.S.A.: Episodes, v. 10, p. 271-276.

Penrose, R. A. F., 1895, Economic geology, in Warren, H. L. J., and Stride, Robert, Cripple Creek and Colorado Springs, Illustrated: Colorado Springs, Colorado, Warren and Stride, 104 p.

Pesman, M. W., 1967, Meet the natives: Denver, Smith-Brooks Printing, 219 p.

Raisz, Erwin, 1954, Landforms of the United States, 6th. rev. ed.: Cambridge, Massachusetts, Erwin Raisz, scale 1:4,435,200.

Scott, G. R., 1975, Cenozoic surfaces and deposits in the Southern Rocky Mountains, in Curtis, B. F., ed., Cenozoic history of the Southern Rocky Mountains: Geological Society of America Memoir 144, p. 227-248.

Sprague, Marshall, 1953, Money mountain - the story of Cripple Creek gold: Boston, Little Brown, 342 p.

Sprague, Marshall, 1976, Colorado, a bicentennial history: New York, W. W. Norton, 204 p.

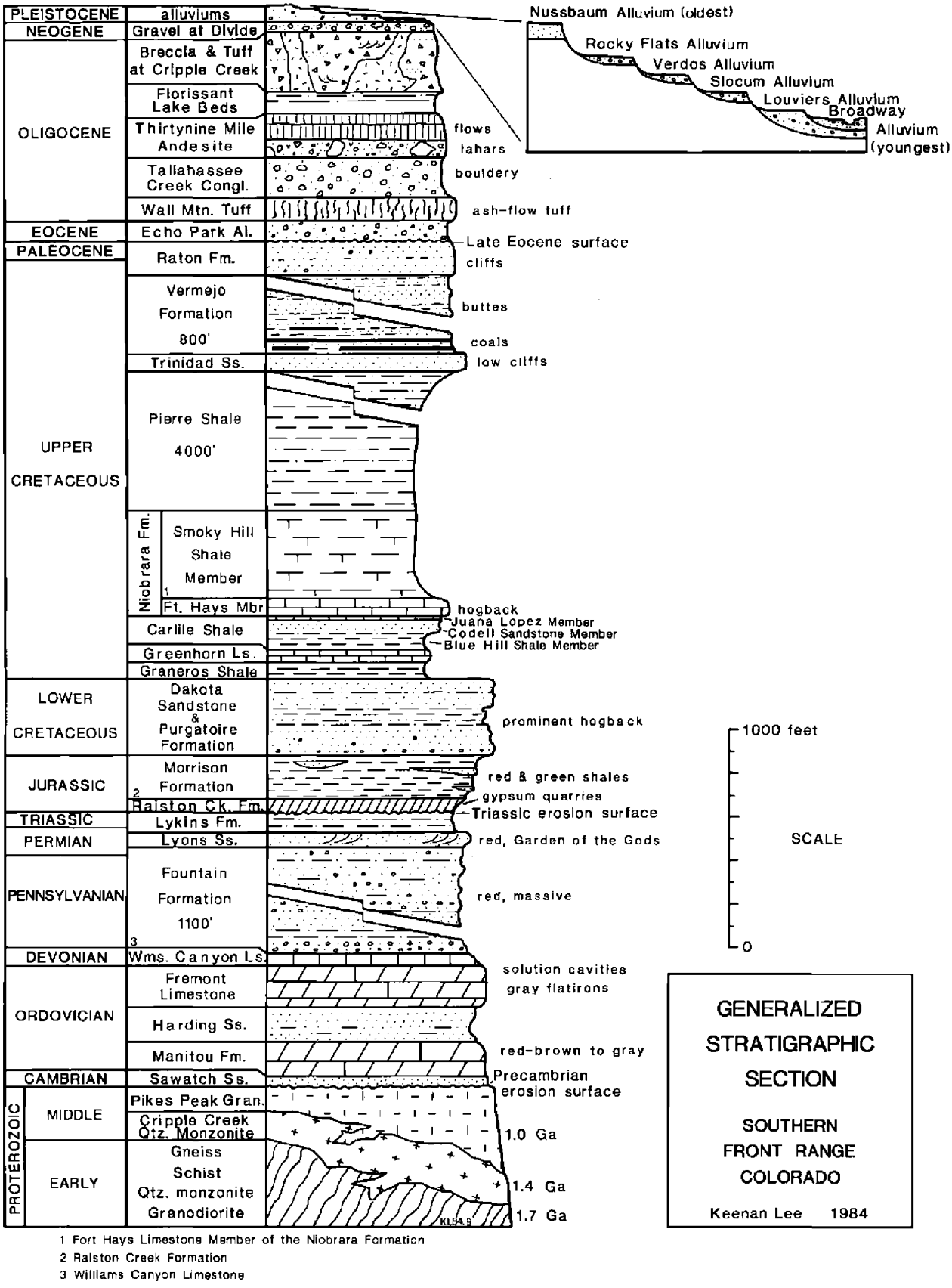

FIGURE 4 Generalized stratigraphic section of the southern Colorado Front Range.

Time	Depositional or Igneous Event	Tectonism
Quaternary	Alpine glaciation	Neogene to Quaternary orogeny uplift, tilting, block faulting
Neogene	Gravels at Divide	
Oligocene	Ash flows Andesitic volcanism	
Oligocene	Gravels	
~~ Late Eocene Surface ~~~~		
Eocene		Laramide orogeny
Cretaceous	Marine sedimentation	
Jurassic	Fluvial sedimentation	
~~ Triassic Erosion Surface ~~~~		
Pennsylvanian	Bajada sedimentation	Ancestral Rocky Mountain orogeny
Mississippian	Karsting	Epeirogeny
Devonian	Shelf sedimentation	
Cambrian	Marine transgression	
~~ Precambrian Erosion Surface ~~~~		
~ 1.0 Ga	Pikes Peak Granite	Pikes Peak plutonism
~ 1.4 Ga	Cripple Creek Quartz Monzonite	Silver Plume disturbance
~ 1.7 Ga	Early Proterozoic gneisses	Boulder Creek orogeny

FIGURE 5 Generalized geologic history of the southern Colorado Front Range.

Taylor, R. B., 1975, Neogene tectonism in south-central Colorado, in Curtis, B. F., ed., Cenozoic history of the Southern Rocky Mountains: Geological Society of America Memoir 144, p. 211-226.

Trimble, D. E., 1980, Cenozoic tectonic history of the Great Plains contrasted with that of the Southern Rocky Mountains: A synthesis: The Mountain Geologist, v. 17, p. 59-69.

Wagenbach, Lorraine, and Thistlewood, J. E., 1987, Golden: The 19th Century, a Colorado chronicle: Littleton, Colorado, Harbinger House, 113 p.

LIMONITE MAPPING WITH LANDSAT MULTISPECTRAL SCANNER DATA AT CRIPPLE CREEK, COLORADO

Keenan Lee
Colorado School of Mines, Golden, Colorado
U.S. Geological Survey, Denver, Colorado

Abstract. Sulfide mineral deposits commonly have limonitic outcrops that can be a guide to exploration. The Landsat Multispectral Scanners (MSS) have already acquired data over most of the world's land surface that can be used to map limonite. By knowing the spectral reflectance properties of limonite and other common surface materials, a geologist using remote sensing can interactively process the digital images to produce a limonite anomaly map.

A Landsat 1 MSS image was processed for an area around the Cripple Creek - Victor mining district in the southern Rocky Mountains. Ratios of the four spectral bands were computed, transformed into a color-space, and the color coordinates used to produce maps of limonitic areas. Interactive interpretation refined the limonite maps to a final exploration map.

Limonitic areas on the exploration map correspond to redbeds, maturely weathered biotite-rich gneisses, pink granites, and hydrothermally altered and mineralized rocks. Redbeds can be identified by their outcrop pattern, but field checking is required to discriminate hydrothermal limonite from weathered mafic minerals and pink granite. In areas around the Cripple Creek - Victor mining district that are relatively free of trees, limonitic areas on the map correspond well with areas of hydrothermal mineralization, primarily gold-silver tellurides.

INTRODUCTION

From digitally processed Landsat MSS images, an experienced photogeologist can derive a small-scale geologic map with basic structural and lithologic information. Through lineament analysis, one can derive structural information beyond the apparent features interpreted by direct photo interpretation, such as anticlines and faults, to interpret basement control (see Lee and others, this publ.). In addition, through proper data processing, one can look beyond apparent color differences on an MSS image to seek subtle spectral variations that relate to mineral deposits. Specifically, we can look for limonite that may be related to sulfide deposits.

The term "limonite" is taken to mean any of several ferric oxide, hydroxide, or sulfate compounds, or mixtures thereof (Blanchard, 1968), that absorb strongly in the ultraviolet and the visible blue. Common minerals in this group are hematite, goethite, jarosite, and ferrihydrite.

If pyritization accompanies economic mineralization, as is often the case, the pyrite will weather at the surface to form limonite. A gossan may form, or more commonly, a limonite staining occurs. This limonite is capable of being remotely sensed, even in quite small quantities.

It is necessary to know the spectral properties of a material in order to successfully identify it. The spectral reflectance of limonite is well known to have characteristic features that serve to identify it (Hunt, 1980 and Hunt and Ashley, 1979). Basically, the limonite compounds have absorption bands (that is, low reflectance) in the blue region of the visible and near 0.9 micrometers (near-infrared), both regions that are sensed by the Landsat MSS. Figure 1 shows reflectance spectra of some rocks from the Cripple Creek - Victor area; all except CCV8405 show these limonite spectral characteristics.

METHODS

By combining the different MSS bands into one color-composite image, one can more readily see differences that occur in more than one spectral band. Rowan and others (1974) showed, in a classic study, how limonitic surfaces can be enhanced on a specific type of image, the color-ratio-

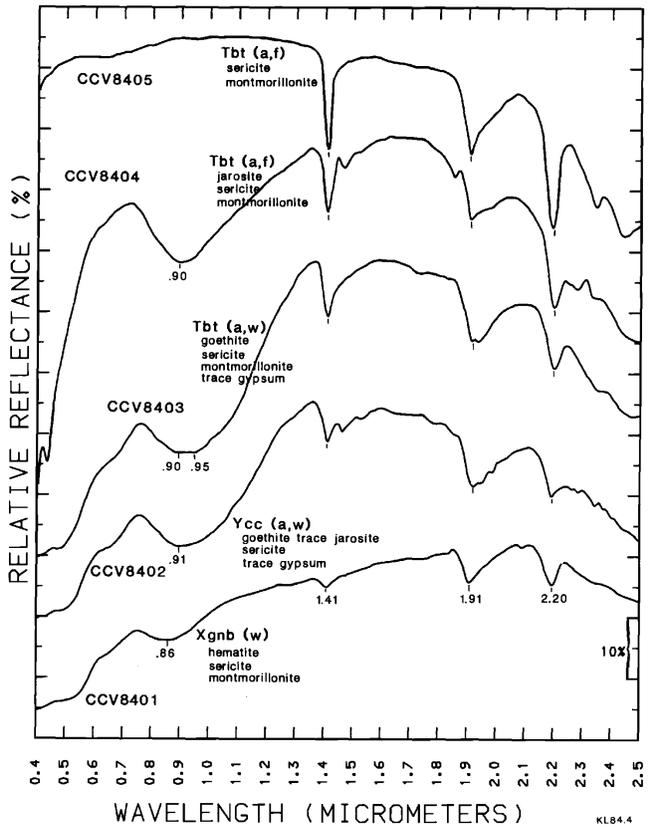

FIGURE 1 Spectral reflectance of rocks from the Cripple Creek - Victor area. a, altered hydrothermally; f, fresh surface; Tbt, tuff breccia at Cripple Creek; w, weathered surface; Xgnb, Early Proterozoic biotite gneiss; Ycc, Middle Proterozoic Cripple Creek Quartz Monzonite.

composite (CRC) image, where MSS bands are ratioed and the ratios are color coded. The basic processing and analysis procedures used to produce the images of the Cripple Creek area are diagrammed in figure 2. An EROS computer-compatible tape (CCT) was "preprocessed" to reformat the image, to destripe it (equalize the six detectors), and to geometrically correct it for skew effect of the earth's rotation (Raines and others, 1978). After the effect of vegetation was masked out by procedures developed by Knepper and Raines (1985), all of the images were contrast enhanced. Individual bands were ratioed to maximize spectral variations and to minimize illumination differences caused by slope aspect. The CRC processed for Cripple Creek, for example, used the MSS Band 4/Band 5 (B4/B5) ratio coded red, B6/B7 coded green, and B4/B6 coded blue. Limonitic surfaces thus would appear green (Rowan and others, 1974; Raines and others, 1978). Other researchers color code band ratios differently, but the methodology described here would not change.

In order to seek systematic differences in the green pixels that may relate to different types of limonite, and to quantitatively analyze these differences, the ratios were transformed to Munsell color coordinates--hue, value, and chroma. Raines (1977) developed this transformation, which digitally converts the three ratio values of an individual pixel in a CRC into Munsell coordinates. With these, differences in greens--that is, different limonitic areas--can be defined numerically (Raines and Knepper, 1983).

At this point, interpretative geologic input is required to select the hue interval of interest. In this study, the hue of interest is that corresponding to limonite on hydrothermally altered rocks. By studying the hues of an exposure of such rock southeast of Cripple Creek, and by comparing it with hues of apparently unaltered rock, the hue range for hydrothermal limonite was defined as digital numbers (DN) 33 through 73. A thematic image highlighting those pixels whose hue falls within this range was prepared by encoding the limonitic pixels red on a background black and white image of Band 7. (Note: because this publication does not support color illustrations, these images cannot be shown.)

The limonite map shows several limonitic areas. For mineral exploration, it would be advantageous to separate hydrothermal limonitic areas from other, non-hydrothermally altered limonitic areas, so additional criteria need to be defined.

Photogeologic interpretation of a Band 7 image revealed that the Cripple Creek altered area had a lower infrared reflectance, DN's less than 75, than limonitic sedimentary rocks to the south. Creating a subset of the limonitic pixels that also have Band 7 DN's of 74 or less eliminated some of these sedimentary rocks and produced an anomaly map that was more useful. In a similar manner, a Munsell value of about 105 or less was useful for further separating out known hydrothermal limonite from economically uninteresting rocks.

RESULTS

The resulting exploration map shows limonite anomalies that are similar spectrally to the known hydrothermally altered area at Cripple Creek. There are four main anomalies: A southern, banded anomaly clearly corresponds to sedimentary rocks. The most prominent pattern corresponds to red beds of the Pennsylvanian

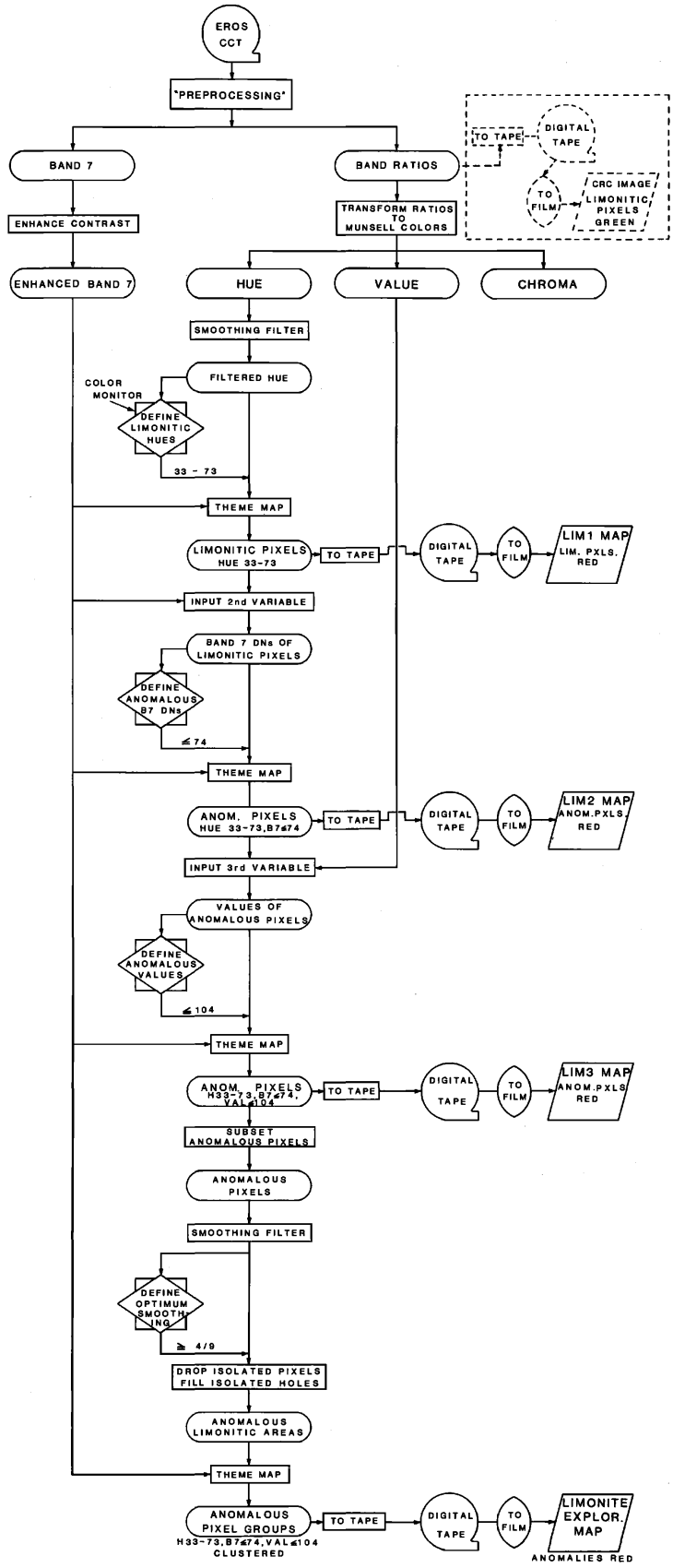

FIGURE 2 Flow diagram of digital processing and interactive decisions used to produce limonite anomaly images at Cripple Creek.

and Permian Fountain Formation (arkose and red mudstones) and the Permian and Triassic Lykins Formation (red mudstones).

The second group of anomalies corresponds to a gray, plagioclase-quartz-biotite gneiss. A reflectance spectrum measured from a weathered surface of this gneiss clearly shows the characteristic limonite shape, and an absorption peak at 0.86 micrometers serves to identify hematite (fig. 1, CCV8401). In this case, the hematite is derived from weathering of the biotite; in hand specimen, many of the biotite sheets are mottled with hematite films.

The third group of anomalies has limonitic pixels that are clearly related to exposures of Pikes Peak Granite. The direct cause of the anomaly, established through reflectance spectroscopy, is hematite, although the source of the hematite itself has not been defined. Two possible source mechanisms are suggested, and indeed, there is evidence that each may contribute. One source is the normal weathering and decomposition of the mafic minerals, as described above. The Pikes Peak Granite is a biotite granite, and some of the biotites show hematite stains. A second source is the abundant red feldspars in the granite. The pink to red color of potassium feldspars is commonly attributed to substitution of ferric iron for aluminum, with some exsolution of ferric oxide along fractures and cleavage planes (Hunt and others, 1973).

The fourth group of limonite anomalies is the Cripple Creek area, where the anomalies are clearly related to hydrothermal alteration and mineralization. The limonitic pixels correspond closely to the Cripple Creek volcanic structure and to volcanic outliers of breccia, tuff, and phonolite intrusions. A map of the limonite distribution is given in figure 3. This map affords the opportunity to compare critically the remote sensing results with mineralization, as indicated by the realistic measure of past mining activity.

Limonite anomalies correspond well with mining activity where trees are absent. Where limonite anomalies overlap with forested areas (fig. 3, B, C, D, G, H, I), airphoto interpretation shows tree densities varying from zero to 30 percent, suggesting that limonite can be mapped where tree cover is less than about 30 percent. Three areas with mining activity and no trees do not appear limonitic (fig. 3, E, J, K). One of these, K, is a large mine dump from deep workings that probably were below the oxidized zone, and the tailings thus were pyritic rather than limonitic. Areas A and F (fig. 3) are possible exploration targets.

CONCLUSIONS

Because the hydrothermal solutions often produced pyrite as well as gold and silver minerals, pyrite oxidation ultimately led to the formation of limonite at the surface, and these minerals have diagnositic spectral reflectance properties. Landsat MSS data, when digitally processed to enhance these limonitic features, provide an image base upon which a geologist interpreter can interactively and iteratively map anomalous limonitic areas.

These techniques are applicable to diverse terrains. Interactive processing of images in the Saudi Arabian desert separated limonitic anomalies caused by sand dunes and alluvium from hydrothermal limonite associated with metallic mineral occurrences (Lee, 1985). In alpine tundra areas of the San Juan Mountains, screening of surficial deposits, combined with vegetation mapping, produced a map of hydrothermal alteration in the Lake City caldera (Lee, 1986).

This case study of the Cripple Creek - Victor mining district, although not an example of an actual exploration effort, does serve to illustrate one approach to using remote sensing in exploration geology. Were the Cripple Creek - Victor gold deposits unknown, the remote sensing exploration methodology used here would have guided explorationists to this site.

REFERENCES

Blanchard, Roland, 1968, Interpretation of leached outcrops: Nevada Bureau of Mines Bulletin 66, 196 p.

Hunt, G. R., 1980, Electromagnetic radiation: the communication link in remote sensing, in Siegal, B. S., and Gillespie, A. R., eds., Remote sensing in geology: New York, John Wiley, p. 5-45.

Hunt, G. R., and Ashley, R. P., 1979, Spectra of altered rocks in the visible and near-infrared: Economic Geology, v. 74, p. 1613-1629.

Hunt, G. R., Salisbury, J. W., and Lenhoff, C. J., 1973, Visible and near-infrared spectra of minerals and rocks: VII. Acidic igneous rocks: Modern Geology, v. 4, p. 217-224.

Knepper, D. H., Jr., and Raines, G. L., 1985, Determining stretch parameters for lithologic discrimination on Landsat MSS band-ratio images: Photogrammetric Engineering and Remote Sensing, v. 51, p. 63-70.

Lee, Keenan, 1985, Interactive digital image analysis of Landsat MSS images for mapping

MAPPING HYDROTHERMAL ALTERATION WITH LANDSAT THEMATIC MAPPER DATA

Daniel H. Knepper, Jr.
U.S. Geological Survey, Denver, Colorado

Abstract. The association of hydrothermally altered rocks with mineral deposits has long been recognized and applied as an exploration tool. Landsat Multispectral Scanner (MSS) data provide a means of mapping ferric iron oxides and hydroxides (limonite), some of which may be related to altered rocks. Landsat Thematic Mapper (TM) data duplicate this capability and extend detection and mapping to other common alteration minerals, such the clay minerals, carbonates, and micas. In addition, TM data have nearly three times the spatial resolution of MSS data, so mapping potentially hydrothermally altered rocks can be conducted in greater detail.

The key to successfully applying TM data to mapping altered rocks is the design of images that enhance the spectral contrasts between the alteration minerals and other minerals and materials. Band ratio images are most commonly used to measure broad differences between selected parts of spectral reflectance curves and detect the presence of absorption bands that are characteristic of the alteration minerals. Although the interpretation of these images is not without the danger misidentifying altered rocks, an experienced geologist can usually detect probable false anomalies and focus attention on those anomalies most likely to be related to hydrothermal alteration.

INTRODUCTION

Hydrothermal alteration is the process by which the mineral structure and composition of rocks are altered by circulating heated fluids composed mostly of water. These same hydrothermal fluids also act to concentrate certain elements, often forming rich hydrothermal mineral deposits. Altered host rocks are common in areas containing mineral deposits associated with igneous and metamorphic events (porphyry copper, vein and hot springs gold, etc.) as well as with roll-front type uranium deposits. Finding and mapping hydrothermally altered rocks using satellite remote sensing data provides a means for relatively rapidly focusing mineral exploration and assessment efforts in areas most likely to contain mineral deposits.

Hydrothermally altered rocks are recognized by the presence of certain mineral species. Some of these minerals, such as alunite and jarosite, form only during the process of hydrothermal alteration and are diagnostic. Other common alteration minerals, such as kaolinite, montmorillonite, and hematite, are also formed during the weathering of both altered and unaltered rocks. Landsat Thematic Mapper (TM) data provide a means of detecting and mapping many of the minerals commonly associated with hydrothermally altered rocks. The information provided by TM data can not be used to identify specific mineral species, nor can it provide unique answers.

Although hydrothermally altered rocks are generally mineralogically and spectrally different from unaltered rocks, false anomalies are not uncommon. For example, sedimentary redbeds, clay-bearing shales, limestone and dolomite strata, and weathered granitic intrusive and volcanic rocks may be spectrally similar to some altered rocks and, consequently, are identified as potentially hydrothermally altered rocks from TM data analysis alone. However, a geologist with experience in mineral deposits and hydrothermal alteration phenomena, and with some geologic knowledge of the study area, can help select those anomalous areas identified on Landsat TM images that are most likely to have been hydrothermally altered.

The alteration minerals that can be detected and mapped with TM data fall into three broad groups: (1) the ferric iron oxide, hydroxide, and sulfate (limonite) minerals (hematite, goethite, jarosite) and (2) the hydroxyl-bearing minerals (clay minerals, micas, etc.), and (3) the hydrated sulfate minerals (gypsum, alunite) and carbonates (calcite, dolomite). Rowan and others (1974) demonstrated that the limonite minerals could be discriminated from other materials using Landsat Multispectral Scanner (MSS) data and that this information could be used to target areas of potentially altered rocks. This same capability is present with TM data, but the delineation of limonitic targets can be done better and in more detail because of the increased spatial resolution

of TM data. In addition, the capability of detecting and mapping hydroxyl-bearing minerals, hydrated sulfates, and carbonates with TM data, the result of spectral bands at 1.6 um and 2.2 um that were not acquired with the MSS system, has significantly expanded the utility of satellite data for targeting areas that may have been hydrothermally altered.

For those readers interested in exploring more deeply the use of TM data for mapping altered rocks, or spectral mapping in general, additional references are included along with those cited in this report.

SPECTRAL CHARACTER OF COMMON ALTERATION MINERALS

One of the most important factors in the successful application of TM data to detecting and mapping areas of hydrothermally altered rocks is the understanding of the spectral character of the alteration minerals relative to the positioning of the TM spectral bands. This information is critical to the design of computer-processed images that will reveal the presence or absence of these minerals.

Spectral curves for the common limonite minerals are shown in Figure 1, along with the spectral bands of data acquired by the Landsat TM system. One characteristic of these minerals is the steep positive slope in the blue, green, and red parts of the spectrum (TM bands 1, 2, and 3, respectively) due to intense absorption in the ultraviolet below 0.4 um. This steep slope, with red>green>blue, accounts for their commonly reddish colors in outcrops. Another characteristic spectral feature of the limonite minerals is an absorption band (reflectance minimum) in the near-infrared that falls largely within TM band 4. Hematite and goethite have no other strong spectral features that can be detected using the TM bands. Jarosite, however, has an additional strong absorption band near 2.2 um that falls within TM band 7 and is typical of the hydroxyl-bearing minerals.

The hydroxyl-bearing minerals, hydrated sulfates, and carbonates all have one or more strong absorption bands that fall within TM band 7 (Figure 2). These absorption bands are diagnostic of the mineral species, but the TM bands are too broad to resolve the important differences between them. Consequently, TM data cannot be used to identify which of these specific minerals may be present based on their diagnostic absorption bands. Some discrimination may be possible, however, based on the general shape of their spectral reflectance curves.

By looking at the relative reflectance values at the TM bands, the hydroxyl-bearing minerals, hydrated sulfates, and carbonates can be grouped according to the gross slopes between TM band 1 and 4, between TM bands 4 and 5, and between TM bands 5 and 7. The first group, represented by chlorite and muscovite (sericite) on Figure 2, have positive slopes on their reflectance curves between TM bands 1 and 4 and between TM bands 4 and 5; between TM bands 5 and 7 their slopes are negative. The second group, represented by calcite, kaolinite, and montmorillonite on Figure 2, has positive slopes between TM bands 1 and 4 and nearly flat slopes between TM bands 4 and 5. The gross slope between TM bands 5 and 7 is negative for this group of minerals. The third group, represented by gypsum and alunite on Figure 2, has positive slopes between TM bands 1 and 4 and negative slopes between TM bands 4 and 5 and between TM bands 5 and 7. These gross differences provide a possible basis for some discrimination within the hydroxyl-bearing minerals, hydrated sulfates, and carbonate minerals, which is discussed in a later section of this report.

Although vegetation is not an alteration mineral, some knowledge of the spectral reflectance characteristics of vegetation is crucial to the design and interpretation of TM images for potentially hydrothermally altered areas. Figure 3 shows an idealized

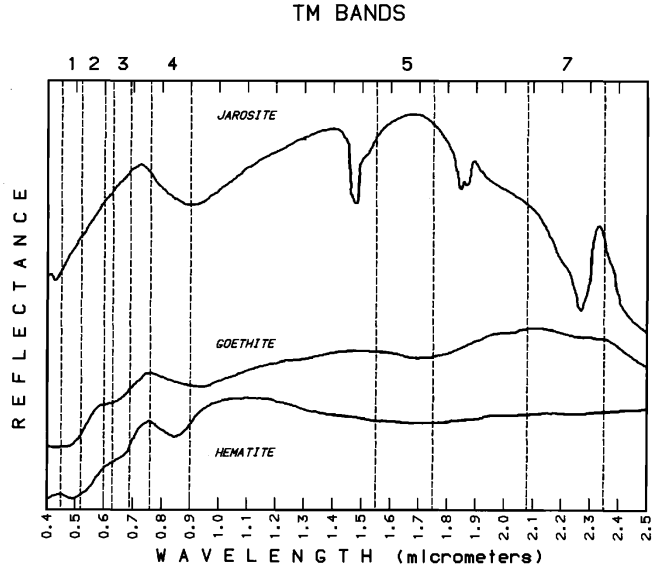

FIGURE 1 Spectral reflectance curves of the common limonite minerals, showing the location of the Landsat Thematic Mapper spectral bands. The curves are offset vertically to allow curve stacking. Curves after Lee and Raines 1984).

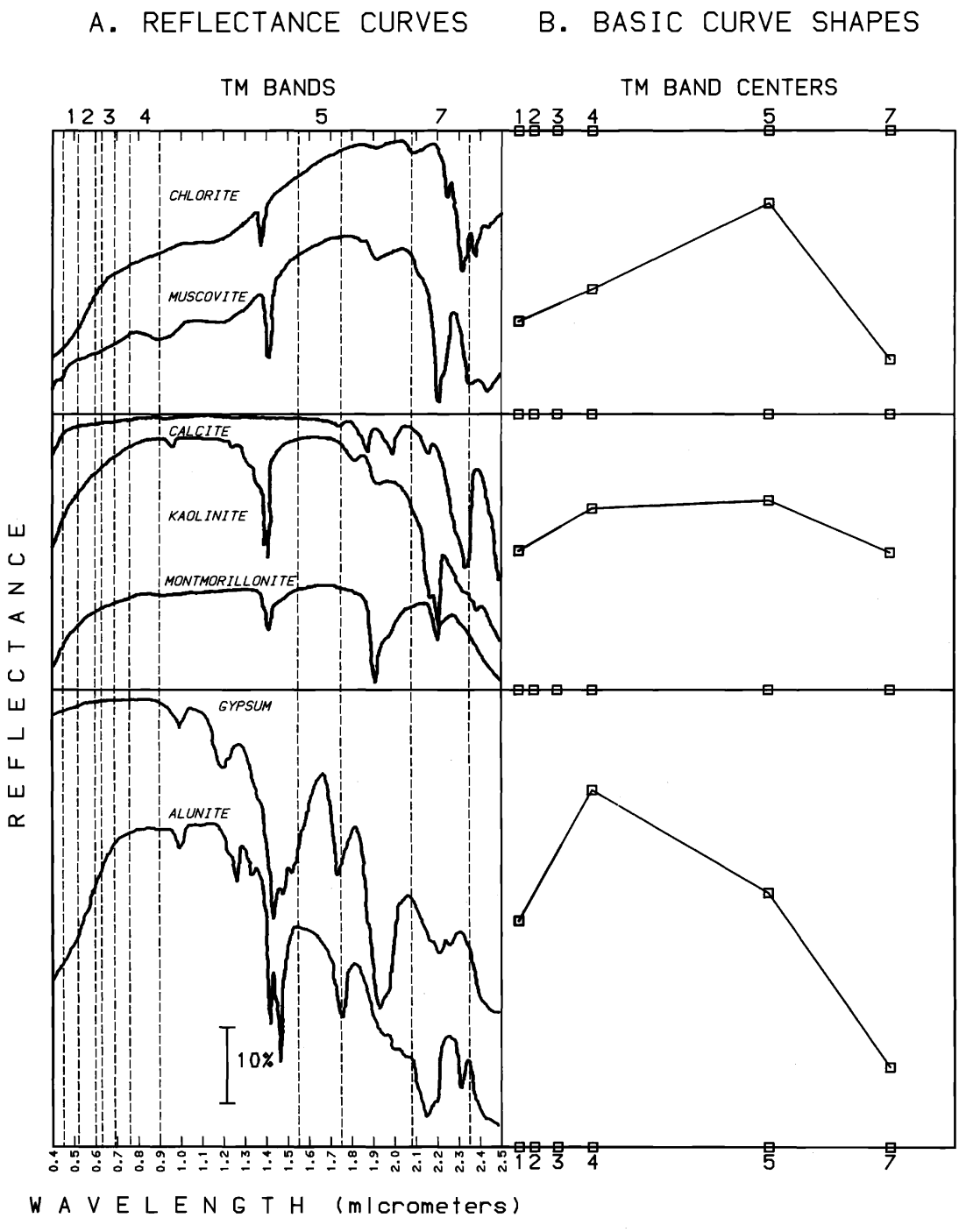

FIGURE 2 A. Spectral curves of common minerals often associated with hydrothermally altered rocks, showing the location of the Landsat Thematic Mapper spectral bands. The curves are offset vertically to allow curve stacking. Curves from Roger Clark (U.S. Geological Survey, unpublished data).
B. A method of grouping the minerals based on the basic shapes of their reflectance curves.

spectral reflectance curve for vegetation. Curves for different types of vegetation are similar in shape and differ mostly in the magnitude of the reflectance. Vegetation, in general, has a small reflectance maximum in TM band 2 (which is why vegetation appears green) and a sharp rise in reflectance in the near-infrared (TM band 4). At longer wavelengths, the reflectance gradually decreases through the range of the TM spectral bands.

With some knowledge of the spectral reflectance characteristics of alteration minerals and vegetation and the spectral bands of Landsat TM, a scheme for processing TM data can be defined that will provide a means of discriminating areas of potential hydrothermally altered rocks exposed at the earth's surface.

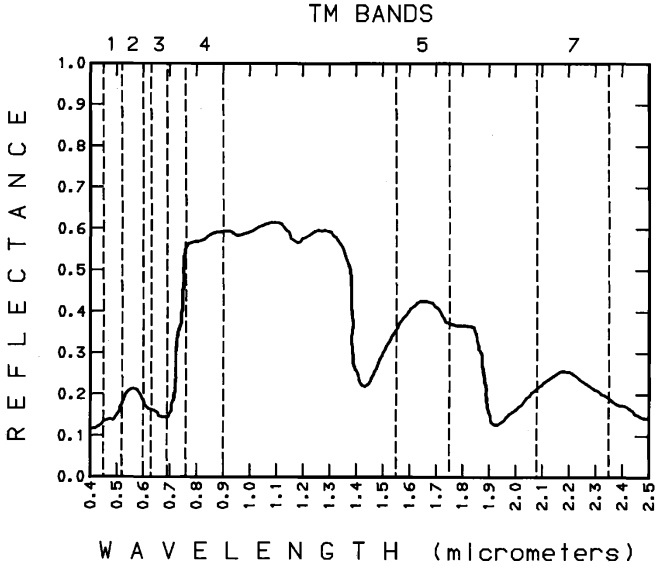

FIGURE 3 Idealized spectral reflectance curve for vegetation, showing the location of the Landsat Thematic Mapper spectral bands. Curve from Raines and Canney (1980).

IMAGE DESIGN

Designing TM image products is the process of selecting those bands, combinations of bands, and ratios of bands that will best depict the spectral features of interest. For mapping hydrothermally altered rocks, the most common approach is the use of a combination of three band-ratios, because ratioing subdues the effects of topography (uneven illumination) and enhances spectral contrast. The three ratios commonly used are each designed to accomplish a specific goal: (1) separate the hydroxyl-bearing minerals, hydrated sulfates, carbonates, and vegetation from other materials, (2) separate the limonite minerals from other materials, and (3) separate vegetation from other materials. The three ratio images are then combined into a color-ratio composite image that displays the mineral groups and vegetation in unique colors.

A Common Alteration Mapping Image

To test for an absorption band near 2.2 um, TM band 7 is used in combination with TM band 5 to produce the TM5/7 ratio. Where an absorption band is present in the vicinity of 2.2 um, the TM5/7 ratio is large (Figure 2). The TM5/7 ratio does an excellent job of delineating the hydroxyl-bearing minerals, hydrated sulfates, and carbonates, but it must be used with caution because vegetation also produces a large TM5/7 ratio due to the relatively rapid fall-off of reflectance with increasing wavelength in the near-infrared (Figure 3). To solve this ambiguity, the TM3/4 ratio (or TM5/4) is commonly used to identify the vegetation. TM band 4 occurs where the reflectance of vegetation characteristically increases rapidly toward longer wavelengths, and the TM3/4 (and TM5/4) ratio becomes very small for vegetated terrain (Figure 3).

Numerous ratios have been tried to delineate the limonite minerals on TM data; however, the most commonly used ratio is TM3/1. This ratio provides a measure of the general slope of the spectral reflectance curve in the visible part of the spectrum. Where the slope is steep and positive, such as for limonite, the TM3/1 ratio becomes relatively large (Figure 1).

The three designed TM ratio images can be combined into a single color-composite image for interpretation on a video display or on color film. Each ratio is assigned a primary color - red, green, or blue - and the color of each pixel on the composite is a function of the value of the ratios and the color assignments. The choice of color assignments for specific ratios is largely a matter of personal choice. However, because the human eye is more responsive to variations in red, yellow, and green than to blue, the ratio perceived as containing the least important information is often chosen as the blue ratio. As an example, consider a color-ratio composite (CRC) image with TM5/7 in red, TM3/1 in green, and TM3/4 in blue. Table 1 summarizes the resulting colors for alteration minerals and vegetation.

An experienced remote sensing geologist will interpret the color on this color-ratio composite image in a geologic context, eliminating most areas that are not related

TABLE 1 Resultant Colors of Alteration Minerals and Vegetation on a Color-ratio Composite Image Prepared with TM5/7 in Red, TM3/1 in Green, and TM3/4 in Blue

MATERIAL	TM5/7 (red)	TM3/1 (green)	TM3/4 (blue)	RESULTANT COLOR
HYDRATED SULFATE, CARBONATE and HYDROXYL-BEARING MINERALS	HIGH	LOW	MODERATE to LOW	**MAGENTA**
LIMONITE (Hematite, goethite)	LOW	HIGH	MODERATE to HIGH	**GREEN to CYAN**
LIMONITE (Jarosite)	HIGH	HIGH	MODERATE to HIGH	**YELLOW to WHITE**
HYDRATED SULFATE, CARBONATE, and HYDROXYL-BEARING MINERALS and LIMONITE	HIGH	HIGH	MODERATE TO HIGH	**YELLOW to WHITE**
VEGETATION	HIGH	LOW	VERY LOW	**RED**

to hydrothermally altered rocks. However, micas in metamorphic and igneous rocks, limestone and dolomite strata, and limonite minerals in alluvial deposits and in naturally weathered rocks of various lithologies can produce signatures that are impossible to distinguish from altered rocks. Therefore, all "anomalous" areas should be field checked to determine the type and extent of hydrothermal alteration and any associated mineralization. Existing geologic maps can be used to prioritize areas for field investigation according to the rock type in which the anomalies occur and the type of mineral deposits known to occur in the area.

Although standard color-ratio composite images contain one ratio designed to identify vegetation (the TM3/4 ratio in the above example), the color-composite display of the ratios often results in only a subtle color difference between the vegetation and the alteration minerals with strong absorption in TM band 7. For the above CRC image, hydroxyl-bearing minerals, hydrated sulfate, and carbonates should appear magenta, while vegetation is red. This color difference is often difficult to discern unambiguously and could increase the chances of the identification of false anomalies. To reduce the possibility of identifying false anomalies, a vegetation mask can be prepared using any of several different methods. One method that works well is to transform the three bands of TM data used to prepare a standard false-color, or color-infrared (CIR), composite image (TM bands 4-red, 3-green, and 2-blue) in to Munsell (HSV) color space consisting of hue, saturation (chroma), and value (brightness). On a standard CIR composite image, vegetation is uniquely displayed in shades of red, which can be identified from the hue Munsell transform. Each image pixel that is a red hue can be identified and used to prepare a mask to eliminate vegetation from the color-ratio composite image (Knepper and Raines, 1985; Magee and others, 1986).

Alternative Alteration Mapping Images

Although color-ratio composite images consisting of TM5/7, TM3/1, and either TM3/4 or TM5/4 are most commonly used for hydrothermal alteration mapping using TM data, it is important to understand that other images are possible, especially for specific purposes. For example, a CRC image can be designed especially for detecting and mapping variations in limonite due to mineralogy or concentration. As before, the TM3/1 ratio provides a good measure of the steepness of the reflectance curve in the visible part of the spectrum, which is the

primary criterion for identifying the limonite minerals. A TM2/3 ratio can be used to provide a measure of how red the material appears: the redder the material relative to green, the smaller the TM2/3 ratio should be. This ratio also does good job of separating out green vegetation because the TM band 2 is large relative to the TM band 3 making the TM2/3 ratio very large for vegetation. The third ratio that could be used is the TM3/4. As was discussed above, this ratio can be used to characterize the presence and strength of an absorption band near .9 um due to ferric iron (Figure 1). By color-coding this CRC image as TM3/1 red, TM2/3 green, and TM3/4 blue, limonitic materials appear in shades of red, orange, yellow, and magenta, while vegetation is green (Table 2).

This limonite CRC image is being tested in several geographic areas and appears to do a good job of displaying variations in limonite in arid regions. Additional experiments are being conducted to determine whether other color-coding schemes may enhance the display of limonite variations.

In all studies using TM data to identify and map hydrothermally altered rocks encountered in the literature, the TM5/7 ratio is the only image generated for identifying the hydroxyl-bearing minerals, hydrated sulfates, and carbonates. However, based on the earlier discussion of the gross reflectance characteristics of these minerals (Figure 2), it should be possible to design an image that will further separate them. For example, one ratio (TM5/7) could be used to detect the presence of an absorption band at 2.2 um (TM band 7). Another ratio (TM5/4) could be used to measure the general slope of the reflectance curve between TM bands 4 and 5, which is positive and steep to moderate (TM5/4 is $>>$ 1.0) for the micas and jarosite, negative (TM5/4 $<<$ 1.0) for alunite and gypsum, and approximately flat (TM5/4 =1.0) for calcite and the clay minerals (Figures 1 and 2). A third ratio (TM7/4) could be used to separate the micas because, in spite of strong absorption in TM band 7, the gross slope between TM bands 4 and 7 is positive (TM7/4 $>=$ 1.0), unlike the clay minerals, sulfates, and carbonates (Figure 2). In addition, the sulfate minerals gypsum and alunite might also be separated with the TM7/4 ratio because their slopes between TM bands 4 and 7 are so strongly negative (TM7/4 $<<$ 1.0) To apply a CRC image to mapping altered rocks using these ratio combinations, it would probably be necessary to apply a mask as discussed above to eliminate possible

TABLE 2 Resultant Color for Limonite and Vegetation on a Color-ratio Composite Image Prepared from TM3/1 (red), TM2/3 (green), and TM3/4 (blue)

MATERIAL	TM3/1 (red)	TM2/3 (green)	TM3/4 (blue)	RESULTANT COLOR
LIMONITE WITH WEAK .9 BAND and BROWN COLOR	HIGH	MODERATE	LOW	**ORANGE;YELLOW**
LIMONITE WITH STRONG .9 BAND and RED COLOR	HIGH	LOW	HIGH	**MAGENTA**
LIMONITE WITH WEAK .9 BAND and RED COLOR	HIGH	LOW	LOW	**RED**
LIMONOTE WITH STRONG .9 BAND and BROWN COLOR	HIGH	MODERATE	HIGH	**PALE MAGENTA**
VEGETATION	LOW	HIGH	LOW	**GREEN**

false anomalies due to vegetation. The potential for this TM band-ratio combination is currently being evaluated at the U.S. Geological Survey.

The preceeding discussion of image design assumed a situation where there is only a single detectable mineral or vegetation within a TM picture element (pixel). In practice, we are faced with the possibility of signals from several mineral species, as well as cultural and atmospheric features and vegetation, being recorded in the TM band radiances for each pixel, a condition known as the "mixed pixel" problem. Because of the broadness of the TM bands and their limited number, there appears to be little that can be done to resolve this problem, although their has been some success in removing the spectral effects of vegetation (Fraser and Green, 1987). The potential for misinterpretations due to mixed pixels is a recognized limitation of TM data, and other types of remote sensing data as well, but experience has shown that this limitation does not appear to be serious nor should it restrict attempts to apply Landsat TM data to mapping hydrothermally altered rocks.

REFERENCES CITED AND SELECTED BIBLIOGRAPHY

Abrams, Michael, 1986, Mapping the Oman ophiolite using TM data: Proceedings, Fifth Thematic Conference on Remote Sensing for Exploration Geology, ERIM, 29 September-2 October 1986, Reno, Nevada, p. 85-95.

Abrams, M., Ashley, R., Rowan, L. Goetz, A., and Kahle, A., 1977, Mapping hydrothermal alteration in the Cuprite mining district, Nevada, using aircraft scanner images for the spectral region 0.46 to 2.35 microns: Geology, V. 5, p. 713-718.

Abrams, M.J., Brown, David, Kepley, Larry, and Sadowski, Ray, 1983, Remote sensing for porphyry copper deposits in southern Arizona: Economic Geology, V. 78, no. 4, p. 591-604.

Bailey, G.B., Dwyer, J.L., and Podwysocki, M.H., 1985, Evaluation of Landsat Thematic Mapper data for geologic mapping in semi-arid terrains: Proceedings, International Symposium on Remote Sensing of Environment, Fourth Thematic Conference, Remote Sensing for Exploration Geology, ERIM, April 1-4, 1985, San Francisco, p. 325-326.

Banninger, C., 1986, Discrimination of geobotanical anomalies in rugged alpine terrain using Landsat Thematic Mapper data: Proceedings, Fifth Thematic Conference on Remote Sensing for Exploration Geology, ERIM, 29 September-2 October 1986, Reno, Nevada, p. 813-816.

Banninger, C., 1986, Relationship between soil and leaf metal content and Landsat MSS and TM acquired canopy reflectance data: Proceedings, 7th International Symposium, International Society of Photogrammetry and Remote Sensing (ISPRS), Enschede, The Netherlands, p. 195-200.

Brickey, D.W., 1986, The use of Thematic Mapper imagery for mineral exploration in the sedimentary terrane of the Spring Mountains, Nevada: Prodeedings, Fifth Thematic Conference on Remote Sensing for Exploration Geology, Reno, Nevada, 29 September-2 October 1986, p. 607-613.

Buckingham, W.F. and Sommer, S.E., 1983, Mineralogical characterization of rock surfaces formed by hydrothermal alteration and weathering - Application to remote sensing: Economic Geology, V. 78, p. 664-674.

Crippen, R.E., 1986, The regression intersection method of adjusting image data for band ratioing: Proceedings, Fifth Thematic Conference on Remote Sensing for Exploration Geology, ERIM, 29 September-2 October 1986, Reno, Nevada, p. 407-416.

Elvidge, C.D., 1986, Use of calibration targets in the measurement of 2.22 um mineral absorption features in Thematic Mapper data: Proceedings, Fifth Thematic Conference on Remote Sensing for Exploration Geology, ERIM, 29 September-2 October 1986, Reno, Nevada, p. 427-438.

Elvidge, C.D. and Lyon, R.J.P., 1984, Mapping clay alteration in the Virginia Range-Comstock Lode, Nevada, with airborne Thematic Mapper imagery: Proceedings, Third Thematic Conference on Remote Sensing for Exploration Geology, ERIM, 16-19 April 1984, Colorado Springs, Colorado, p. 162-170.

Elvidge, C.D. and Lyon, R.J.P., 1985, Estimation of the vegetation contribution to the 1.65um/2.22um ratio in airborne Thematic Mapper imagery of the Virginia Range, Nevada: International Journal of Remote Sensing, V. 6, p. 75-88.

Fielding, E.J., 1985, Lithologic discrimination of volcanic and sedimentary rocks by spectral examination of Landsat TM data from the Puna, Central Andes Mountains: Prodeedings, Fourth Thematic Conference on Remote Sensing for Exploration Geology, ERIM, 1-4 April 1985, San Francisco, California, p. 619-630.

Fraser, S.J., and Green, A.A., 1987, A software defoliant for geological analysis of band ratios: International Journal of Remote Sensing, v. 8, no. 3, p. 525-532.

Goetz, A.F.H., Rock. B.N., and Rowan, L.C., 1983, Remote sensing for exploration: an overview: Economic Geology, V. 78, p. 573-590.

Harding, A.E., Garrard, G.R., and Girones, E.O., 1986, Exploration for mercury and lead-zinc-silver using the airborne Thematic Mapper, Alamaden area, Spain: Proceedings, Fifth Thematic Conference on Remote Sensing for Exploration Geology, ERIM, 29 September-2 October 1986, Reno, Nevada, p. 601-606.

Huckerby, J.A., Magee, R., Moore, J.McM., and Coates, D., 1986, Thematic mapper applied to alteration zone mapping for gold exploration in south-east Spain: Proceedings, Fifth Thematic Conference on Remote Sensing for Exploration Geology, Reno, Nevada, 29 September-2 October 1986, p. 591-599.

Hunt, G.R., 1977, Spectral signatures of particulate minerals in the visible and near infrared: Geophysics, v. 42, p. 501-513.

Hunt, G.R. and Ashley, R.P., 1979, Spectra of altered rocks in the visible and near infrared: Economic Geology, V. 74, p. 1613-1629.

Hunt, G.R., and Salisbury, J.W., 1970, Visible and near-infrared spectra of mineral and rocks: I. Silicate minerals: Modern Geology, v. 1, p. 283-300.

_____, 1971, Visible and near-infrared spectra of minerals and rocks: II. Carbonates: Modern Geology, v. 2, p.23-30.

_____, 1976a, Visible and near-infrared spectra of minerals and rocks: XI. Sedimentary rocks: Modern Geology, v. 5, p. 211-217.

_____, 1976b, visible and near-infrared spectra of minerals and rocks: XII. Metamorphic rocks: Modern Geology, v. 5, p. 219-228.

Hunt, G.L., Salisbury, J.W., and Lenhoff, C.J., 1971a, Visible and near-infrared spectra of minerals and rocks: III. Oxides and hydroxides: Modern Geology, v. 2, p. 195-205.

_____, 1971b, Visible and near-infrared spectra of minerals and rocks: IV. Sulphides and sulphates: Modern Geology, v. 5, p.1-14.

_____, 1972, Visible and near-infrared spectra of minerals and rocks: V. Halides, phosphates, arsenates, vanadates, and borates: Modern Geology, v. 3, p. 121-132.

_____, 1973a, Visible and near-infrared spectra of minerals and rocks: VI. Additional silicates: Modern Geology, v. 4, p. 85-106.

_____, 1973b, Visible and near-infrared spectra of minerals and rocks: VII. Acidic igneous rocks: Modern Geology, v. 4, p. 217-224.

_____, 1973c, Visible and near-infrared spectra of minerals and rocks: VIII. Intermediate igneous rocks: Modern Geology, v. 4, p. 237-244.

_____, 1974, Visible and near-infrared spectra of minerals and rocks: IX. Basic and ultrabasic igneous rocks: Modern Geology, v. 5, p. 15-22.

Kepper, J.C., Lugaski, T.P., and MacDonald, J.S., 1986, Discrimination of lithologic units, alteration patterns and major structural blocks in the Tonopah, Nevada, area using Thematic Mapper data: Proceedings, Fifth Thematic Conference on Remote Sensing for Exploration Geology, ERIM, 29 September-2 October 1986, Reno, Nevada, p. 97-115.

Knepper, D.H., Jr. and Raines, G.L, 1985, Determining stretch parameters for lithologic discrimination on Landsat MSS band-ratio images: Photogrammetric Engineering and Remote Sensing, v. 51, no. 1, p. 63-70.

Kruse, F.A., 1986, Digital mapping of alteration zones in a hydrothermal system using Landsat Thematic Mapper data - An example from the Northern Grapevine Mountains, Nevada/California: Proceedings, Fifth Thematic Conference on Remote Sensing for Exploration Geology, ERIM, 29 September-2 October 1986, Reno Nevada, p. 393.

Lee, Keenan, and Raines, G.L, 1984, Reflectance spectra of alteration minerals: U.S. Geological Survey Open-File Report 84-0096, 1 chart.

Loughlin, W.P. and Tawfiq, M.A., 1985, Discrimination of rock types and alteration zones from airborne MSS data - The Samran-Shayban and Mahad Adh Dhahab areas of Saudi Arabia: Proceedings, Third Thematic Conference on Remote Sensing for Exploration Geology, ERIM, San Francisco, California, 1-4 April 1985, p. 207-225.

Magee, R.W., Moore, J.M., and Brunner, Jake, 1986, Thematic Mapper data applied to mapping hydrothermal alteration in south west New Mexico: Proceedings, Fifth Thematic Conference on Remote Sensing for Exploration Geology, ERIM, 29 September-2 October 1986, Reno, Nevada, p. 373-382.

McBride, J. H., Fielding, E.J., and Isacks, B.L., 1986, Discrimination and supervised classification of volcanic flows of the Puna-Altiplano, central Andes Mountains, using Landsat TM data: Proceedings, Fifth Thematic Conference on Remote Sensing for Exploration Geology, ERIM, 29 September-2 October 1986, Reno, Nevada, p. 693-702.

Miller, N.L. and Elvidge, C.D., 1985, The iron absorption index - a comparison of ratio-based and baseline-based techniques for the mapping of iron oxides: Proceedings, Fourth Thematic Conference on Remote Sensing for Exploration Geology, ERIM, San Francisco, California, 1-4 April 1985, p. 405-415.

Mouat, D.A., Myers, J.S., and Miller, N.L., 1986, An integrated approach to the use of Landsat TM data for gold exploration in west central Nevada: Proceedings, Fifth Thematic Conference on Remote Sensing for Exploration Geology, Reno, Nevada, 29 September-2 October 1986,p. 615-626.

Peters, D.C., 1983, Use of airborne multi-spectral scanner data to map alteration related to roll-fromt uranium migration: Economic Geology, V. 78, p. 641-653.

Podwysocki, M.H., Segal, D.B., and Abrams, M.J., 1983, Use of multispectral scanner images for assessment of hydrothermal alteration in the Marysvale, Utah, mining area: Economic Geology, V. 78, p.675-687.

Raines, G.L, and Canney, F.C., 1980, Vegetation and geology, in Siegal, B.S., and Gillespie, A.R., eds., Remote sensing in geology: New York, Wiley, p.365-380.

Rowan, L.C., Wetlaufer, P.H., Goetz, A.F.H., Billingsley, F.C., and Stewart, J.H., 19074, Discrimination of rock types and detection of hydrothermally altered areas in south-central Nevada by the use of computer-enhanced ERTS images: U.S. Geological Survey Professional Paper 883, 35 p.

LANDSAT LINEAMENT ANALYSIS OF THE SOUTHERN COLORADO FRONT RANGE

Keenan Lee, Hayati Koyuncu, and Andrea J. Gallagher
Colorado School of Mines, Golden, Colorado
U.S. Geological Survey, Denver, Colorado

Lineament analysis is used to help interpret regional structure, to aid in locating buried structures, and to map fractures. In regional syntheses, lineament analysis may define structural fabric of a terrane and focus attention on domain boundaries or zones of weakness. Some analyses are directed toward detection of basement structures, primarily faults.

Basement faults, especially if recurrent, influence depositional patterns and thus influence hydrocarbon accumulations, both in controlling development and distribution of reservoir facies and in formation of trapping conditions (Perry and Lee, 1986). Basement faults, as zones of weakness, may influence emplacement of igneous intrusions and therefore the localization of hydrothermal systems.

Fractures may directly influence metal deposition by controlling fluid flow along fracture permeability. As such, fractures have been considered the plumbing system for numerous metal deposits. Fractures likewise may be of some importance in hydrocarbon accumulations. In the Florence field of the Canon City embayment, the second oldest oil field in the U.S.A., production is from fracture permeability in the Cretaceous Pierre Shale.

METHODS

Linear Feature Mapping

Linear features were mapped on part of a Landsat Thematic Mapper (TM) image that covers approximately a one degree by one degree area of the southern Colorado Front Range. The area of coverage is shown in figure 1, and a single-band image of about the same area is shown in Lee and others (this publ., p. 34). The TM data were radiometrically corrected and geographically registered, and Bands 2, 3, and 4 were used to make a color-infrared (CIR) composite. This CIR image was then used as the basis for photogeologic interpretation of linear features.

"Linear features" include all natural straight features, regardless of length, that the photo interpreter was able to see in the image. Most linear features correspond to linear topographic features, usually valleys

Miller, N.L. and Elvidge, C.D., 1985, The iron absorption index - a comparison of ratio-based and baseline-based techniques for the mapping of iron oxides: Proceedings, Fourth Thematic Conference on Remote Sensing for Exploration Geology, ERIM, San Francisco, California, 1-4 April 1985, p. 405-415.

Mouat, D.A., Myers, J.S., and Miller, N.L., 1986, An integrated approach to the use of Landsat TM data for gold exploration in west central Nevada: Proceedings, Fifth Thematic Conference on Remote Sensing for Exploration Geology, Reno, Nevada, 29 September-2 October 1986,p. 615-626.

Peters, D.C., 1983, Use of airborne multi-spectral scanner data to map alteration related to roll-fromt uranium migration: Economic Geology, V. 78, p. 641-653.

Podwysocki, M.H., Segal, D.B., and Abrams, M.J., 1983, Use of multispectral scanner images for assessment of hydrothermal alteration in the Marysvale, Utah, mining area: Economic Geology, V. 78, p.675-687.

Raines, G.L, and Canney, F.C., 1980, Vegetation and geology, in Siegal, B.S., and Gillespie, A.R., eds., Remote sensing in geology: New York, Wiley, p.365-380.

Rowan, L.C., Wetlaufer, P.H., Goetz, A.F.H., Billingsley, F.C., and Stewart, J.H., 19074, Discrimination of rock types and detection of hydrothermally altered areas in south-central Nevada by the use of computer-enhanced ERTS images: U.S. Geological Survey Professional Paper 883, 35 p.

LANDSAT LINEAMENT ANALYSIS OF THE SOUTHERN COLORADO FRONT RANGE

Keenan Lee, Hayati Koyuncu, and Andrea J. Gallagher
Colorado School of Mines, Golden, Colorado
U.S. Geological Survey, Denver, Colorado

Lineament analysis is used to help interpret regional structure, to aid in locating buried structures, and to map fractures. In regional syntheses, lineament analysis may define structural fabric of a terrane and focus attention on domain boundaries or zones of weakness. Some analyses are directed toward detection of basement structures, primarily faults.

Basement faults, especially if recurrent, influence depositional patterns and thus influence hydrocarbon accumulations, both in controlling development and distribution of reservoir facies and in formation of trapping conditions (Perry and Lee, 1986). Basement faults, as zones of weakness, may influence emplacement of igneous intrusions and therefore the localization of hydrothermal systems.

Fractures may directly influence metal deposition by controlling fluid flow along fracture permeability. As such, fractures have been considered the plumbing system for numerous metal deposits. Fractures likewise may be of some importance in hydrocarbon accumulations. In the Florence field of the Canon City embayment, the second oldest oil field in the U.S.A., production is from fracture permeability in the Cretaceous Pierre Shale.

METHODS

Linear Feature Mapping

Linear features were mapped on part of a Landsat Thematic Mapper (TM) image that covers approximately a one degree by one degree area of the southern Colorado Front Range. The area of coverage is shown in figure 1, and a single-band image of about the same area is shown in Lee and others (this publ., p. 34). The TM data were radiometrically corrected and geographically registered, and Bands 2, 3, and 4 were used to make a color-infrared (CIR) composite. This CIR image was then used as the basis for photogeologic interpretation of linear features.

"Linear features" include all natural straight features, regardless of length, that the photo interpreter was able to see in the image. Most linear features correspond to linear topographic features, usually valleys

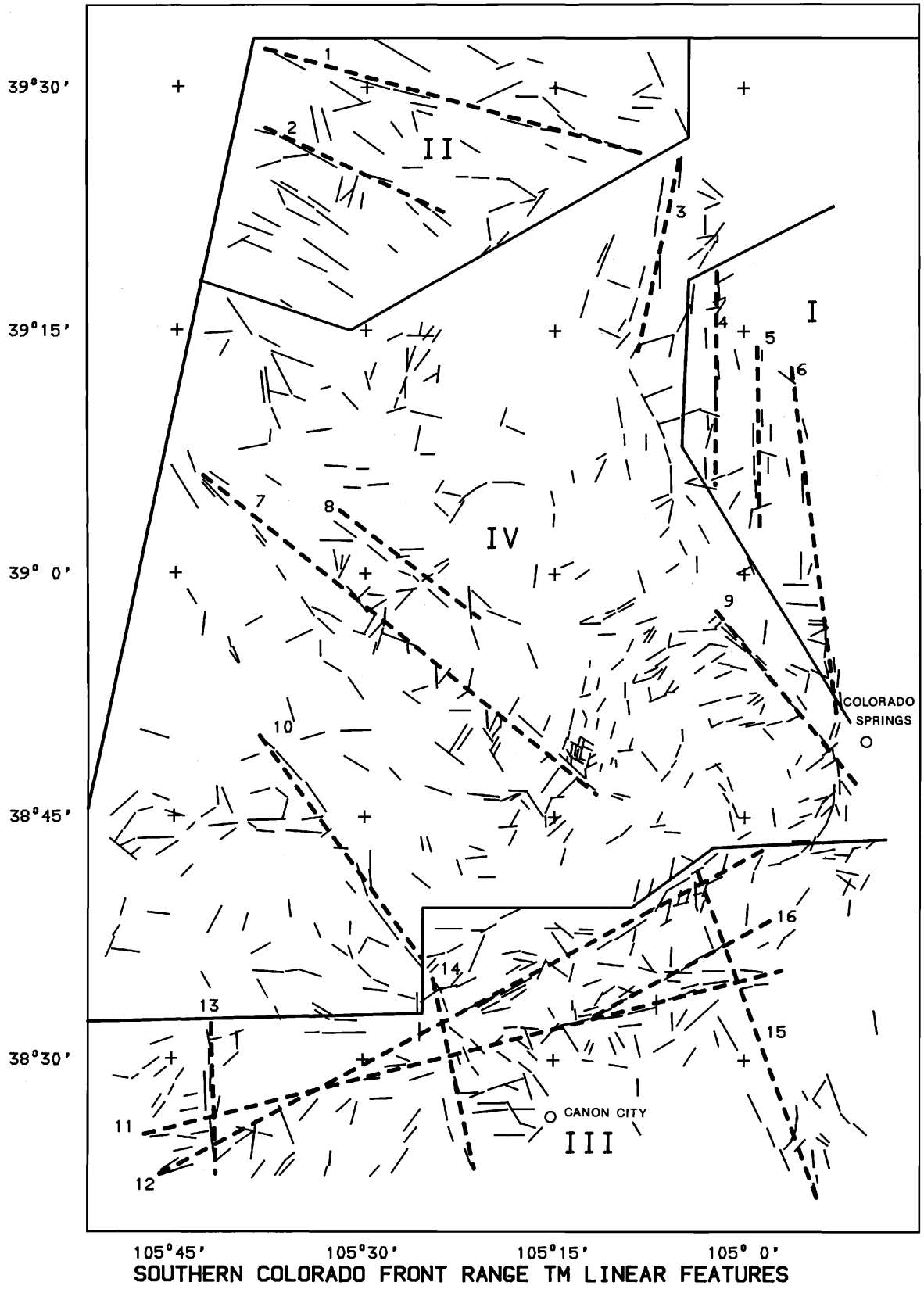

FIGURE 1 Southern Colorado Front Range area showing linear features mapped from Landsat Thematic Mapper image. Dashed lines are lineaments derived from analysis of the linear features. Domains are separated by solid lines and numbered I-IV.

of uncertain geologic nature, while others correspond to mappable geologic features. ("Lineaments" are elongate zones of linear features, derived from statistical analysis and interpretation of linear features, as discussed below).

Linear Feature Analysis

The linear features must be digitized to allow subsequent statistical analysis (for the methodology of this and subsequent data reduction techniques, see Sawatzky and Raines, 1981). The digital linear feature data are then available for frequency analysis of length and orientation.

Figure 2 shows a length-frequency histogram of linear features from the central part of the study area (domain IV in fig. 1; the original data set was subdivided into smaller areas, or domains, that grouped linear features of similar orientation). The 447 linear features range from less than 0.2 km to a maximum of about 5 km. Median length is about 1.7 km (significantly shorter than linear features from similar studies using MSS images; it is too early to know if this relationship will prove to be the case consistently).

LENGTH INTERVAL		FREQUENCY + + + +
0.00	0.20	1
0.20	0.40	1
0.40	0.60	3 **
0.60	0.80	17 **********
0.80	1.00	18 **********
1.00	1.20	45 **********
1.20	1.40	56 **********
1.40	1.60	59 **********
1.60	1.80	59 **********
1.80	2.00	47 **********
2.00	2.20	33 **********
2.20	2.40	30 **********
2.40	2.60	21 **********
2.60	2.80	13 ********
2.80	3.00	11 *******
3.00	3.20	7 ****
3.20	3.40	5 ***
3.40	3.60	7 ****
3.60	3.80	6 ****
3.80	4.00	2 *
4.00	4.20	0
4.20	4.40	1
4.40	4.60	3 **
4.60	4.80	0
4.80	5.00	1
5.00	5.20	1

FIGURE 2 Histogram of linear feature lengths. Range is 0.2 to 5.2 km, with the median length of about 1.7 km.

Azimuth-frequency analysis is used to study significant directional trends in the data. Figure 3 is a histogram of linear feature azimuths, by one degree increments, from domain IV (fig. 1). These data have been length-weighted to give more emphasis to longer features, and the histogram is smoothed by a three-point moving average. A strong northwest trend is apparent in the data. The solar azimuth will selectively subdue linear features with a northwest orientation (Sawatzky and Lee, 1974), and the interpreter should at least be cognizant of this bias if not actually correcting for the effect (Briceno and Lee, 1984).

The geographic distribution of individual trends of linear features can be seen by plotting subsets of the data, for example, only those linear features in domain IV that fall in the statistically significant azimuthal interval of N33W to N55W (fig. 4). Clusters of linear features, especially elongate clusters, can be seen more clearly by contouring the concentration, or density, of linear features (fig. 4).

Lineament Interpretation

As used in this report, a "lineament" is an elongate zone of aligned linear features. Except for some lineaments that appear clearly in the image itself, the recognition of lineaments is based on linear feature analysis and is the final interpretation of this analysis. The basis of lineament recognition is interpreting linear trends, or clusters, of mapped linear features. For example, a homogeneous area with a single fracture direction would show linear features distributed uniformly over the image, and one statistically significant trend would emerge in the azimuth-frequency analysis, but no lineament would be mapped.

To interpret lineaments by the methodology used here, one normally selects a significant azimuth trend and analyzes only that subset of linear features oriented within that azimuth interval. Contouring their density distribution aids in interpreting aligned concentrations of linear features. Referring again to figure 4, the contoured data show several concentrations that are elongate in the direction of the linear features. Four lineaments are interpreted from these data, as mapped in figure 4.

RESULTS

Figure 1 shows the results of a lineament interpretation of the study area. Sixteen lineaments have been interpreted, as shown by the long, solid lines in figure 1. Of these, one lineament corresponds to a fold-fault pair in sedimentary rocks, one correlates poorly with mapped faults, seven lineaments are related to more than one fault, and seven others correspond clearly and directly to faults or fault zones.

An example of the latter case, where the

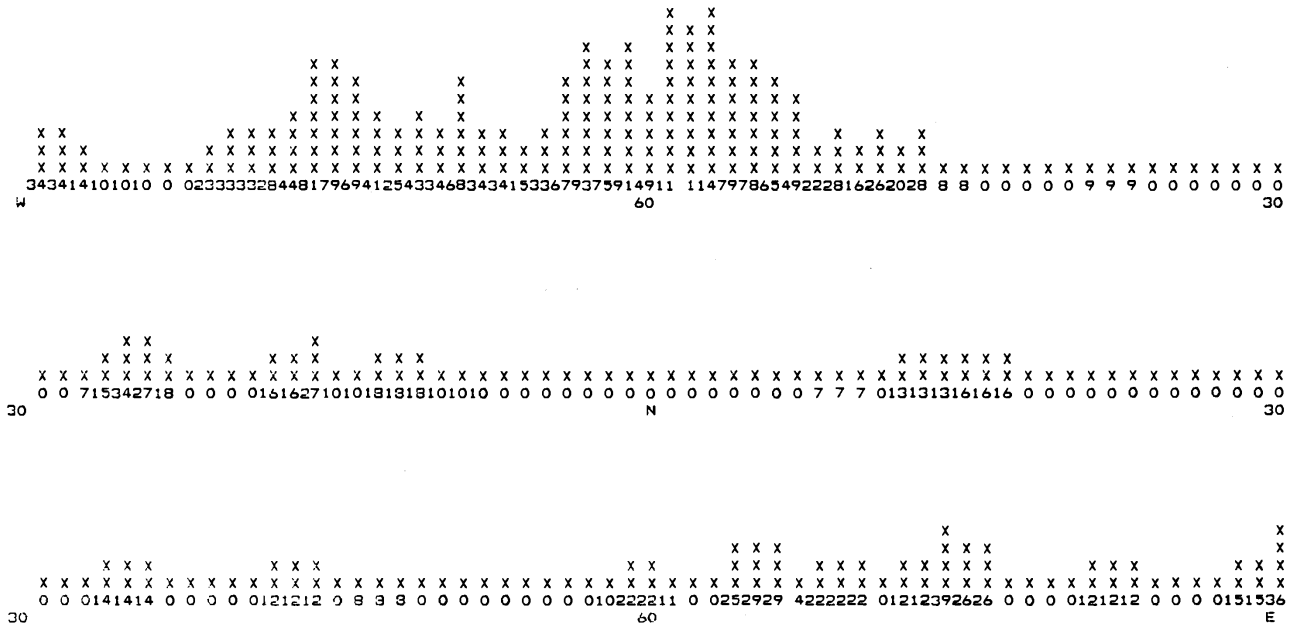

FIGURE 3 Histogram of linear feature azimuths. Data have been length-weighted to emphasize longer features.

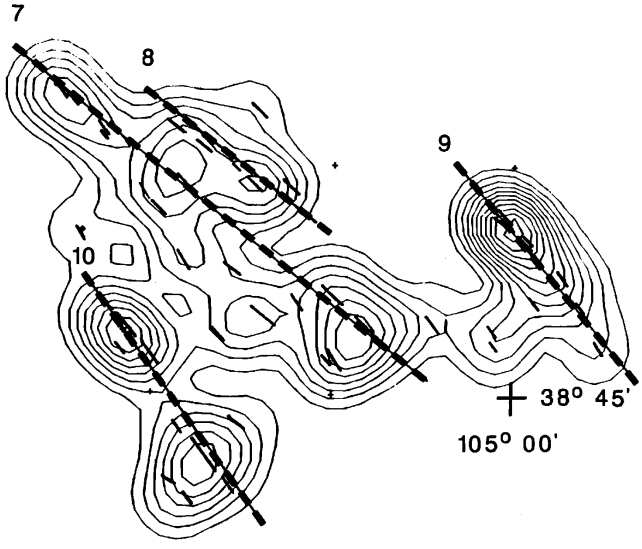

FIGURE 4 Subset of linear features with azimuths between N33W and N55W. Concentrations of linear features are shown by contours (interval is arbitrary). Also shown are the four lineaments interpreted from these data.

lineament is directly correlated with a fault, is shown in figure 5. The lineament, defined on the basis of the eleven linear features shown, is represented by a dashed line. Also shown in the figure are the traces of the Ute Pass fault zone (this fault, and the ones shown in subsequent figures, are from the 1:250,000 geologic map by Scott and others, 1978).

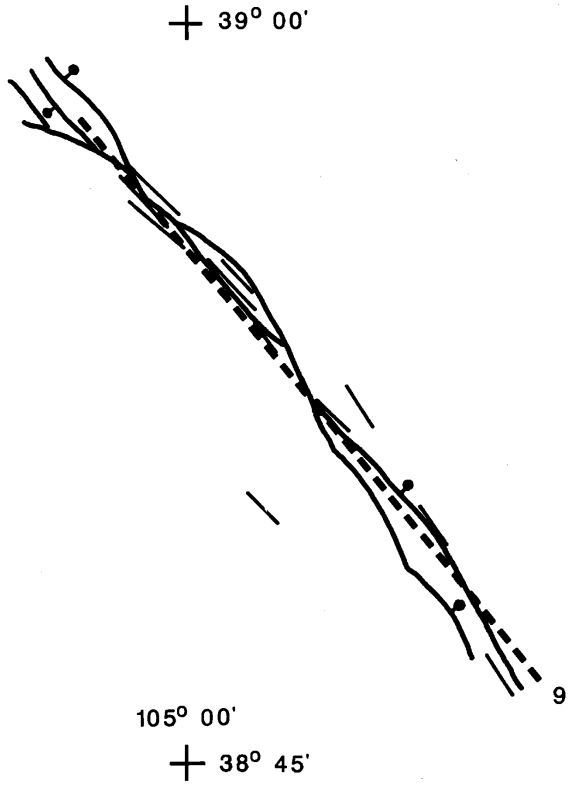

FIGURE 5 Lineament (dashed line) derived from linear features corresponds directly to the Ute Pass fault zone.

Figure 6 shows the relationship of a lineament (dashed line) to a fold structure (dotted line) in sedimentary rocks, in this case a monocline in Cretaceous marine carbonates and shales (Salt Canyon monocline). The fold may well represent the edge of a basement block over which sedimentary rocks have been draped. On the downdraped side are several subparallel faults.

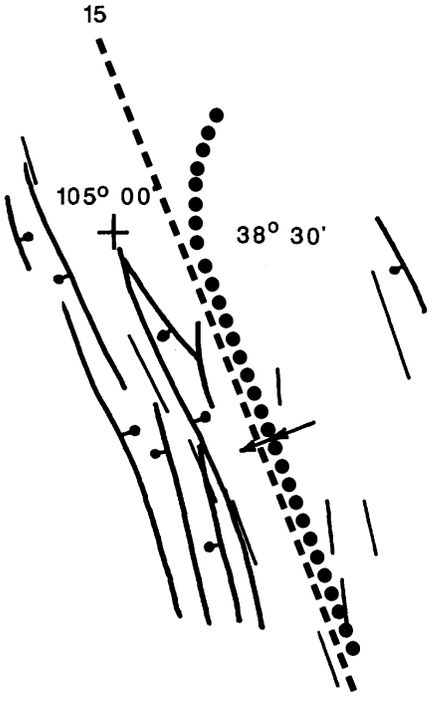

FIGURE 6 Lineament (dashed line) derived from linear features in Cretaceous sedimentary rocks. Lineament corresponds to the Salt Canyon monocline (dotted line), with normal faults on the downdraped side.

One of the most important lineaments in the study area does not correlate well with any single fault, but it represents a fault zone (fig. 7). It is considered important because it is in the position of the offset of the Precambrian mountain front, where the linear front, extending south from Golden, is offset in the Canon City embayment some 30 miles (50 km) to the southwest.

DISCUSSION

Some critics of lineament analysis would suggest that if one cannot touch a linear feature on the ground, that it is not "real". Adherents of the approach to

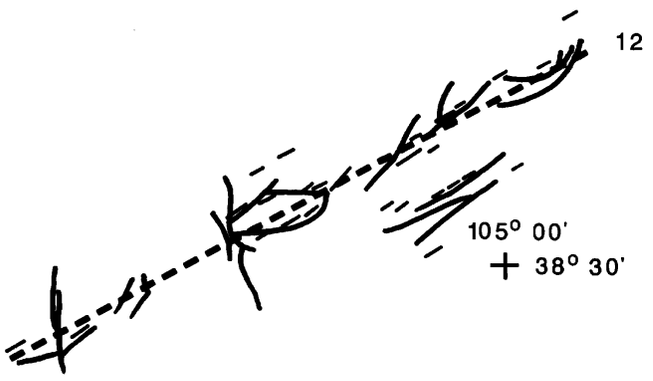

FIGURE 7 Lineament (dashed line) does not correspond well with mapped faults, although segments of numerous faults lie along the lineament.

lineament interpretation illustrated here, on the other hand, generally give little significance to an individual linear feature. There are three cases in this analysis, however, in which the linear features seemingly are more significant than the derived lineament. An example is shown in figure 8, where a lineament was interpreted based on 15 linear features. Although the lineament coincides with portions of three faults, there is not a strong correlation with any. The linear features, on the other hand, show a very strong correlation, with 11 of the 15 features coinciding with a fault trace. In this case the linear features better define the faults than does the lineament. It may be that in this area there is considerably better exposure of basement than one normally encounters.

In most lineament analyses, lineaments are interpreted that are parallel to the linear features, as is the case for all of the examples shown here. It may be that this is the result of studies done in the central-

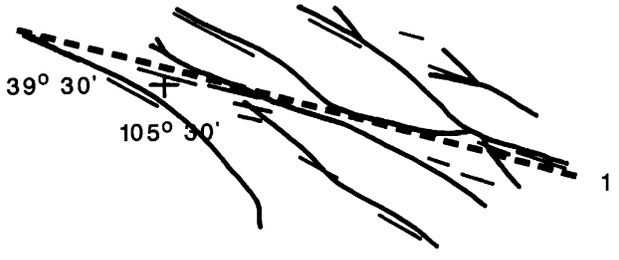

FIGURE 8 Lineament (dashed line) does not correspond well with mapped faults, although several fault segments are coincident with lineament. linear features themselves better define the position of fault traces.

western U.S.A., where dominantly vertical displacements on basement faults propagate to the surface as fractures parallel to the fault. If wrench faulting occurs, however, one might expect en echelon fractures to be oriented some 60 degrees to the main fault (and lineament). Such a case was encountered along the Anatolian fault in Turkey (Lee, 1983), and a possible example is shown for the study area in figure 9. North-northeast oriented linear features occur in a northwest-trending zone adjacent to the main trace of the Ute Pass fault zone. If these were the result of shear, one would expect right-lateral displacement. The geologic map shows no strike-slip movement here, but on a northwest extension of the fault, such displacement does occur.

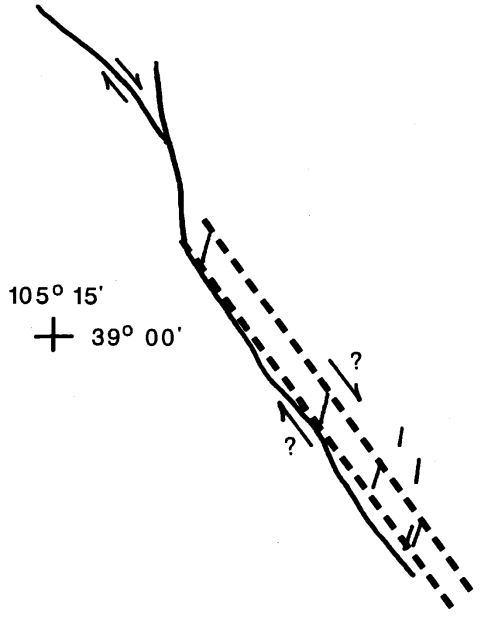

FIGURE 9 A questionable lineament (paired dashed lines) defined by linear features of a different orientation. The en echelon linear features are at about a 50-degree angle to the lineament. Main trace of the Ute Pass fault system is shown just south of this lineament.

SUMMARY

Interpretation of TM imagery of the southern Colorado Front Range led to mapping of 622 linear features. Median length of the linear features was about 1.7 km, with a maximum length of about 5 km. Azimuth-frequency analysis defined statistically significant trends in the data. Subsets of linear features in these trend intervals were plotted, and their areal density was contoured. From these contour maps, lineaments were interpreted.

The lineament interpretation was compared with published geologic maps. Of the 16 interpreted lineaments, one correlated with a fold-fault pair in sedimentary rocks. One lineament corresponded poorly with mapped faults. Seven lineaments were related to faults or fault systems but did not coincide well with individual traces. Seven lineaments correlated clearly and directly with mapped faults. In a few cases, the linear features better defined the faults than did the derived lineaments.

Lineament analysis provides a methodology to obtain structural information from satellite images. This information in turn may be used as exploration guides for hydrocarbons and mineral deposits.

REFERENCES

Briceno, H. O., and Lee, Keenan, 1984, Applications of Landsat images to geological mapping in a tropical jungle environment-Caroni River Basin, Venezuela, in Teleki, P., and Weber, C., eds., Remote Sensing for Geological Mapping, Orleans, France, 1984, Proceedings: International Union of Geological Sciences Publication 18, p. 161-175.

Lee, Keenan, 1983, Landsat analysis for uranium exploration in northeastern Turkey: U.S. Geological Survey Open-File Report 83-99, 18 p.

Perry, S. L., and Lee, Keenan, 1987, Lineaments of the Northern Denver Basin and their paleotectonic and hydrocarbon significance, in International Symposium on Remote Sensing of the Environment, 5th Thematic Conference, Remote Sensing for Exploration Geology, Reno, Nevada, 1986, Proceedings: Ann Arbor, Environmental Research Institute of Michigan, p. 335-346.

Sawatzky, D. L., and Lee, Keenan, 1974, New uses of shadow enhancement: Remote Sensing of Earth Resources, v. 3, p. 1-18.

Sawatzky, D. L., and Raines, G. L., 1981, Geologic uses of linear feature maps from small-scale images, in O'Leary, D. W., and Earle, J. L., eds., 3rd International Conference New Basement Tectonics, Proceedings: Denver, Basement Tectonics Committee, p. 91-100.

Scott, G. R., Taylor, R. B., Epis, R. C., and Wobus, R. A., 1978, Geologic map of the Pueblo 1° x 2° quadrangle, south-central Colorado: U.S. Geological Survey Miscellaneous Investigations Map I-1022, 1:250,000.

IMAGING SPECTROMETRY - AN INTRODUCTION

Fred A. Kruse
Center for the Study of Earth from Space (CSES)
Cooperative Institute for Research in Environmental Sciences (CIRES)
University of Colorado, Boulder

INTRODUCTION

Imaging spectrometry is "the simultaneous acquisition of images in many narrow, contiguous spectral bands" (Goetz and others, 1985). Analysis of imaging spectrometer data allows extraction of a detailed spectrum for each picture element (pixel) of the image (fig. 1). Broad-band remote sensing systems, such as the Landsat Multispectral Scanner (MSS) and Landsat Thematic Mapper (TM), drastically undersample the information content available from a reflectance spectrum (fig. 2). An imaging spectrometer, on the other hand, samples at close intervals and provides a spectrum that very much resembles one measured on a laboratory instrument (fig. 3).

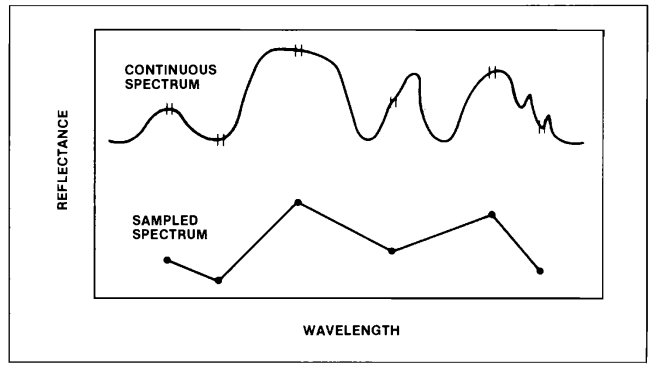

FIGURE 2 Effect of undersampling a spectrum (from Goetz, 1984). Double tick marks on continuous spectrum represent sample points.

BACKGROUND, RECENT RESEARCH RESULTS, AND FUTURE PLANS

The first imaging spectrometer was the Airborne Imaging Spectrometer (AIS), designed at the Jet Propulsion Laboratory and flown during the 1984 through 1986 flight seasons on NASA's C-130 aircraft. The AIS was an experimental instrument designed to test two-dimensional, near-infrared, area-array

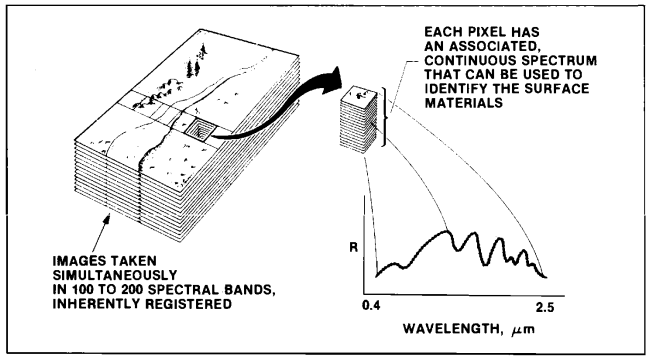

FIGURE 1 The imaging spectrometer concept (from Goetz, 1984).

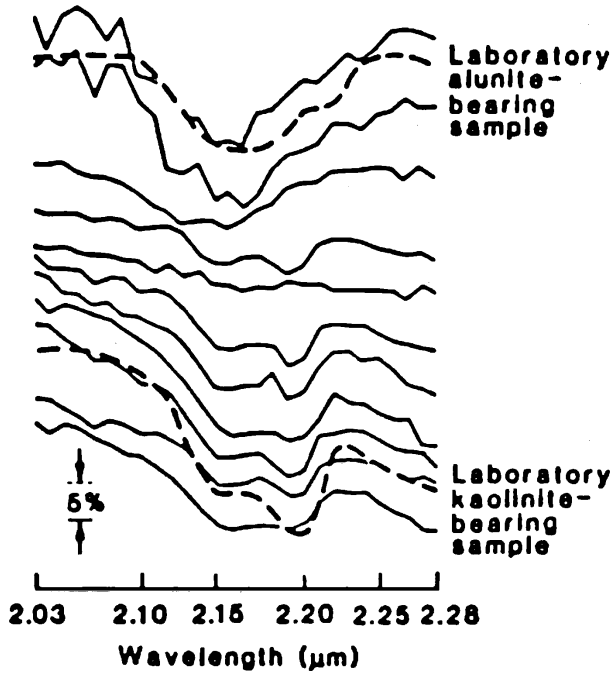

FIGURE 3 Examples of Airborne Imaging Spectrometer (AIS) spectra from Cuprite, Nevada (solid lines), compared with laboratory spectra for alunite and kaolinite (dashed lines) (after Goetz and others, 1985).

detectors. This instrument imaged 32 (AIS-1) or 64 (AIS-2) cross-track pixels simultaneously, collecting data in 128 contiguous, narrow channels (9.3 nm [AIS-1] or 10.6 nm [AIS-2]) from approximately 1.2 to 2.4 μm (Vane and others, 1983). The AIS detector was composed of a 32 X 32 or 64 X 64 area-array, HgCdTe detector sandwiched with a silicon, charge-coupled device multiplexer (Rode and others, 1982; Wellman and others, 1983; Goetz and others, 1985). The spectrometer was stepped through four (AIS-1) or two (AIS-2) grating positions in the time it took to advance one pixel on the ground in order to obtain the 128 spectral bands. Ground resolution was from about 10 m to 15 m, depending on flight altitude.

Several investigators have reported on the application of the data for characterization of mineral deposits or petroleum resources. Goetz and others (1985) identified and mapped the minerals kaolinite and alunite at Cuprite, Nevada (fig. 3). Kruse and others (1985a, 1985b, 1986) and Kruse (1987, 1988) identified areas of sericite (fine-grained muscovite) alteration and argillic alteration (montmorillonite) using the AIS-1 and AIS-2 instruments. Additionally, the AIS allowed identification and mapping of the minerals calcite and dolomite based upon differences in their near-infrared reflectance spectra. Hutinspiller and Taranik (1986) identified kaolinite and other clay minerals using AIS data at Virginia City, Nevada (the Comstock). Feldman and Taranik (1986) used AIS data to identify altered areas in volcanic terrain with kaolinite, montmorillonite, and illite. Lyon (1986, 1987) has successfully mapped both kaolinitic and sericitic alteration at Yerington, Nevada, with the AIS. Pieters and Mustard (1986, 1987), using the AIS to map mineral components associated with an ultramafic dike in Utah, were able to identify and spectrally unmix serpentine, gypsum, and clay-bearing components of the dike. Dykstra and Segal (1985) reported reasonable correlation between laboratory spectra and AIS spectra for studies at the Recluse oil field in Wyoming. Lang and others (1985, 1987) described "spectral stratigraphy" and improved lithologic mapping using the AIS data in combination with Thematic Mapper images for the Wind River/Bighorn basin area, Wyoming.

Several scientists reported preliminary results with the AIS in Australia (Huntington and others, 1986; Macklin and others, 1987), however, vegetation and instrument problems hindered these investigations. As exemplified by the Australian problems, few AIS studies were attempted in vegetated terrain. A geobotanical study by Milton and others (1986) at Pilot Mountain, North Carolina, however, suggests that variation between AIS spectra of vegetation may be useful for discriminating plant communities, and indirectly, lithologic variation.

The current Airborne Visible/Infrared Imaging Spectrometer (AVIRIS) is the second generation of imaging spectrometers. It is a 224-channel instrument utilizing the spectral range 0.41 to 2.45 μm in approximately 10 nm-wide bands (Porter and Enmark, 1987). The addition of the visible region of the spectrum will allow mapping of iron oxide mineralogy and likely will improve vegetation mapping capabilities. The AVIRIS is flown aboard the NASA U-2 and ER-2 aircraft at an altitude of 20 km, with an instantaneous field of view of 20 m and a swath width of about 10 km. It utilizes a linear array of discrete detectors and four individual spectrometers to collect data simultaneously for the 224 bands in a 614 pixel-wide swath perpendicular to the flight line. The second dimension of the image is provided by the forward motion of the aircraft, which moves the ground field of view of the array of 614 detectors along the terrain.

The AVIRIS was flown during 1987 and will be reflown during 1989; evaluation of the earlier data is underway. Preliminary geologic results have been reported by Vane (1987) for images of Cuprite, Nevada. The minerals kaolinite, alunite, and buddingtonite were successfully identified from spectra extracted from the AVIRIS data (fig. 4). Data were collected from about 20 sites in the United States, and investigators reported on the results of their investigations in June, 1988. One exciting geologic result is the identification of minerals containing rare earth elements (REE) associated with carbonatites at Mountain Pass, California (Rowan and others, 1988). Noise problems in the AVIRIS data limited the usefulness of most data obtained during the 1987 flight season. Data from AVIRIS flights during 1987 at Canon City and Cripple Creek, Colorado, were not useful for geologic mapping because of the signal-to-noise problems. Significant improvements have since been made, and we anticipate that the 1989 data will have better signal-to-noise characteristics that will allow mineralogical mapping at these sites.

A 64-channel imaging spectrometer developed by Geophysical Environmental Research (GER), flown during 1987 and 1988, is the first commercial instrument of its kind. The GER imaging spectrometer (GERIS) collects data from 0.43 to 2.5 μm in 64 channels of varying width. The 24 visible and infrared bands

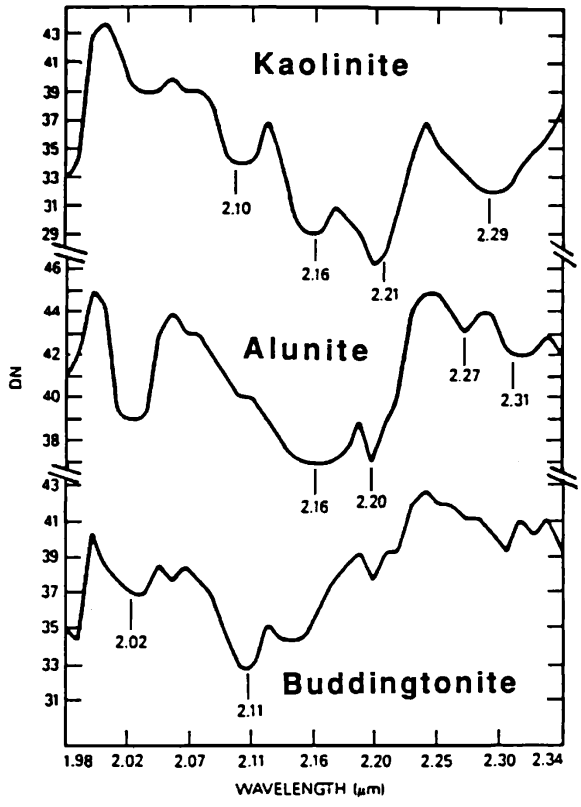

FIGURE 4 Single-pixel Airborne Visible/Infrared Imaging Spectrometer (AVIRIS) spectra from Cuprite, Nevada, for the minerals kaolinite, alunite, and buddingtonite (after Vane, 1987).

between 0.43 and 0.972 are 23 nm wide, the 8 bands in the infrared between 1.08 and 1.8 μm are 120 nm wide, and the 32 bands from 1.99 to 2.5 μm are 16 nm wide. First results from data flown at Cuprite, Nevada, are promising. Spectra have been extracted directly from the image data, and kaolinite, alunite, and buddingtonite have been successfully identified (Kruse and others, 1988). An example of an alunite spectrum extracted from the GER data is shown in figure 5, with a laboratory spectrum for comparison.

A satellite instrument called the High Resolution Imaging Spectrometer (HIRIS) will be launched around 1995 as part of the Earth Observing System (EOS), providing spectral measurements in 192 bands between 0.4 and 2.5 μm with a regional (30-50 km) field of view and a 30 m instantaneous field of view. Additionally, an instrument called the Moderate Resolution Imaging Spectrometer will provide an 1800 km swath with 1 km resolution and present new opportunities for synergism between a very high resolution instrument (HIRIS) and an instrument with repeat global coverage capabilities.

IMAGE PROCESSING

Analysis of imaging spectrometer data requires sophisticated image processing techniques. The first requirement is to calibrate wavelength accurately. Laboratory measurements of the instrument provide the initial wavelength calibration, and an additional check can be made by locating known atmospheric absorption features in the imaging spectrometer data. Atmospheric carbon dioxide absorption bands at 1.265, 1.575, 1.610, 2.005, and 2.055 μm and narrow atmospheric water vapor bands at 0.94 and 1.13 μm are useful for wavelength-calibration of the data in the infrared (Kneisyz and others, 1980; Vane, 1987). In the visible and photographic infrared portion of the spectrum, narrow atmospheric water bands at

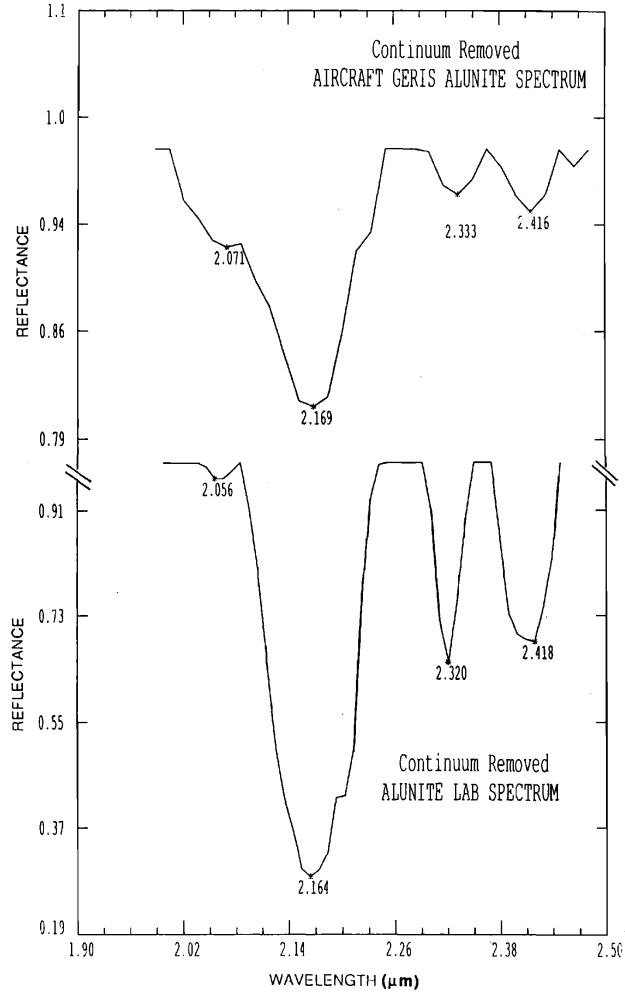

FIGURE 5 Comparison of GER imaging spectrometer spectrum of alunite at Cuprite, Nevada, with a laboratory spectrum of alunite.

0.69, 0.72, and 0.76 μm can be used to calibrate wavelengths.

Imaging spectrometer data often require cosmetic processing to remove instrument artifacts. Data-line dropout is a common problem with unprocessed (raw) data from these experimental sensors. The standard procedure is to replace the individual bad line with the pixel-by-pixel average of the two adjacent lines. Additionally, a pronounced striping pattern in the flightline direction often was observed in the AIS images. This pattern was caused by varying DC offsets in detectors. Procedures for removal of the striping are described in Dykstra and Segal (1985) and Kruse (1987, 1988).

Much of the variability in brightness (digital numbers or DN) in raw imaging spectrometer data can be attributed to illumination differences caused by topography and albedo differences between rock types. It is important to remove these differences to allow extraction of the spectral information. The "equal energy normalization" procedure (Jet Propulsion Laboratory, 1984, 1985) normalizes the data by scaling the sum of the DN's in each spectrum (each pixel) to a constant value. The effect of the normalization is to shift all the spectra to nearly the same overall relative brightness.

After albedo differences in the spectra are removed, the next step is to convert the data to reflectance so that individual spectra can be compared directly with laboratory data for mineral identification. Ideally the aircraft data would be calibrated to absolute reflectance, but this requires onboard calibration for each flight, which was not available for the AIS data. An alternative to onboard calibration is to use a standard area on the ground to calibrate the data (Roberts and others, 1985); however, this approach requires a prior knowledge of each site. Another approach is to use the properties of the data themselves to calculate an approximation of the reflectance. One such approximation, defined as "internal average relative (IAR) reflectance" (Kruse and others, 1985a, 1985b; Kruse, 1987, 1988), is calculated by determining an average spectrum for a single flightline or for all flightlines acquired on an individual mission. Each spectrum (pixel with n channels) in the flightline is then divided by the average spectrum. The resulting spectra represent reflectance relative to the average spectrum and resemble laboratory spectra acquired of the same materials. The IAR reflectance technique has the added advantage of effectively removing the majority of atmospheric effects, because the average spectrum contains contributions from the atmosphere. However, if the flight crosses an area that has wide variation in ground elevation or if the atmosphere is not uniform along the flightline, the global average will not completely remove the effects of the atmosphere. Also note that the average spectrum used to calculate the IAR reflectance spectrum may itself have spectral character related to mineral absorption features. This can adversely affect the appearance of the IAR reflectance spectra and limit their usefulness in comparisons with laboratory data. A technique similar to the IAR reflectance procedure (logarithmic residuals) has been successfully demonstrated by Green and Craig (1985) and Huntington and others (1986).

ANALYSIS AND DISPLAY

Derivation of a reflectance spectrum for each pixel of an image is only the first step. Once reflectance spectra have been obtained, then the sheer volume of the data requires that efficient algorithms for mineral identification be utilized to analyze the data. Several investigators are developing techniques for extraction of spectral information from imaging spectrometer data. One approach involves binary encoding and spectral matching using a reference library (Mazer and others, 1987). Another, more sophisticated approach relies on removal of a continuum from the data and automated extraction of spectral information (Green and Craig, 1985; Kruse and others, 1986; Kruse, 1987, 1988; Yamaguchi and Lyon, 1986; and Clark and others, 1987). Algorithms for identification of spectral mixtures and deconvolution of mixed spectra are being developed by Pieters and Mustard (1986, 1987, 1988) and Smith and Adams (1985).

Display of imaging spectrometer data is more complex than displaying three bands as an RGB color composite. The information present in the imaging spectrometer data simply cannot be fully displayed in one, or even 10, color images. A combination of spectral and spatial domains must be used to fully display the compositional information present in the data. One way of displaying some of the data is as color-coded, stacked spectra showing all the spectra for one pixel column along a flightline (Marsh and McKeon, 1983; Kruse and others, 1985a, 1985b; Kruse, 1987, 1988; Huntington and others, 1986). Another simple way to display part of the data is as a reflectance image for an

individual band. Individual spectra or groups of spectra may be plotted. Finally, automated extraction of pixels with specific spectral features or mineralogy can be used to produce a thematic map showing the distribution of individual minerals.

REFERENCES

Clark, R. N., King, T. V. V., and Gorelick, N. S., 1987, Automatic continuum analysis of reflectance spectra: in Proceedings, Third AIS Workshop, 2-4 June, 1987, JPL Publication 87-30, Jet Propulsion Laboratory, Pasadena, California, p. 138-142.

Dykstra, J. D., and Segal, D. B., 1985, Analysis of AIS data of the Recluse Oil Field, Recluse, Wyoming: in Proceedings, AIS Workshop, 8-10 April, 1985, JPL Publication 85-41, Jet Propulsion Laboratory, Pasadena, California, p. 86-91.

Feldman, Sandra, and Taranik, J. V., 1986, Identification of hydrothermal alteration assemblages using Airborne Imaging Spectrometer data: in Proceedings, 2nd Airborne Imaging Spectrometer (AIS) Data Analysis Workshop, 6-8 May, 1986, JPL Publication 86-35, Jet Propulsion Laboratory, Pasadena, California, p. 96-101.

Goetz, A. F. H., 1984, High spectral resolution remote sensing of the land: in Proceedings, Society of Photo-Optical Instrumentation Engineers, v. 475, Remote Sensing, p. 56-68.

Goetz, A. F. H., Vane, Gregg, Solomon, J. E., and Rock, B. N., 1985, Imaging spectrometry for earth remote sensing: Science, v. 228, p. 1147-1153.

Green, A. A., and Craig, M. D., 1985, Analysis of aircraft spectrometer data with logarithmic residuals: in Proceedings, AIS Workshop, 8-10 April, 1985, JPL Publication 85-41, Jet Propulsion Laboratory, Pasadena, California, p. 111-119.

Huntington, J. F., Green, A. A., and Craig, M. D., 1986, Preliminary Geological investigation of AIS Data at Mary Kathleen, Queensland, Australia: in Proceedings, 2nd Airborne Imaging Spectrometer (AIS) Data Analysis Workshop, 6-8 May, 1986, JPL Publication 86-35, Jet Propulsion Laboratory, Pasadena, California, p. 109-131.

Hutinspiller, Amy, and Taranik, J. V., 1986, Detection of hydrothermal alteration at Virginia City, Nevada, using Airborne Imaging Spectrometry (AIS): in Proceedings, 2nd Airborne Imaging Spectrometer (AIS) Data Analysis Workshop, 6-8 May, 1986, JPL Publication 86-35, Jet Propulsion Laboratory, Pasadena, California, p. 102-108.

Jet Propulsion Laboratory, 1984, Airborne Imaging Spectrometer, Science Investigator's Guide to AIS DATA: Jet Propulsion Laboratory, Pasadena, California, 15 p.

Jet Propulsion Laboratory, 1985, Airborne Imaging Spectrometer, Science Investigator's Guide to AIS DATA: Jet Propulsion Laboratory, Pasadena, California, 14 p.

Kneisyz, F. X., Shettle, E. P., Gallery, W. P., Chetwynd, J. H., Jr., Abreu, L. W., Selby, J. E. A., Fen, R. W., and McClatchey, R. A., 1980, Atmospheric transmittance/radiance: Computer Code LOWTRAN: AFCRL Environmental Research Paper No. 697, AFCRL-80-0067.

Kruse, F. A., Knepper, D. H., and Clark, R. N., 1986, Use of digital Munsell color space to assist interpretation of imaging spectrometer data -- Geologic examples from the northern Grapevine Mountains, California and Nevada: in Proceedings of the 2nd Airborne Imaging Spectrometer (AIS) Data Analysis Workshop, 6-8 May, 1986, JPL Publication 86-35, Jet Propulsion Laboratory, Pasadena, California, p. 132-137.

Kruse, F. A., Raines, G. L., and Watson, Kenneth, 1985a, Analytical techniques for extracting geologic information from multichannel airborne spectroradiometer and airborne imaging spectrometer data: in Proceedings, International Symposium on Remote Sensing of Environment, Fourth Thematic Conference, "Remote Sensing for Exploration Geology", San Francisco, California 1-4 April, 1985, Environmental Research Institute of Michigan, Ann Arbor, p. 309-324.

Kruse, F. A., Raines, G. L., and Watson, Kenneth, 1985b, Analytical techniques for extracting mineralogical information from multichannel airborne imaging spectrometer data (Abs.): in Proceedings, AIS Workshop, 8-10 April, 1985, JPL Publication 85-41, Jet Propulsion Laboratory, Pasadena, California, p. 105.

Kruse, F. A., 1987, Mapping hydrothermally altered rocks in the northern Grapevine Mountain, Nevada and California with the Airborne Imaging Spectrometer: in Proceedings, Third AIS Workshop, 2-4 June, 1987, JPL Publication 87-30, Jet Propulsion Laboratory, Pasadena, California, p. 148-166.

Kruse, F. A., 1988, Use of Airborne Imaging Spectrometer data to map minerals associated with hydrothermally altered rocks in the northern Grapevine Mountains, Nevada and California: Remote Sensing of Environment, v. 24, no. 1, p. 31-51.

Kruse, F. A., Calvin, W. M., and Seynec, Oliver, 1988, Automated extraction of absorption features from Airborne Visible/Infrared Imaging Spectrometer (AVIRIS) and Geophysical and Environmental Research Imaging Specrometer (GERIS) data: in Proceedings of the 1st AVIRIS Performance Evaluation Workshop, Jet Propulsion Laboratory (in press).

Lang, H. R., Paylor, E. D., and Adams, S., 1985, Remote stratigraphic analysis: Combined TM and AIS results in the Wind River/Bighorn basin area, Wyoming: in Proceedings, AIS Workshop, 8-10 April, 1985, JPL Publication 85-41, Jet Propulsion Laboratory, Pasadena, California, p. 32-34.

Lang, H. R., Adams, S. L., Conel, J. E., McGuffie, B. A., Paylor, E. D., and Walker, R. E., 1987, Multispectral remote sensing as stratigraphic tool, Wind River Basin and Big Horn Basin areas, Wyoming: American Association Petroleum Geologists Bulletin, v. 71, no. 4, p. 389-402.

Lyon, R. J. P., 1986, Comparison of the 1984 and 1985 AIS data over the Sigatse Range (Yerington), Nevada: in Proceedings, 2nd Airborne Imaging Spectrometer (AIS) Data Analysis Workshop, 6-8 May, 1986, JPL Publication 86-35, Jet Propulsion Laboratory, Pasadena, California, p. 86-95.

Lyon, R. J. P., 1987, Evaluation of AIS-2 (1986) data over hydrothermally altered granitoid rocks of the Singatse Range (Yerington) Nevada and comparison with 1985 AIS-1 data: in Proceedings, Third AIS Workshop, 2-4 June, 1987, JPL Publication 87-30, Jet Propulsion Laboratory, Pasadena, California, p. 107-119.

Macklin, Steve, Munday, Tim, and Hook, Simon, 1987, preliminary results from an investigation of AIS-1 data over an area of epithermal alteration: Plateau, Northern Queensland, Australia: in Proceedings, Third AIS Workshop, 2-4 June, 1987, JPL Publication 87-30, Jet Propulsion Laboratory, Pasadena, California, p. 120-131.

Marsh, S. E., and McKeon, J. B., 1983, Integrated analysis of high-resolution field and airborne spectroradiometer data for alteration mapping: Economic Geology, v. 78, no. 4, p. 618-632.

Mazer, A. S., Martin, M., Lee, M., and Solomon, 1987, Image processing software for imaging spectrometry: in Proceedings, 31st Annual International Technical Symposium, 16-21 August, 1987, Society of Photo-Optical Instrumentation Engineers, v. 834, p. 136-139.

Milton, N. M., Walsh, P. A., and Purdy, T. L., 1986, Geobotanical studies at Pilot Mountain, North Carolina, using the Airborne Imaging Spectrometer: in Proceedings, 2nd Airborne Imaging Spectrometer (AIS) Data Analysis Workshop, 6-8 May, 1986, JPL Publication 86-35, Jet Propulsion Laboratory, Pasadena, California, p. 162-170.

Pieters, C. M., and Mustard, J. F., 1986, Abundance and distribution of mineral components associated with Moses Rock (Kimberlite) diatreme: in Proceedings, 2nd Airborne Imaging Spectrometer (AIS) Data Analysis Workshop, 6-8 May, 1986, JPL Publication 86-35, Jet Propulsion Laboratory, Pasadena, California, p. 81-85.

Pieters, C. M., and Mustard, J. F., 1987, Abundance and distribution of ultramafic microbreccia in Moses Rock Dike: Quantitative application of mapping spectroscopy: Journal of Geophysical Research, v. 92, no. B10, p. 10376-10390.

Pieters, C. M., and Mustard, J. F., 1988, Exploration of crustal/mantle material for the Earth and Moon using reflectance spectroscopy: Remote Sensing of Environment, v. 24, no. 1, p. 151-178.

Porter, W. M., and Enmark, H. T., 1987, A system overview of the Airborne Visible/Infrared Imaging Spectrometer (AVIRIS): in Proceedings, 31st Annual International Technical Symposium, 16-21 August, 1987, Society of Photo-Optical Instrumentation Engineers, v. 834, p. 22-31.

Roberts, D. A., Yamaguchi, Y., and Lyon, R. J. P., 1985, Calibration of Airborne Imaging Spectrometer Data to percent reflectance using field spectral measurements: in Proceedings, Nineteenth International Symposium on Remote Sensing of Environment, Ann Arbor, Michigan, october 21-25, 1985.

Rode, J. P., Vural, K., Blackwell, J. D., Cox, F. A., and Lin, W. N., 1982, Characterization of a 32 X 32 HgCdTe focal plane: Proceedings of the IRIS Specialty Group on Infrared Detectors, San Diego, California.

Rowan, Larry, Crowley, James, and Meyer, David, 1988, Assessment of inflight performance over the Mountain Pass carbonatite, California: in Proceedings of the 1st AVIRIS Performance Evaluation Workshop, Jet Propulsion Laboratory (in press).

Smith, M. O., and Adams, J. B., 1985, Interpretation of AIS images of Cuprite, Nevada using constraints of spectral mixtures: in Proceedings, AIS Workshop, 8-10 April, 1985, JPL Publication 85-41, Jet Propulsion Laboratory, Pasadena, California, p. 62-67.

Vane, Gregg, Goetz, A. F. H., and Wellman, J. B., 1983, Airborne Imaging Spectrometer: A new tool for remote sensing: IEEE Transactions on Geoscience and Remote Sensing, v. GE-22, no. 6, p. 546-549.

Vane, Gregg, 1987, First results from Airborne Visible/Infrared Imaging Spectrometer (AVIRIS): in Proceedings, 31st Annual International Technical Symposium, 16-21 August, 1987, Society of Photo-Optical Instrumentation Engineers, v. 834, p. 166-174.

Wellman, J. B., Goetz, A. F. H., Herring, M., and Vane, Gregg, 1983, An imaging spectrometer experiment for the Shuttle: Proceedings 1983 International Geoscience and Remote Sensing Symposium (IGARS), IEEE cat. no. 83CH1837-4.

Yamaguchi, Yasushi, and Lyon, R. J. P., 1986, Identification of clay minerals by feature coding of near-infrared spectra: in Proceedings, International Symposium on Remote Sensing of Environment, Fifth Thematic Conference, "Remote Sensing for Exploration geology", Reno, Nevada, 29 September- 2 October, 1986, Environmental Research Institute of Michigan, Ann Arbor, p. 627-636.

REMOTE SENSING IN EXPLORATION GEOLOGY FIELD TRIP
DENVER - COLORADO SPRINGS - CANON CITY - ROYAL GORGE - CRIPPLE CREEK

Keenan Lee[1], Daniel H. Knepper, Jr.[2], and Fred A. Kruse[3]

0.0 START. DENVER intersection I-25 and US-6. Go south on I-25. Figure 1 shows route of field trip. [9.0 (distance in miles to the next point)]

9.0 Skyline to west shows late Eocene erosion surface, above which Pikes Peak (14,110 ft, 4,301 m), at 1 o'clock, rose as a monadnock. Mt. Evans, another of Colorado's "fourteeners", is at 3:30. [17.8]

26.8 Castle Rock, above town of same name, is capped by Oligocene Castle Rock Conglomerate, which rests on 36 Ma Wall Mountain Tuff, a rhyolite ash-flow tuff. This ash-flow tuff was important in deciphering the Tertiary tectonic history of the Front Range; its presence at Castle Rock demonstrates that the Front Range did not exist as a mountain range in early Oligocene time, since the source is in South Park, on the west side of the present Front Range. [19.2]

46.0 Monument Hill, elevation 7,352 ft (2,241 m), forms the divide between the north-flowing Platte River drainage and the south-flowing Arkansas River. [16.4]

62.4 Exit 146. Turn right (west) on Garden of the Gods road. [2.6]

65.0 Turn left (south) on 30th Street. [1.5]

66.5 Turn right (west) on Gateway Road. Ahead is the Garden of the Gods. [0.4]

66.9 Stop sign. Turn right (north) on scenic loop. This is the Gateway Rocks area. Main red rocks are Permian Lyons Sandstone, a fine grained, well sorted shoreline sandstone that has been tilted vertically and faulted during the Laramide orogeny. As the road turns south again, the stratigraphically lower red conglomerates of the Pennsylvanian and Permian Fountain Formation come into view. The contact is a vertical or slightly overturned fault. [0.8]

67.7 Stop sign. Turn left to the Hidden Inn. [0.1]

67.8 STOP 1A. Hidden Valley Trading Post. Scenic and rest stop. 30 minutes. Turn around, proceed to south. [0.4]

[1]Colorado School of Mines, Golden, Colorado and U.S. Geological Survey, Denver, Colorado
[2]U.S. Geological Survey, Denver, Colorado
[3]University of Colorado, Boulder, Colorado

Smith, M. O., and Adams, J. B., 1985, Interpretation of AIS images of Cuprite, Nevada using constraints of spectral mixtures: in Proceedings, AIS Workshop, 8-10 April, 1985, JPL Publication 85-41, Jet Propulsion Laboratory, Pasadena, California, p. 62-67.

Vane, Gregg, Goetz, A. F. H., and Wellman, J. B., 1983, Airborne Imaging Spectrometer: A new tool for remote sensing: IEEE Transactions on Geoscience and Remote Sensing, v. GE-22, no. 6, p. 546-549.

Vane, Gregg, 1987, First results from Airborne Visible/Infrared Imaging Spectrometer (AVIRIS): in Proceedings, 31st Annual International Technical Symposium, 16-21 August, 1987, Society of Photo-Optical Instrumentation Engineers, v. 834, p. 166-174.

Wellman, J. B., Goetz, A. F. H., Herring, M., and Vane, Gregg, 1983, An imaging spectrometer experiment for the Shuttle: Proceedings 1983 International Geoscience and Remote Sensing Symposium (IGARS), IEEE cat. no. 83CH1837-4.

Yamaguchi, Yasushi, and Lyon, R. J. P., 1986, Identification of clay minerals by feature coding of near-infrared spectra: in Proceedings, International Symposium on Remote Sensing of Environment, Fifth Thematic Conference, "Remote Sensing for Exploration geology", Reno, Nevada, 29 September- 2 October, 1986, Environmental Research Institute of Michigan, Ann Arbor, p. 627-636.

REMOTE SENSING IN EXPLORATION GEOLOGY FIELD TRIP
DENVER - COLORADO SPRINGS - CANON CITY - ROYAL GORGE - CRIPPLE CREEK

Keenan Lee[1], Daniel H. Knepper, Jr.[2], and Fred A. Kruse[3]

0.0 START. DENVER intersection I-25 and US-6. Go south on I-25. Figure 1 shows route of field trip. [9.0 (distance in miles to the next point)]

9.0 Skyline to west shows late Eocene erosion surface, above which Pikes Peak (14,110 ft, 4,301 m), at 1 o'clock, rose as a monadnock. Mt. Evans, another of Colorado's "fourteeners", is at 3:30. [17.8]

26.8 Castle Rock, above town of same name, is capped by Oligocene Castle Rock Conglomerate, which rests on 36 Ma Wall Mountain Tuff, a rhyolite ash-flow tuff. This ash-flow tuff was important in deciphering the Tertiary tectonic history of the Front Range; its presence at Castle Rock demonstrates that the Front Range did not exist as a mountain range in early Oligocene time, since the source is in South Park, on the west side of the present Front Range. [19.2]

46.0 Monument Hill, elevation 7,352 ft (2,241 m), forms the divide between the north-flowing Platte River drainage and the south-flowing Arkansas River. [16.4]

62.4 Exit 146. Turn right (west) on Garden of the Gods road. [2.6]

65.0 Turn left (south) on 30th Street. [1.5]

66.5 Turn right (west) on Gateway Road. Ahead is the Garden of the Gods. [0.4]

66.9 Stop sign. Turn right (north) on scenic loop. This is the Gateway Rocks area. Main red rocks are Permian Lyons Sandstone, a fine grained, well sorted shoreline sandstone that has been tilted vertically and faulted during the Laramide orogeny. As the road turns south again, the stratigraphically lower red conglomerates of the Pennsylvanian and Permian Fountain Formation come into view. The contact is a vertical or slightly overturned fault. [0.8]

67.7 Stop sign. Turn left to the Hidden Inn. [0.1]

67.8 STOP 1A. Hidden Valley Trading Post. Scenic and rest stop. 30 minutes. Turn around, proceed to south. [0.4]

[1]Colorado School of Mines, Golden, Colorado and U.S. Geological Survey, Denver, Colorado
[2]U.S. Geological Survey, Denver, Colorado
[3]University of Colorado, Boulder, Colorado

68.2 Take left fork. [1.0]

69.2 STOP 1B. Ridge Road High Point. Camera obscura, the oldest remote sensing imaging system known. Unique opportunity to walk inside one of these forerunners of our modern cameras. Proceed southward. [0.8]

70.0 Turn left (east) on US-24. [3.1]

73.1 Turn right (south) on I-25. [1.1]

74.2 Exit 140. Turn right (south) on Colo-115. [9.4]

83.6 To the right (west) are vertical beds of Cretaceous Dakota Fm. and Lyons Sandstone where they emerge from beneath the Cheyenne Mtn. reverse fault (see geologic map in Lee, this publication, figure 3). Cheyenne Mtn. is composed of Middle Proterozoic Pikes Peak Granite thrust 4000-8000 ft (1200-2400 m) over sedimentary rocks, mostly Cretaceous Pierre Shale (see stratigraphic section in Lee, this publication, figure 4). [3.4]

87.0 Fountain sandstones and conglomerates in road cuts. These red beds stand out as bright yellow-green on MSS and TM color-IR images. [6.7]

93.7 Crest of the Red Creek arch, a broad anticline plunging southeast off the south end of the Front Range, separating the Denver basin from the Canon City embayment to the southwest. [7.7]

101.4 STOP 2. Overview of the Canon City embayment with Wet Mountains on the skyline, the basin in front of them, the plains to the southeast, the Cretaceous sedimentary rocks ahead dipping into the basin, and the Precambrian gneiss of the Front Range to the right. [6.1]

107.5 Turn right (west) on U.S.-50. Road over Quaternary pediment gravels on Pierre Shale. Road crosses several gentle folds of the Canon City structural embayment. [8.9]

116.4 Enter Canon City, which bills itself as the "Climate Capitol of Colorado". [3.1]

119.5 Mouth of Arkansas River Canyon (Royal Gorge) on left. Ahead Fountain Formation underlies valley, Dakota Sandstone forms ridge on right, and Ordovician Manitou Formation, Harding Sandstone, and Fremont Limestone form the slopes on the left. [7.3]

126.8 Turn left (south) on Fremont County 3A. [4.3]

131.1 STOP 3. Royal Gorge. Canyon cut into Early Proterozoic rocks, here migmatitic gneisses. Fairly flat surface on both sides of canyon is an exhumed and slightly eroded surface that beveled ancestral Rocky Mountains in late Paleozoic and early Mesozoic time. Royal Gorge drainage probably was superposed onto Precambrian rocks during Laramide arching and formed a shallow drainage on the late Eocene erosion surface. The downcutting occurred during Neogene to Quaternary uplift that has averaged about 50 m/my. Scott's (1975) figures for Clear Creek near Golden show downcutting rates of about 13 m/my for Miocene, 42 m/my for Pliocene, and 75 m/my for Quaternary. (Are we approaching the climax of the Neoquat orogeny?) The Royal Gorge bridge is 321.6 m (1055 ft) above the Arkansas River. Turn around. [4.3]

135.4 Turn left (west) on U.S.-50. [1.2]

136.6 Turn right (north) on Colo-9. [2.7]

139.3 Pierre Shale underlies valley in a complexly faulted graben. Mountains to left, right and ahead are upthrust Precambrian plutonic rocks. Vertical Dakota Sandstone beds to right along flanking thrust faults. Currant Creek fault system extends beyond the image in figure 1; total length from South Park through Wet Mtns. more than 140 km. Demonstrable Neogene movement (Taylor, 1975). [5.9]

145.2 Turn right (east) on Fremont County-11. [3.6]

148.8 Crossing the unconformity that represents a late Eocene erosion surface. Oligocene Tallahassee Creek Conglomerate lies on weathered Cripple Creek Quartz Monzonite. The significance of this late Eocene surface (LES) has only recently been recognized, but its existence forced reinterpretation of Cenozoic tectonism. With a widespread extent of probably more than 10,000 km^2 (Epis and Chapin, 1975), it indicates that our present Rocky Mountains (the fourth generation) are quite young. [0.5]

149.3 Sharp right bend in road as it emerges onto a low-relief upland surface that approximates the LES. Here the surface is covered with a thin veneer of Tallahassee Creek Conglomerate; to the north, Oligocene Thirtynine Mile Andesite lies on the LES. We will be traveling on the LES until tomorrow midday. Major elevation changes during this time will represent block faulting offsets from Neogene to Quaternary orogeny. The LES is readily mapped in this area on Landsat

images by its textural and color characteristics. Pikes Peak on skyline to the northeast. [1.9]

153.8 Descending into High Park. Bare Hills ahead (11:30 through 3 o'clock) are a relatively thick pile of Tallahassee Creek Conglomerate, with some Thirtynine Mile Andesite and a few knobs of phonolite. This conglomerate and the Echo Park Alluvium are host rocks for uranium mineralization. [3.3]

157.1 View ahead to the northeast shows the approximate LES of High Park in the lower foreground. Mount Pisgah, the volcano-shaped hill on the skyline immediately left of Pikes Peak, rests on the LES in the Cripple Creek area. The Cripple Creek block has been uplifted about 1500 ft relative to High Park. [1.9]

159.0 Wall Mountain Tuff to right, a rhyolite ash flow tuff, is important because it marks the onset of volcanism in earliest Oligocene time, preserves and dates the regional post-Laramide erosion surface, and serves as a datum for determining the location and magnitude of middle to late Cenozoic block faulting. [5.0]

164.0 Turn right (north), still on Teller County-11. [4.2]

168.2 Turn left (north) on Teller County-1. [4.4]

172.6 Low divide between south-flowing Four-Mile Creek and north-flowing Four-Mile Creek is composed of Oligocene lahars and lavas that dammed ancestral Four-Mile Creek to form lake Florissant, in which the famous lake beds accumulated. [2.3]

174.9 Turn left (west). [0.1]

175.0 STOP 4. Florissant Fossil Beds National Monument. The deposits consist dominantly of volcanic detritus and are less than 150 ft (45.9 m) thick. Tuffaceous shales and mudstones, near the middle of the sequence, contain most of the delicately preserved fossil plant and insect remains; andesitic tuffs and mudflows underlying them preserve petrified stumps and logs of giant Sequoia trees. The sediments and their enclosed flora and fauna indicate that ancient lake Florissant existed under climatic conditions that were warm, perhaps even subtropical. K/Ar age determinations indicate the lake existed during early Oligocene time, about 34 Ma. Turn around. [0.1]

175.1 Turn right (south) on Teller County-1. [6.7]

181.8 Intersection Teller County-1 and Teller County-11. Continue straight toward Cripple Creek. [0.8]

182.6 Leave volcanics and enter Pikes Peak Granite. The road up the valley ahead follows the contact (fault?) between the Cripple Creek Quartz Monzonite (1.4 Ga), on the right, and the Pikes Peak Granite (1.0 Ga), on the left. [6.1]

188.7 Cross Long Hungry Gulch. The heritage of place names in the Cripple Creek area reflects a geologic overprint (Rhyolite Mountain, Carbonate Hill, Trachyte Knob) onto the miners' boom-or-bust attitudes of eternal optimism (Gold Hill, Galena Hill, Copper Mtn., Beacon Hill, Rosebud Hill - note: all highs) and, probably all too frequently, harsh realism (Poverty Gulch, Cripple Creek, Dead Ox Gulch, Long Hungry Gulch - all lows). [0.9]

189.6 Cripple Creek city limits. Elevation 9495 ft. See fig. 2 for geologic sketchmap and route through Cripple Creek-Victor mining district. At first intersection, turn right, go one block, turn left onto Bennett Avenue, the main street of Cripple Creek. [0.7]

190.3 Stop sign at intersection of Bennett Ave. and 2nd St. Continue straight ahead through town on Colo-67. [2.5]

192.8 Turn sharp right (south) on Teller County-41, Range View Road. [0.3]

193.1 STOP 5. Observation point with overview of Cripple Creek. Cripple Creek was founded in 1891, shortly after Bob Womack discovered gold along Poverty Gulch in October of 1890. Peak production and population occurred in 1900, when the district population was greater than 50,000 and Cripple Creek had more than 25,000 residents. 1980 census showed 641 residents. Most of the buildings now remaining were built immediately after the fires of April 1896 destroyed most of the city. In 1901, Cripple Creek boasted 41 first class hotels. Panoramic view counter-clockwise from north: open basin of South Park with Mosquito and Sawatch ranges on horizon; landmark Mt. Pisgah due west not quite up to horizon; long benches of Thirtynine Mile volcanic field in middle ground; peaks of Sangre de Cristo Range, notched by Hayden Pass just above Bare Hills and High Park; left of Sangres are Wet Mtns. In

immediate foreground are headwaters of Cripple Creek, from the gentle slopes of Mineral Hill, to right of Mt. Pisgah, down which turquoise washes into Cripple Creek gutters, around to Poverty Gulch just to south, where Bob Womack sank the first shaft at the El Paso discovery. Limonite mapping on Landsat images delineates well the mineralized area of mining district (see Lee, this publ.). [0.8]

193.9 Turn sharp right (west). [0.8]

194.7 Turn left (south) on Colo-67 at Molly Kathleen gold mine, back to town. [1.7]

196.4 The Imperial Hotel, a half block north of Bennett Avenue on 3rd Street, is the only one of Cripple Creek's original hotels still standing. It was built in 1896, shortly after the disasterous fires that destroyed much of the original town. With the exception of two years during World War II it has been in continuous operation. Much of the guest-room furniture is of 1900 vintage (with the exception of modern springs and mattresses on beds). The hotel is famous for summer performances of serious melodrama.

END OF DAY 1.

Day 2

0.0 Intersection of Bennett Ave. and 2nd Street. Proceed south on Colo-67 toward Victor. [2.1]

2.1 STOP 1 Anaconda townsite. Contact of Cripple Creek Quartz Monzonite breccia and tuff at Cripple Creek (Tbt, fig. 2). Hydrothermal alteration of both rocks makes recognition of contact difficult, and the contact is complex. The Cripple Creek district is a gold-silver district with ore minerals deposited within or along the borders of a mass of Tertiary breccia and tuff dropped down into Precambrian rocks. The main Cripple Creek volcanics are in an elliptical structure trending northwest, two miles wide and about four miles long, with the city of Cripple Creek on the northwest and Victor on the south (see fig. 2). The breccia-Precambrian contact is complex, but generally dips steeply inward. The structure has been described as a crater, caldera, basin, and volcanic subsidence structure. The breccia mass is primarily latite-phonolite and phonolite breccia, but substantial quantities of tuff, arkosic sandstone, conglomerate, and mudstones (with fossil leaves and logs) are also found within

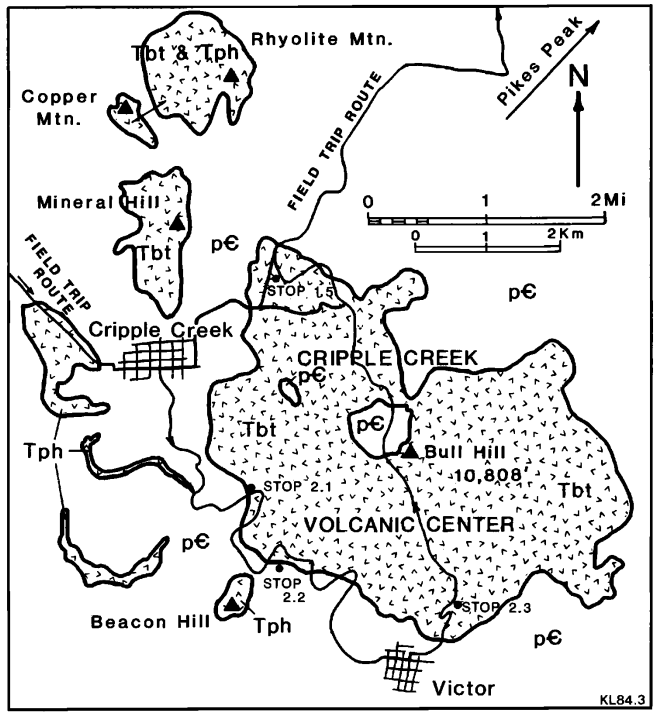

FIGURE 2 Cripple Creek - Victor area with generalized geology and field trip route. Tbt, tuff and breccia at Cripple Creek; Tph, phonolite; pЄ, undifferentiated Precambrian plutonic and metamorphic rocks.

the structure, and much of the volcanic breccia itself shows sorting and stratification. Koschmann (1947) suggests the structure was subsiding before and during Oligocene to Miocene volcanism along steep faults with a dominant northwest trend.

Most of the ore deposits occur as veins, with some small irregular masses and at least one pipelike rubble mass (the Cresson "blowout"). Vein deposits are concentrated around the edge of the breccia and near intrusions within the breccia pile, with some veins extending as much as 2000 ft (600 m) into the Precambrian rocks. Veins characteristically occur as short individual veins in long, narrow zones, perhaps reflecting deeper fissure control (Koschmann, 1947). Primary ore minerals are gold-silver-tellurides (calaverite, sylvanite, krennerite, petzite, and hessite) in a gangue of quartz, dolomite, fluorite, and pyrite. The gold:silver ratio is about 10:1, with free gold found only where the tellurides have been oxidized. Ore solutions originated below the roots of the breccia mass, and three or four

phases of hydrothermal solutions passed upward and outward (Loughlin and Koschmann, 1935). Alteration extends beyond the ore zones, with Precambrian rocks showing less alteration than breccias. Sodium minerals show potassic alteration. Volcanic groundmass shows sericitic alteration, and plagioclase phenocrysts have altered to clay. Although there is no alteration zonation defined, there has been considerable overprinting (J. Lufkin, 1984, oral communication). Areas of greatest potassic alteration conform well with high concentrations of gold, silver, tellurium and iron (Gott and others, 1969).

Major mining activity peaked in 1900, with production that year of 878,000 ounces of gold. Cumulative production is about 20 million ounces of gold and 2 million ounces of silver. Mining declined from 1900 to 1933, when the gold price was raised from $20.67 to $35 per ounce. Some mines reopened in early 1934, and activity was about to increase when the Carlton deep drainage tunnel was finished in 1941, but the war effort in 1942 closed most mines. When gold prices rose following deregulation in 1964, increased activity, but little production, followed. Today's ore deposits are yesterday's tailings piles, as most activity is directed toward gold extraction by heap leaching old mine dump material. [1.5]

3.6 STOP 2. Carlton Mill of Cripple Creek and Victor Gold Mining Company, operated by Texas Gulf, which holds the rights to most of the land in the district. Current (1988) activities concentrate on heap leaching. Brief tour of operation. [2.0]

5.6 Enter Victor, Colorado. Elevation 9,693. Victor was founded in 1893 as gold mining extended southward from Cripple Creek. Called the "City of Mines" partly because of extensive mining when gold veins were found to extend under the city itself. Most of city was destroyed by fire of 1899, but was immediately rebuilt. Population peaked in 1900 at 12,000; 1980 residents numbered 266, not including town's donkeys. Roadsign proclaims Lowell Thomas's birth, but not Jack Dempsey's first fight at the Gold Coin Club. Continue 1 1/2 blocks past city hall. [0.4]

6.0 Turn left (north), go one block, turn right, go 1 1/2 blocks. [0.2]

6.2 Turn left (north) onto Range View Road. [0.8]

7.0 STOP 3. Road to Ajax mine. Discussion of imaging spectrometry and AVIRIS imaging of Cripple Creek-Victor mining district. [1.6]

8.6 PHOTO STOP. Brief stop for picture taking. Vista very similar to yesterday's last stop at Tenderfoot Hill, but with front lighting. Observation point at 10,500 ft (3,200 m). Bull Hill to right is high point of area at 10,808 ft (3,294 m). Conifers are mostly bristlecone pine (Pinus aristata, aka foxtail pine), with subordinate Engelmann spruce (Picea engelmannii) and quaking aspen (Populus tremuloides). [1.4]

10.0 View of Pikes Peak at 2 o'clock. Valleys on southwest side of Pikes Peak were glaciated during Wisconsinan, showing well developed Bull Lake and Pinedale end moraines. [0.2]

10.2 Take right fork. [1.0]

11.2 Rejoin Colo-67. Turn right. Contact of volcanics and Pikes Peak Granite. [2.4]

13.6 View ahead of end moraine of Bull Lake glaciation. Boulders strewn across flood plain ahead were carried by catastrophic stream flow resulting from breaching of earth dam in terminal moraine (Holocene outwash?). [3.4]

17.0 Enter old railroad tunnel. Road follows old railroad bed for most of distance from Cripple Creek to Divide. This was one of three railroads serving Cripple Creek and Victor. The others came up Phantom Canyon from Florence, and up the Corley Mountain Highway (Gold Camp Road) from Colorado Springs. [6.5]

23.5 Roadcuts in gravel at Divide. These deposits are well discriminated on Landsat images. [2.8]

26.3 Turn right (east) on US-24. [4.2]

30.5 View at 10:00 of Devil's Head, which stands above the late Eocene surface on Rampart Range and is composed of Pikes Peak Granite; grassy area in foreground is gravel at Divide. Highway is on gravel at Divide, following the approximate paleochannel. Gravel ahead descends to about 8600 ft (2,600 m) elevation. Directly ahead is a patch of Divide gravel on the Rampart Range LES, which is in the paleodownstream direction, that is at about 9400 ft (2,865 m), indicating nearly 1000 ft (305 m) of Neogene to Quaternary offset on the Ute Pass fault. [2.6]

33.1 Woodland Park, elevation 8465. Continue through town on US-24. [7.4]

40.5 Bust, Colo. Alternative to Pikes Peak. [5.0]

45.5 View of unconformity between Sawatch Sandstone (Cambrian) and Pikes Peak Granite on both sides of highway. Sawatch dips steeply off southeast flank of Rampart Range into Manitou embayment. In the next five miles (8 km), road goes stratigraphically upward through steeply dipping sedimentary section from Cambrian to Cretaceous. [5.6]

51.1 Turn left (north) on I-25. [67.8]

118.9 I-25 and US-6. Beginning point of road log. End of road log.

Acknowledgment: Parts of road log are modified from Epis and others (1976).

REFERENCES

Epis, R. C., and Chapin, C. E., 1975, Geomorphic and tectonic implications of the post-Laramide, late Eocene erosion surface in the Southern Rocky Mountains, in Curtis, B. F., ed., Cenozoic history of the Southern Rocky Mountains: Geological Society of America Memoir 144, p. 45-74.

Epis, R. C., Scott, G. R., Taylor, R. B., and Sharp, W. N., 1976, Petrologic, tectonic, and geomorphic features of central Colorado, in Epis, R. W., and Weimer, R. J., eds., Studies in Colorado field geology: Colorado School of Mines Professional Contribution 8, p. 301-322.

Gott, G. B., McCarthy, J. H., Jr., Van Sickle, G. H., and McHugh, J. B., 1969, Distribution of gold and other metals in the Cripple Creek District, Colorado: U.S. Geological Survey Professional Paper 625-A, 17 p.

Koschmann, A. H., 1947, Structural control of the gold deposits of the Cripple Creek District, Teller County, Colorado: U.S. Geological Survey Bulletin 955-B, 60 p.

Loughlin, G. F., and Koschmann, A. H., 1935, Geology and ore deposits of the Cripple Creek District, Colorado: Colorado Scientific Society Proceedings, v. 13, no. 6, p. 217-435.

Scott, G. R., 1975, Cenozoic surfaces and deposits in the Southern Rocky Mountains, in Curtis, B. F., ed., Cenozoic history of the Southern Rocky Mountains: Geological Society of America Memoir 144, p. 227-248.

Taylor, R. B., 1975, Neogene tectonism in south-central Colorado, in Curtis, B. F., ed., Cenozoic history of the Southern Rocky Mountains: Geological Society of America Memoir 144, p. 211-226.

REMOTE SENSING APPLIED TO HYDROCARBON EXPLORATION IN THE DENVER/JULESBURG BASIN, COLORADO

Ronald W. Marrs
Department of Geology and Geophysics, University of Wyoming, Laramie

INTRODUCTION

Remote sensing is used routinely for geologic mapping and structural analysis in many petroleum provinces around the world. The regional coverage provided by Landsat, SPOT, and other global imaging systems gives us a better perspective of sedimentary basins, overthrust belts, and other petroleum provinces. This new view is particularly effective for developing regional syntheses. Both the synoptic view and the expanded spectral capabilities of these new systems have wide application for "basin analysis" and hydrocarbon exploration. This paper reviews those applications that are most appropriate for exploration in the Denver/Julesburg (DJ) basin and similar areas.

GEOLOGIC SETTING

The DJ basin lies on the extreme eastern edge of the Rocky Mountain Foreland Basins province (fig. 1). It is asymmetric to the west; and the deepest part, which lies very near the Colorado Front Range, is filled with some 4000 meters of Paleozoic through Tertiary sedimentary rocks. The Colorado Front Range was thrust over the western margin of the basin along the Golden fault.

33.1 Woodland Park, elevation 8465. Continue through town on US-24. [7.4]

40.5 Bust, Colo. Alternative to Pikes Peak. [5.0]

45.5 View of unconformity between Sawatch Sandstone (Cambrian) and Pikes Peak Granite on both sides of highway. Sawatch dips steeply off southeast flank of Rampart Range into Manitou embayment. In the next five miles (8 km), road goes stratigraphically upward through steeply dipping sedimentary section from Cambrian to Cretaceous. [5.6]

51.1 Turn left (north) on I-25. [67.8]

118.9 I-25 and US-6. Beginning point of road log. End of road log.

Acknowledgment: Parts of road log are modified from Epis and others (1976).

REFERENCES

Epis, R. C., and Chapin, C. E., 1975, Geomorphic and tectonic implications of the post-Laramide, late Eocene erosion surface in the Southern Rocky Mountains, in Curtis, B. F., ed., Cenozoic history of the Southern Rocky Mountains: Geological Society of America Memoir 144, p. 45-74.

Epis, R. C., Scott, G. R., Taylor, R. B., and Sharp, W. N., 1976, Petrologic, tectonic, and geomorphic features of central Colorado, in Epis, R. W., and Weimer, R. J., eds., Studies in Colorado field geology: Colorado School of Mines Professional Contribution 8, p. 301-322.

Gott, G. B., McCarthy, J. H., Jr., Van Sickle, G. H., and McHugh, J. B., 1969, Distribution of gold and other metals in the Cripple Creek District, Colorado: U.S. Geological Survey Professional Paper 625-A, 17 p.

Koschmann, A. H., 1947, Structural control of the gold deposits of the Cripple Creek District, Teller County, Colorado: U.S. Geological Survey Bulletin 955-B, 60 p.

Loughlin, G. F., and Koschmann, A. H., 1935, Geology and ore deposits of the Cripple Creek District, Colorado: Colorado Scientific Society Proceedings, v. 13, no. 6, p. 217-435.

Scott, G. R., 1975, Cenozoic surfaces and deposits in the Southern Rocky Mountains, in Curtis, B. F., ed., Cenozoic history of the Southern Rocky Mountains: Geological Society of America Memoir 144, p. 227-248.

Taylor, R. B., 1975, Neogene tectonism in south-central Colorado, in Curtis, B. F., ed., Cenozoic history of the Southern Rocky Mountains: Geological Society of America Memoir 144, p. 211-226.

REMOTE SENSING APPLIED TO HYDROCARBON EXPLORATION IN THE DENVER/JULESBURG BASIN, COLORADO

Ronald W. Marrs
Department of Geology and Geophysics, University of Wyoming, Laramie

INTRODUCTION

Remote sensing is used routinely for geologic mapping and structural analysis in many petroleum provinces around the world. The regional coverage provided by Landsat, SPOT, and other global imaging systems gives us a better perspective of sedimentary basins, overthrust belts, and other petroleum provinces. This new view is particularly effective for developing regional syntheses. Both the synoptic view and the expanded spectral capabilities of these new systems have wide application for "basin analysis" and hydrocarbon exploration. This paper reviews those applications that are most appropriate for exploration in the Denver/Julesburg (DJ) basin and similar areas.

GEOLOGIC SETTING

The DJ basin lies on the extreme eastern edge of the Rocky Mountain Foreland Basins province (fig. 1). It is asymmetric to the west; and the deepest part, which lies very near the Colorado Front Range, is filled with some 4000 meters of Paleozoic through Tertiary sedimentary rocks. The Colorado Front Range was thrust over the western margin of the basin along the Golden fault.

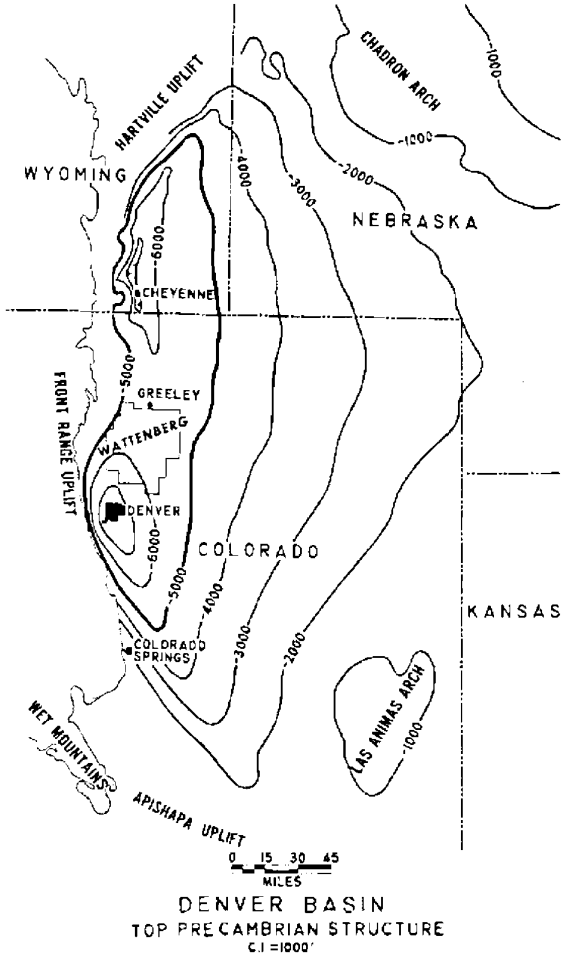

FIGURE 1 Denver-Julesburg basin showing structure contours on the Precambrian surface and the Wattenberg oil and gas field (from Matuszczak, 1973).

Sedimentary units are overturned or dip steeply basinward on the west side of the basin, but dips are relatively shallow around the other margins of the DJ basin. The stratigraphic sequence consists of cyclic marine, shoreline, and continental sediments associated with shallow seas that repeatedly transgressed across the area in response to regional tectonism. This sequence comprises an impressive array of petroleum source rocks and reservoir sandstones (Fig. 2).

More than 800 petroleum fields with cumulative production and reserves estimated to be in excess of 700MM bbl have been discovered in the DJ basin (Pruitt, 1978). Production is from basin-flank folds and from stratigraphic traps. The chief petroleum source rocks are thick Cretaceous shales. Reservoir units are typically fluvial channel or deltaic sandstones (Weimer, 1978, 1980), eolian or shoreline sandstone bodies, or porous chalks and fractured carbonates. Historically, the structural traps have been easier to find, but the stratigraphic traps are frequently larger. Exploration methods that can effectively locate fractures associated with buried structures or tectonic boundaries that control depositional patterns are becoming increasingly important to petroleum interests in the DJ basin.

REMOTE SENSING TECHNIQUES

Several remote sensing techniques have proven useful in regional evaluations. The seven-channel Landsat Thematic Mapper (TM) is particularly effective for regional lithologic mapping, because in addition to visible and near-infrared spectral bands that have long been available from the Landsat Multispectral Scanner (MSS), the TM mid-infrared data provide information on sand/shale ratios. Multispectral image interpretations are normally quite effective for rock, soil, and vegetation discrimination. In contrast, high spatial resolution is the pre-requisite for structural and geomorphic analysis and for detailed evaluation of individual prospect areas. The necessary resolution may be provided by aerial photography or by high-resolution satellite systems, such as SPOT (10-meter resolution), the Space Shuttle Large-Format Camera (SSLFC), or from a synthetic aperture radar system. Stereoscopic presentation and large area coverage are also extremely important for geologic analysis. So, the ideal geologic remote sensing system would have high spectral definition over a broad range (visible to thermal infrared or beyond), 5- to 10-meter spatial resolution across a large area, and stereoscopic coverage on a seasonal basis. Such a system does not yet exist, but data are available from several systems that meet one or more of these requirements.

Prior to interpretation of the imagery, it is generally advisable to apply corrections and enhancements. The images often contain both geometric and radiometric distortions that should be removed (corrections may include destriping, restoration of lost data values, skew correction, rotation, atmospheric correction, scaling, etc.). If it is desirable to match the imagery to a map base, it may be necessary to mosaic several images and/or to apply an appropriate geometric correction to obtain the desired map projection. Structural and geomorphic detail may be improved by applying high-pass frequency filters or other edge-enhancement routines. Spectral processing may be applied

RELATION OF DEPOSITIONAL SEQUENCES TO ROCKY MOUNTAIN OIL & GAS OCCURRENCE

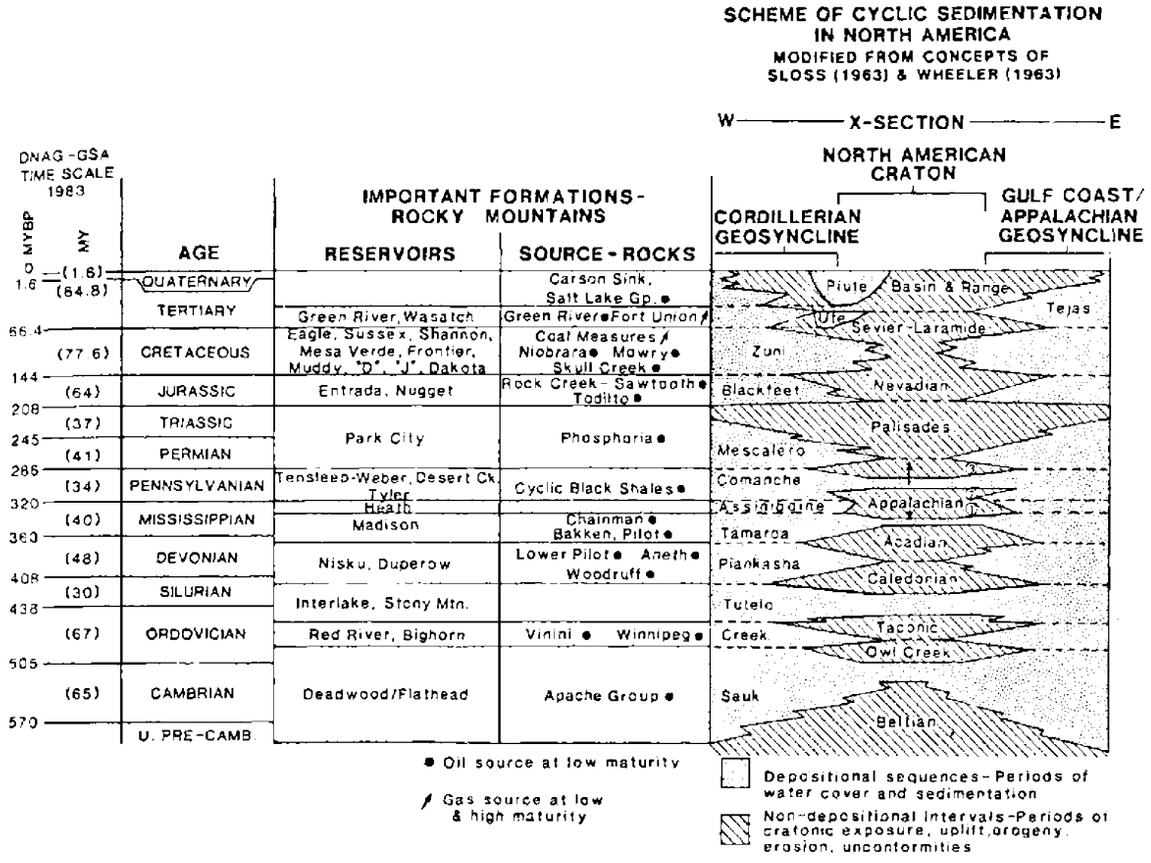

FIGURE 2 Stratigraphic chart keyed to major depositional sequences and the occurrence of reservoirs and source rocks in the Rocky Mountain region (from Meissner and others, 1984).

to condense the information from numerous bands into a single color composite scene and to enhance subtle spectral contrasts. Important algorithms for this type of enhancement compute band ratios, principal components, or other spectral space transformations, and then combine the results into color images.

Application of remote sensing to hydrocarbon exploration usually begins with a geomorphic analysis in which drainage patterns are carefully mapped throughout the region using high-resolution stereoscopic imagery. Unusual circular patterns, radial drainages, aligned offsets, gradient changes, or any peculiar variation from the more typical pattern may serve as an indicator of structure (Elliot, 1958; Berger, 1982). Because the development of landforms is strongly influenced by the lithologic substrata, geomorphic analysis is an aid to lithologic mapping. Statistical analysis of drainage trends or other geomorphic patterns may also prove useful in identifying tectonic lineaments or other regional patterns obscured by younger rocks and soils (Marrs and Raines, 1984; Weimer, 1980).

After careful analysis of geomorphic patterns, it is important to develop a good outcrop map, usually by interpreting enhanced multispectral imagery and from published geologic maps. The final map should represent units as they are seen on the imagery, whether or not they reflect unit boundaries that are normally recognized. If stereoscopic coverage is available, or if slopes can be determined from drainage directions or by comparing with topographic data, bedding attitudes can be added to the map along with faults and structural axes. The result should be similar in almost every respect to a geologic map, except for the fact that interpretation is based upon imagery rather than field data. This

interpreted map should then be carefully evaluated, together with the geomorphic interpretation, to identify possible prospect areas on the basis of favorably situated fractures, folds, or positive geomorphic patterns.

The third step in the remote sensing evaluation of a region is a careful examination of color and tonal patterns on the enhanced multispectral imagery. The purpose is to locate any spectrally "anomalous" regions where soil or vegetation patterns contrast with typical "background" or similar units exposed elsewhere. It is essential to establish "background" based not only upon the textural patterns, relief, and reflectance of each unit, but also upon the normal variation expected in that unit due to lithologic variability, elevation, slope, solar aspect, surface moisture, and other variations that are not considered anomalous. Surface spectral anomalies may represent unusual mineralogical or chemical conditions in the soils, such as those at Cement field, Oklahoma (Donovan and others, 1974) and Table Rock field, Wyoming (Marrs and Paylor, 1987). They also may relate to soil gas anomalies or to stressed vegetation such as at Patrick Draw, Wyoming (Richers and others, 1982) and Lost River, West Virginia (Abrams and others, 1984). Such anomalies are sometimes caused by leakage from petroleum reservoirs.

After compiling interpretations of the geomorphology, lithology, structure, and anomalous features for any region, it is necessary to correlate the results with available field data, measured sections, published maps, geochemical and geophysical surveys, well logs, and production maps. These comparisons aid in selecting those features that give the best indication of known production in an area and allow selection of target areas that are untested. These may then be examined further with high-resolution imagery or with detailed field surveys designed to examine critical characteristics of the target areas. Some may develop into prospects.

REFERENCES

Abrams, M. J., Conel, J. E., and Lang, H. R., 1984, The joint NASA/Geosat test case project: American Association of Petroleum Geologists, v. 2, sections 11, 12, and 13.

Berger, Zeev, 1982, The use of Landsat data for detection of buried and obscured geologic structures in the East Texas Basin, U.S.A.: Environmental Research Institute of Michigan, Second Thematic Conference on Remote Sensing for Exploration geology, Dec. 6-10, 1982, p. 579-589.

Donovan, T. J., Friedman, I., and Gleason, J. D., 1974, Recognition of petroleum-bearing traps by unusual isotopic compositions of carbonate-cemented surface rocks: Geologic Society of America, v. 2, p. 351-354.

Elliot, D. H., 1958, Drainage analysis, Donkey Creek area, Powder River Basin, Wyoming: Wyoming Geologic Association, 13th Annual Field Conference Guidebook, p. 214.

Marrs, R. W., and Paylor, E. D., 1987, Investigation of a surface spectral anomaly at Table Rock gas field, Wyoming: Geophysics, v. 52, no. 7, p. 841-857.

Marrs, R. W., and Raines, G. L., 1984, Tectonic framework of the Powder River Basin, Wyoming and Montana, Interpreted from Landsat imagery: American Association of Petroleum Geologists Bulletin, v. 68, no. 11, p. 1718-1731.

Meissner, F. F., Woodward, J., and Clayton, J. L., 1984, Stratigraphic relationships and distribution of source rocks in the greater Rocky Mountain region: Rocky Mountain Association Geologists Guidebook, p. 11.

Matuszczak, R. A., 1973, Wattenberg field, Denver Basin: Mountain Geologist, v. 19, no. 3, p. 99-105.

Pruitt, J. D., 1978, Statistical and geological evaluation of oil and gas production from the J sandstone, Denver Basin, Colorado, Nebraska, and Wyoming, in Pruitt, J. D., and Coffin, P. E., eds., Energy resources of the Denver Basin: Rocky Mountain Association Geologists Guidebook, p. 9-24.

Richers, D. M., Reed, R. J., Horstman, K. C., Michels, G. D., Baker, R. N., Lundell, L., and Marrs, R. W., 1982, A Landsat soil gas geochemical study of the Patrick Draw Oil Field, Sweetwater Co., Wyoming: American Association Petroleum Geologists Bulletin, v. 66, p. 903-922.

Weimer, R. J., 1978, Influence of Transcontinental Arch on Cretaceous marine sedimentation: a preliminary report, in Pruitt, J. D., and Coffin, P. E., eds., Energy resources of the Denver Basin: Rocky Mountain Association Geologist Guidebook, p. 211-222.

Weimer, R. J., 1980, Recurrent movement on basement faults, a tectonic style for Colorado and adjacent areas, in Kent, H. C., and Porter, K. W., eds., Colorado geology: Rocky Mountain Association Geologists Guidebook, p. 23-35.

REMOTE SENSING IN PETROLEUM EXPLORATION FIELD TRIP: DENVER BASIN, COLORADO

Ronald W. Marrs
Department of Geology and Geophysics, University of Wyoming, Laramie

INTRODUCTION

This one-day field trip will allow participants to examine sedimentary units that are source and/or reservoir rocks for petroleum in the Denver basin. These units exhibit facies variations as we progress northward along the western margin of the basin. We will also see structures that are typical of the western flank of the Denver basin. Both the facies contrasts and the structures are important elements in a basin analysis by remote sensing. The route also traverses a portion of the Wattenberg gas/oil field which is one of the newest and largest producers in the Rocky Mountain region. The character of the surface in the producing area is quite variable and is not amenable to direct detection of underlying petroleum.

ROAD LOG: Morrison, Colorado, to Ft. Collins, Colorado, along the west flank of the Denver basin.

The trip begins at Berthoud Hall on the Colorado School of Mines campus, Golden, Colorado. Figure 1 is a generalized map showing the route and stops. Proceed southeast from campus to 19th street and then SW on 19th to the intersection with U.S. 6, which will be the reference point for this road log. Turn southeast (left) toward Denver.

MILEAGE (mi)

- 0.0 START. GOLDEN intersection U.S. 6 and 19th Street.
- 1.4 Intersection of U.S. 6 with Colorado 93, turn south (right) onto Colorado 93.
- 2.3 Intersection of Colorado 93 and Colorado 26 (Mount Vernon Canyon Road). Continue south on Colorado 26. Jurassic Morrison Formation and the Cretaceous Dakota Group form the imposing hogback on the east (left). (fig. 2, stratigraphic column)
- 3.4 STOP 1. Turn left into parking area just before the I-70 interchange. This spectacular road cut exposes Jurassic and Cretaceous strata. Items of interest at this stop include:
  1. Eastward dipping Cretaceous units that are source and reservoir rocks for most of the petroleum produced in the Denver basin.
  2. The view from the end of the walkway of upper Cretaceous units and the Golden fault.
  3. Green Mountain, composed of Cretaceous sedimentary rocks capped by lower Tertiary conglomerates.

  The walkway along the north side of

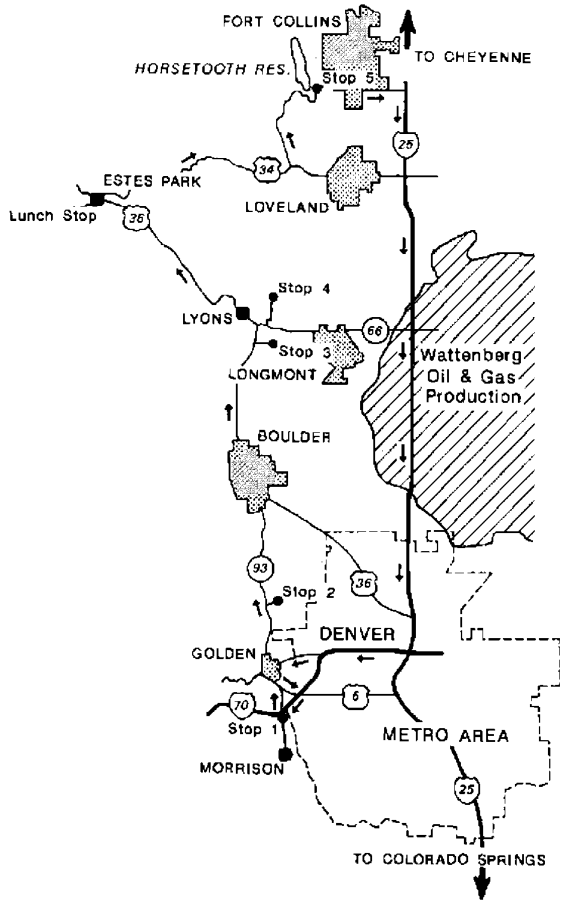

FIGURE 1 Map of field trip route, western Denver basin, Colorado.

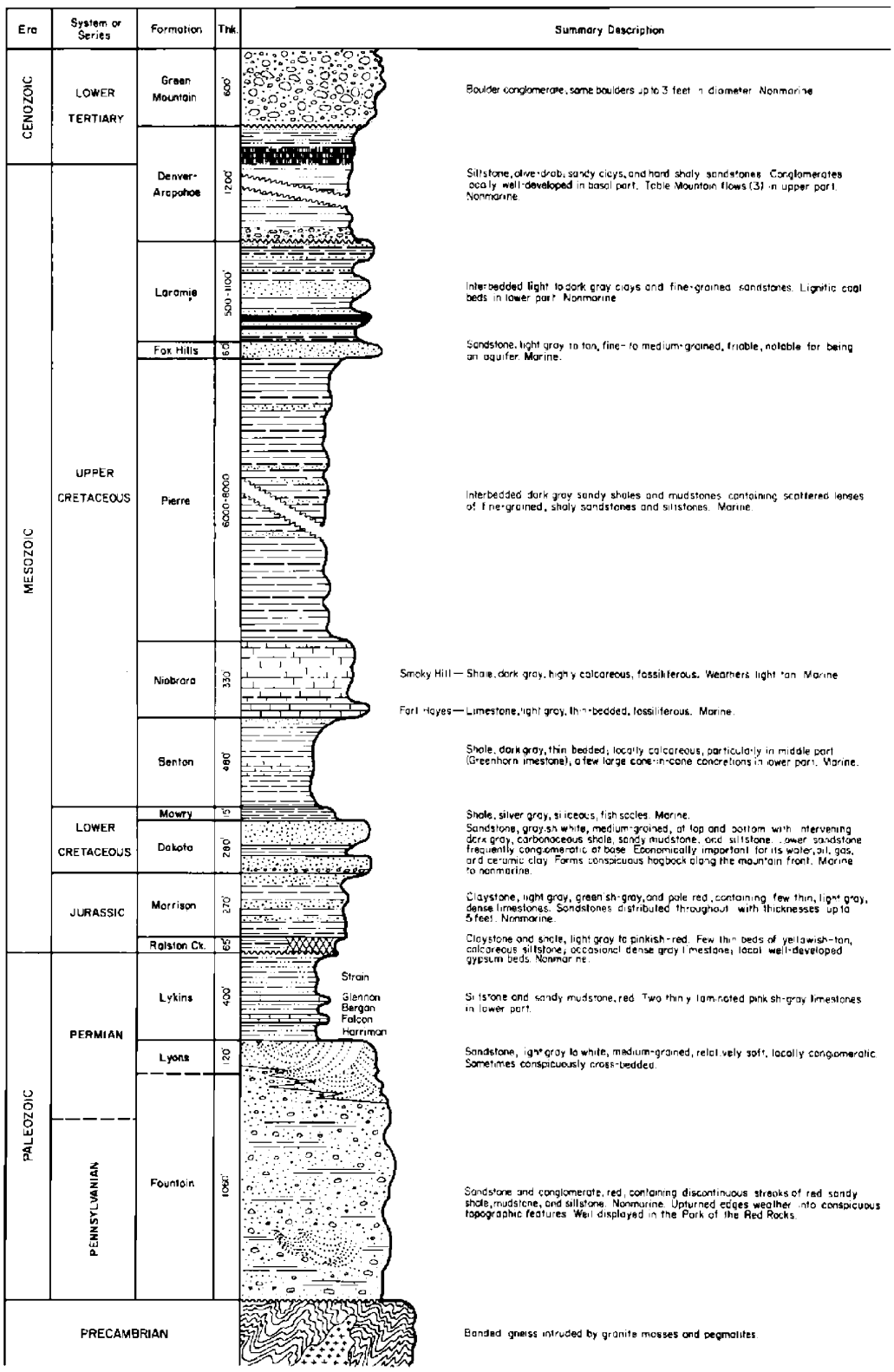

FIGURE 2 Generalized stratigraphic section for the western Denver basin near Golden, Colorado (from Haun, 1960, p. 300).

the road cut extends about 1000 ft east from the parking area and boasts more than a dozen geologic signposts.

7.8 Return to Golden via U.S. 6, but continue on U.S. 6 to its intersection with Colorado 58 at the mouth of Clear Creek Canyon. Turn right (east).

8.4 Washington Street (Colorado 93), turn left (north) toward Boulder, Colorado.

10.4 Hogback ridge of Dakota Sandstone on the west (left) (fig. 3). Mines on the ridge were for clay, used in the manufacture of ceramics.

11.0 Low ridge behind the ranch house (west) is formed by a sandstone of the Cretaceous Laramie Formation.

13.8 Very steeply dipping clay beds of the Laramie Formation exposed in the roadcut.

15.0 STOP 2. Turn right on Leyden Road and go 0.3 miles east (cross Leyden ridge and turn around at ranch house lane). Stop and view the ridge and the old mine where coals of the lower Laramie Formation were mined (this is now a gas storage facility).

15.6 Return to Colorado 93 and proceed northward.

16.4 Tan beds of Cretaceous Pierre Shale crop out along the road.

17.2 Road climbs onto Rocky Flats erosional surface. Intersection with Colorado 72 (Coal Creek Canyon Road). Continue ahead. Flatirons of Pennsylvanian to Permian Fountain Formation lap onto the Front Range uplift (west side of road).

19.2 Idealite cement plant (on the right). Clay for cement is mined from the Pierre Shale.

22.0 Fox Hills Sandstone exposed in roadcut.

26.6 Enter Boulder. Turn right (east) on Baseline Road. University of Colorado on left.

26.8 Go beneath the Denver/Boulder turnpike and turn left (north) onto U.S. 36 (28th Street).

32.2 Junction of U.S. 36 and Colorado 93. Continue northward toward Lyons.

33.3 Table Mesa to the northeast and Haystack Mountain to the east are remnants of old erosional surfaces.

35.4 Fort Hays Limestone Member of the

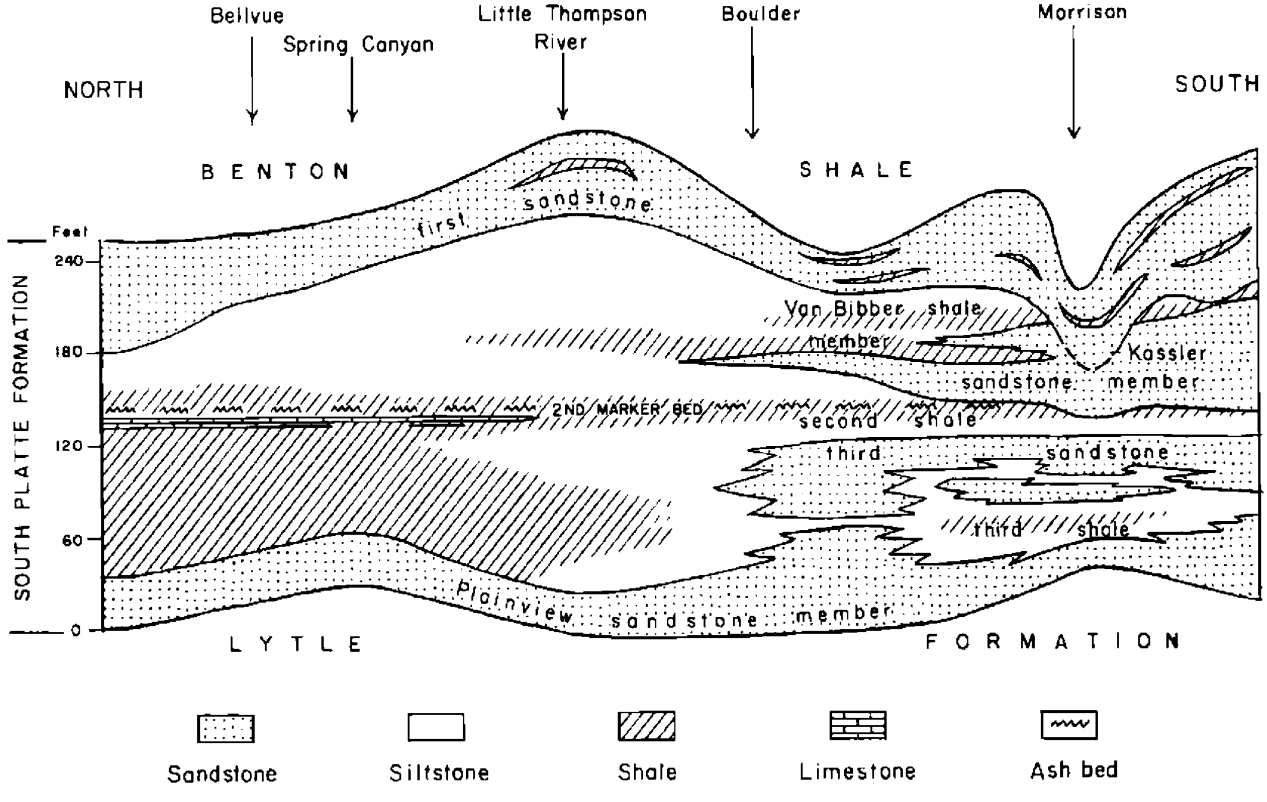

FIGURE 3 Generalized diagram of changing stratigraphy of the Cretaceous Dakota Group (South Platte Formation) along the Colorado Front Range (from Waage and Eicher, 1960, p. 232).

Cretaceous Niobrara Formation crosses U.S. 36 and continues on the right.

38.0 Black shales of the Cretaceous Benton Group exposed in roadcut. Light stringers are bentonite layers. Junction with Colorado 119. Continue ahead.

39.0 Dakota "J" Sand (Muddy) in road cut and continuing northward as a low ridge on the east (right).

40.0 STOP 3. Hygiene Road. Turn right (east) and go 0.3 miles east to quarry gate. Turn around. Quarry north of road is in Smoky Hill Shale Member (Niobrara Formation). Low ridge crossing the road is the Fort Hays Limestone. Examine these outcrops in the roadcut. Also note the view to the north of three anticlines (Rabbit Mountain on the east, Dowe Pass in the center, and another anticline on the west).

40.6 Return to U.S. 36 and proceed north toward Lyons.

42.0 Junction U.S. 36 and Colorado 66. Turn right (east) on Colorado 66.

43.0 Turn north on North 53rd Street (Boulder County 27) at the large water tank.

43.9 Jog to the east about 1 mile and then continue north on North 55th Street.

45.0 STOP 4. Cross canal and turn right into picnic area at the south end of Dowe Pass anticline. Stop for brief discussion of structural style of folds along the east flank of the Colorado Front Range.

47.0 Return to Colorado 66 and turn right (west) to Lyons.

49.0 Junction of Colorado 66 and 7. Go right toward Estes Park. Permian Lyons Sandstone crops out at Lyons where it is quarried for building stone.

51.0 Prominent cliffs on both sides of Colorado 66 west of Lyons are Fountain Formation capped by Lyons Sandstone.

53.0 The Fountain Formation/Precambrian contact crosses the highway near the Stone Mountain RV Park. A thick regolith at the contact makes it difficult to recognize. Proceed up the canyon of the South St. Vrain River to Estes Park. The rocks are Precambrian crystalline units, so just enjoy the scenery.

69.0 LUNCH STOP. Estes Park, Colorado. Please browse or enjoy the sights of Estes Park. Take Colorado 34 east to Drake and Loveland, along the Big Thompson River.

96.0 Turn left (north) at the school onto County Road 27N to Masonville and Horsetooth Reservoir after traversing Fountain Formation through Dakota Sandstone section at the lower end of Big Thompson Canyon. Lyons Sandstone on the left (west) has been quarried extensively. Dakota hogback on the right (east), Morrison Formation in the valley.

98.5 Redbeds exposed at left side of road (on curve) are siltstone and red shales of the Permian to Triassic Lykins Formation.

100.8 Masonville. As we proceed north and east, we see the stratigraphic section repeated by en echelon folds. Milner Mountain, to the northeast, exposes a large block of Precambrian schists and gneisses.

101.1 Turn right (east) on Road 25E. Route crosses a fault and an anticlinal fold.

101.9 Black talc schist on left side of road is Precambrian rock exposed in the core of an anticline.

105.1 Road forks. Continue south (right) on 25E to South Bay area of Horsetooth Reservoir.

108.9 STOP 5. Pull off near the junction of Road 28S. Examine the Cretaceous section in the Spring Creek Canyon road cut and enjoy the sights at Horsetooth Reservoir.

109.5 Road angles down the east side of the Dakota hogback. View to the east is of the city of Fort Collins. The low ridge at the base of the slope is the Fort Hayes Limestone.

110.8 Junction with Road 19S. Turn right (south) on 19S.

111.3 Junction with Road 3D (Harmony Road). Turn left.

117.3 Turn right on I-25 and proceed south toward Denver. I-25 is the main route along the Front Range urban corridor. Good agricultural land is rapidly being consumed by more intensive development.

131.3 Junction with Colorado 66. Route traverses the western portion of the huge Wattenberg gas/oil field. Note that intensive agricultural and other development has disturbed the surface to such a degree that there would be little hope of detecting any surface anomalies or related geologic phenomena associated with this field.

172.0 I-70 interchange. Take I-70 west toward Grand Junction and Golden.

177.5 Junction with Highway 58. Take 58 west to Golden and the Colorado

School of Mines campus.
182.0 Arrive back at Berthoud Hall.

REFERENCES

Haun, J. D., 1960, Geology of mountain front west of Denver, in Weimer, R. J., and Haun, J. D., eds., Guide to the geology of Colorado: Denver, Rocky Mountain Association of Geologists, p. 298-303.

Waage, K. M., and Eicher, D. L., 1960, Dakota Group in northern Front Range area, in Weimer, R. J., and Haun, J. D., eds., Guide to the geology of Colorado: Denver, Rocky Mountain Association of Geologists, p. 230-237.

REMOTE SENSING IN THE CENTRAL VIRGINIA PIEDMONT

Nancy M. Milton, M. D. Krohn, and B. A. Eiswerth
U.S. Geological Survey, Reston, Virginia

In vegetated terrains, remote observation of rocks and soils is not possible, but inferences about substrate can be made from the distribution and vigor of the plant cover. Distinctive floras have long been known to be associated with specific lithologies, such as the serpentine floras described by Rune (1953), Whittaker (1954), and Kruckeberg (1984). Other vegetation communities are limited by water availability, such as phreatophytes in the southwestern United States (Robinson, 1958) and the riverbottom maple and river birch communities of the Atlantic coast (Brush et al., 1977). In some cases, specific plant species are associated with conditions provided by one group of lithologies, but not with those of another group. For example, white pine and white oak are positively correlated with limestone and shale units in Pennsylvania, but negatively correlated with sandstone and conglomerate units (Milton et al., 1982). Such plant ecological relationships are consistent with the theories developed by Gleason (1926) and Hack and Goodlett (1960). Plant distribution is seen as one component of a landscape in a dynamic equilibrium, such that each component is dependent on all other components, and changes in one component affects the others.

In the Appalachian Piedmont physiographic province of Virginia, the humid temperate climate permits the growth of a closed canopy forest, except where modified by land use. Forests cover 70 to 80 percent of the surface, and outcrops are found mainly in stream beds. The vegetation is included in the oak-pine vegetation unit of Braun (1950) and the oak-hickory-pine unit of Kuchler (1964). The major species present are white, black, chestnut, post, northern red, and spanish oaks, hickory, yellow poplar, and red maple. Virginia pine occurs scattered in oak forests and loblolly pine in planted stands. The understory, which includes subcanopy trees, shrubs, and herbs, is usually moderately to very dense and commonly includes one or more of the following: dogwood, holly, blackgum, heaths, and woody vines. Pine forests often have sparse understories of holly, sassafras, and vines. A subunit of oak forest, dominated by chestnut oak, has a sparse to moderate understory composed mainly of ericaceous species. Vegetation along streams is more likely to be composed of one or more of the following species: red maple, river birch, sycamore, green ash, and silver maple.

In central Virginia, the chestnut oak forest grows primarily over lithologies that produce relatively dry soil conditions (Milton and Krohn, 1982). Three such lithologies that have been identified are coarse-grained volcaniclastic and metavolcanic rocks, aluminous schists, and highly weathered upland gravel deposits. The soils developed on the volcanic and gravel units tend to be coarse-textured, and consequently water-holding capacity is low. High concentrations of aluminum in soils inhibits water uptake by plants. The metavolcanic unit is the host rock for many of the gold occurrences in the Virginia Piedmont province.

The Virginia Piedmont province is an area of low relief that has undergone extensive

School of Mines campus.
182.0 Arrive back at Berthoud Hall.

REFERENCES

Haun, J. D., 1960, Geology of mountain front west of Denver, in Weimer, R. J., and Haun, J. D., eds., Guide to the geology of Colorado: Denver, Rocky Mountain Association of Geologists, p. 298-303.

Waage, K. M., and Eicher, D. L., 1960, Dakota Group in northern Front Range area, in Weimer, R. J., and Haun, J. D., eds., Guide to the geology of Colorado: Denver, Rocky Mountain Association of Geologists, p. 230-237.

REMOTE SENSING IN THE CENTRAL VIRGINIA PIEDMONT

Nancy M. Milton, M. D. Krohn, and B. A. Eiswerth
U.S. Geological Survey, Reston, Virginia

In vegetated terrains, remote observation of rocks and soils is not possible, but inferences about substrate can be made from the distribution and vigor of the plant cover. Distinctive floras have long been known to be associated with specific lithologies, such as the serpentine floras described by Rune (1953), Whittaker (1954), and Kruckeberg (1984). Other vegetation communities are limited by water availability, such as phreatophytes in the southwestern United States (Robinson, 1958) and the riverbottom maple and river birch communities of the Atlantic coast (Brush et al., 1977). In some cases, specific plant species are associated with conditions provided by one group of lithologies, but not with those of another group. For example, white pine and white oak are positively correlated with limestone and shale units in Pennsylvania, but negatively correlated with sandstone and conglomerate units (Milton et al., 1982). Such plant ecological relationships are consistent with the theories developed by Gleason (1926) and Hack and Goodlett (1960). Plant distribution is seen as one component of a landscape in a dynamic equilibrium, such that each component is dependent on all other components, and changes in one component affects the others.

In the Appalachian Piedmont physiographic province of Virginia, the humid temperate climate permits the growth of a closed canopy forest, except where modified by land use. Forests cover 70 to 80 percent of the surface, and outcrops are found mainly in stream beds. The vegetation is included in the oak-pine vegetation unit of Braun (1950) and the oak-hickory-pine unit of Kuchler (1964). The major species present are white, black, chestnut, post, northern red, and spanish oaks, hickory, yellow poplar, and red maple. Virginia pine occurs scattered in oak forests and loblolly pine in planted stands. The understory, which includes subcanopy trees, shrubs, and herbs, is usually moderately to very dense and commonly includes one or more of the following: dogwood, holly, blackgum, heaths, and woody vines. Pine forests often have sparse understories of holly, sassafras, and vines. A subunit of oak forest, dominated by chestnut oak, has a sparse to moderate understory composed mainly of ericaceous species. Vegetation along streams is more likely to be composed of one or more of the following species: red maple, river birch, sycamore, green ash, and silver maple.

In central Virginia, the chestnut oak forest grows primarily over lithologies that produce relatively dry soil conditions (Milton and Krohn, 1982). Three such lithologies that have been identified are coarse-grained volcaniclastic and metavolcanic rocks, aluminous schists, and highly weathered upland gravel deposits. The soils developed on the volcanic and gravel units tend to be coarse-textured, and consequently water-holding capacity is low. High concentrations of aluminum in soils inhibits water uptake by plants. The metavolcanic unit is the host rock for many of the gold occurrences in the Virginia Piedmont province.

The Virginia Piedmont province is an area of low relief that has undergone extensive

weathering, resulting in a thick cover of saprolite and clay residuum over the bedrock. Lithologies include mainly lower Paleozoic metasedimentary and metavolcanic rocks expressed in outcrop primarily as mica schists and quartzo-feldspathic gneisses. The rocks have generally been metamorphosed from transitional greenschist to amphibolite facies in a series of NE-trending belts. Interrupting this linear pattern are several granitic intrusions. At least three periods of ductile folding have been recognized. Some of the units have been interpreted to represent a lower Paleozoic island arc sequence. Superimposed upon these Paleozoic rocks are the rift basins and diabase intrusions of Triassic and Early Jurassic age. Along the eastern edge of the area and along several major rivers, highly weathered, well-drained upland gravel deposits, presumably of Tertiary age, cover interfluves. The eastern edge of the Piedmont, called the Fall Line, is a physiographic scarp that separates the crystalline rocks of the Piedmont from the Cretaceous and Cenozoic sedimentary rocks of the Coastal Plain. The western edge of the Piedmont province is marked by the mafic Precambrian and Cambrian rocks of the Blue Ridge province (Bobyarchick et al., 1981; Glover and Tucker, 1979; Pavlides, 1979, 1980; Seiders and Mixon, 1981; Smith et al., 1964; Wier and Pavlides, 1985).

The image study area covers the portion of the Piedmont roughly bounded by the Rappahannock River on the north, the James River on the south, the Coastal Plain boundary (Fall Line) on the east, and the Blue Ridge province on the west (fig. 1). The northwest portion of Landsat MSS image #1854-15071, collected on November 24, 1974, was used to create an inverted-principal-component (IPC) image (Krohn et al., 1981). Statistical data were computed to produce a variance-covariance matrix for MSS bands 4, 5, 6, and 7. The principal components (PC) were normalized at the 25th percentile and filtered by using a high-pass filter on PC 1 for edge enhancement and low-pass filters on PC 3 and 4 to eliminate high frequency noise. The transform matrix was inverted to create the IPC image. The combination of IPC bands 4, 2, and 1 were projected as red, green, and blue, respectively, to enhance the chestnut oak forest unit, which appears yellow in the IPC image. The numeric data used in red, green, and blue color combination were transformed to Munsell coordinates, hue, saturation, and value, respectively. All digital numbers not corresponding to the yellow pixels, as defined using hue and saturation, were nulled, and a parallelepiped classification was used on the masked data set to enable a subsequent cleaning of the image. Pixel groups were digitally overlain on a contrast-enhanced gray-tone MSS band 4 image for purposes of field checking and examining relationships of vegetation units with rock units (fig. 2).

Concentrations of chestnut oak forest, yellow on the IPC image (fig. 2), can be related to three lithologies that produce arid soil conditions. The concentration of areas in the southeastern portion of the image south of the James River are related to extensive mid-Tertiary upland gravel deposits. The NE-trending belt of chestnut-oak through the western part of the image near Lake Anna coincides with the metavolcanic rocks of the Chopawamsic Formation (Pavlides, 1979) that tend to form upland areas. Chestnut oak forests are scattered throughout the schist units on the western edge of the image, and we believe them to be areas of high aluminum from analogies with other lithologies in North Carolina.

The field trip transect crosses part of the Virginia Piedmont province from the town of Ruckersville on the west to Thornburg on the east, crossing most of the major lithologies and vegetation communities of the area. The route is shown on a simplified lithologic map with chestnut oak occurrences marked (fig. 3).

ROADLOG: TRANSECT THROUGH PIEDMONT PROVINCE OF VIRGINIA

From the Convention Center in Washington, D.C., proceed south on 14th Street to Constitution Avenue, turn right (west) to Theodore Roosevelt Bridge. From the bridge, continue west on Interstate 66 about 30 miles to exit, Route (Rt) 29 south at Gainesville. Travel south on Rt 29 about 40 miles to Culpeper, turn south on Rt 15 18 miles to Orange. Between Culpeper and Orange, the route crosses the Triassic Culpeper basin, and, for the last 2.5 miles, the Catoctin Formation phyllites.

The westernmost edge of the mapped transect is in the greenstones of the Catoctin Formation (SC on fig. 3), which support a chestnut-oak forest. The Catoctin Formation forms the eastern margin of the Blue Ridge province. An abrupt vegetation change occurs at the boundary of the Catoctin Formation with the Mesozoic Barboursville basin (Newark Group, SS on fig. 3). Agriculture is the prominent land use across the topographically low basin, and no chestnut oak is found.

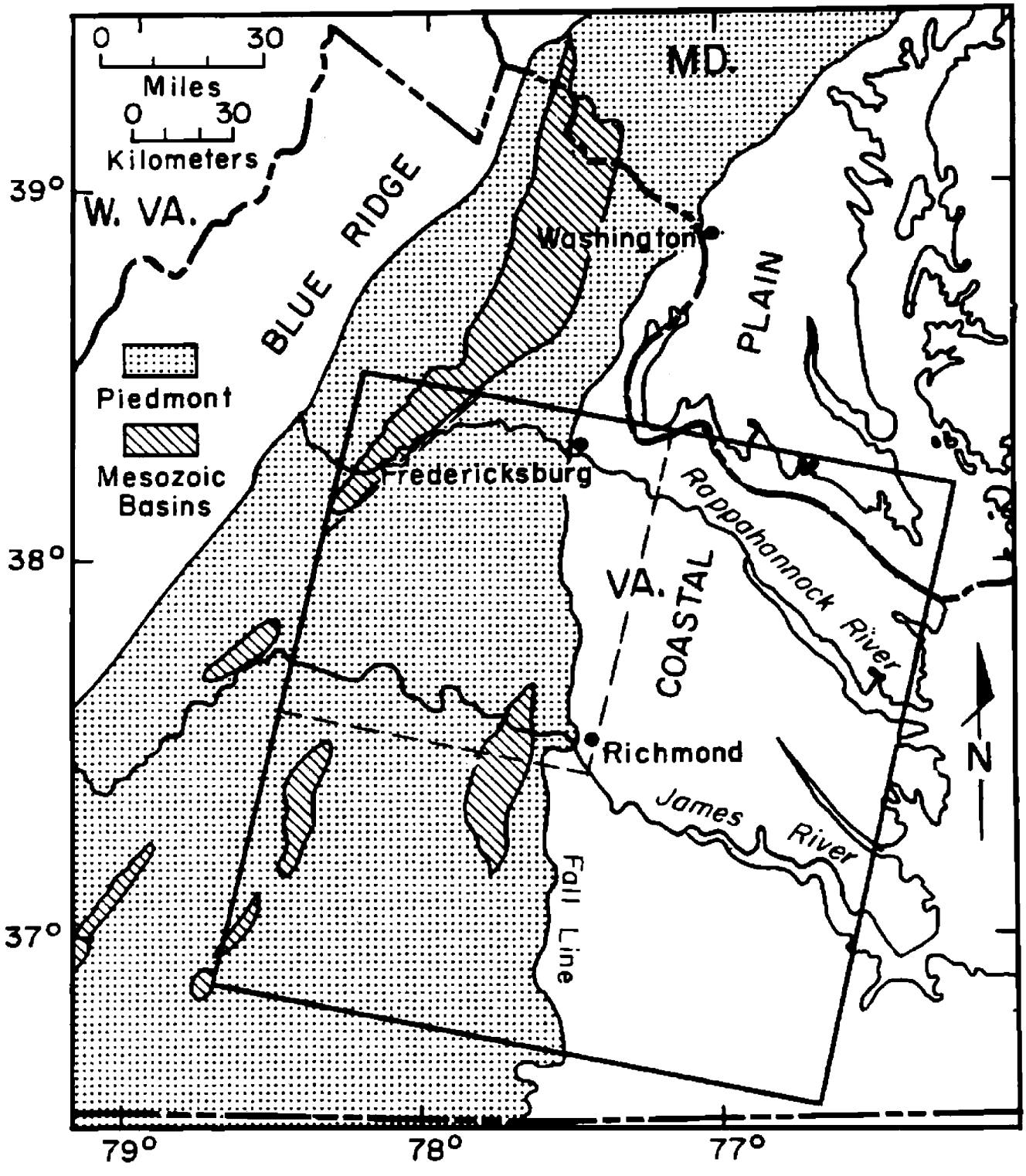

FIGURE 1 Index map showing location of the study area in the central Virginia Piedmont province, U.S.A.

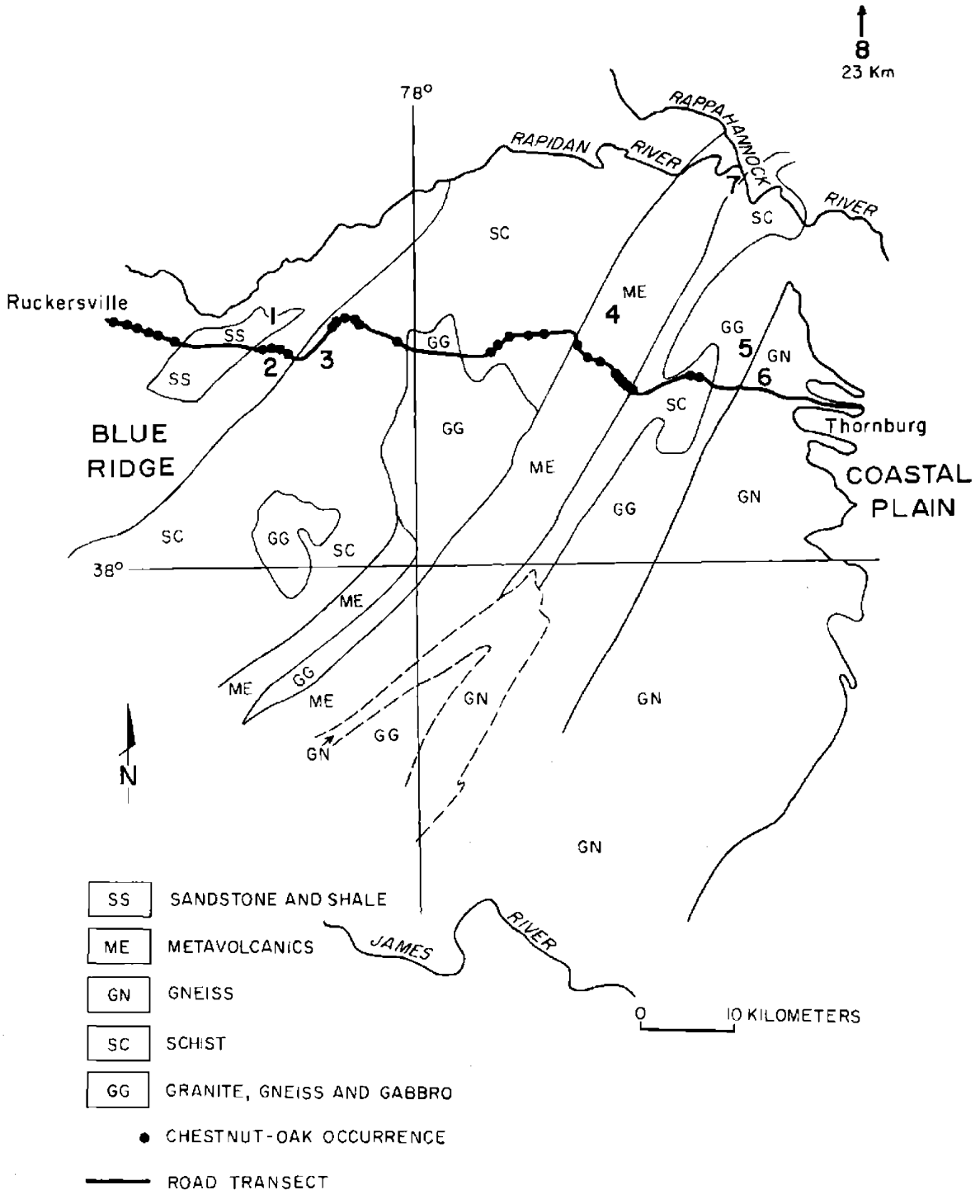

FIGURE 3 Generalized lithologic map of the central Virginia Piedmont showing transect and locations of chestnut-oak occurrences along the transect. Map is derived from Commonwealth of Virginia (1963), Pavlides (1981), and Pavlides (pers. commun.).

STOP 1. Montpelier Station.

From Orange, proceed west on Rt 20 4 miles across the clastic rocks of the Barboursville basin to Montpelier Station, the home of President James Madison. Pull into the parking lot of the National Historic Trust offices for a look at maps and the mixed oak forest.

STOP 2. Gordonsville quad. Metavolcanic rocks of the Catoctin Formation.

From Montpelier Station, continue west on Rt 20 1 mile. Turn left (southeast) on Rt 639. In .75 mile, bear left to stay on Rt 639 (gravel road). Chicken Mountain Road crosses a narrow strip of basic volcanics of the Catoctin Formation. At 2.5 miles, watch for an exposure of Catoctin Formation along the road cut on the left. Note the chestnut-oak forest along the ridge.

STOP 3. Gordonsville quad. Phyllites of the Evington Group.

Rt 639 continues across a strip of limestones on which no chestnut oak grows, and enters the Piedmont province near the crossing of Rt 15. At Madison Run, proceed left (northeast) on Rt 647, and immediately watch for outcrops of phyllite to the left of the road behind the ruins.

Continue on Rt 647 1.6 miles to the right on Rt 688 (becomes Rt 612). After 5 miles, turn right (northeast) on Rt 631. (This road is unmarked, so watch for dumpsters on the right). From here to North Pamunkey Church, the transect crosses the phyllitic schists of the Evington group, which support scattered stands of chestnut-oak. In 1.1 mile, turn right (east) on Rt 629.

From North Pamunkey Church, the route crosses one of the granitoid intrusions. No chestnut-oak is found for nine miles until the transect crosses back into schists near Danton. At Danton, turn left (north) on Rt 651 5.6 miles to a left on Rt 601 to Paytes. From Paytes, proceed right (southeast) on Rt 608 about .9 mile, take the right fork onto Rt 606. Near this point, the transect crosses into the Chopawamsic Formation metavolcanics, with abundant chestnut-oak. No vegetation boundary occurs at the metavolcanic-schist boundary, but an abrupt change is seen at the town of Margo, where the route crosses into granite. No chestnut-oak is found on the granite, nor on the granitic gneiss to the east. Proceed on Rt 606 about 12 miles to Post Oak, about 4 miles further to Snell, and 6 miles on to Thornburg.

Proceed to Chancellorsville Battlefield Visitor's Center for lunch, on Rt 3 in Chancellorsville quad. Quantico Formation.

STOP 4. Chancellorsville quad. Saprolite of the metavolcanic rocks of the Chopawamsic Formation. Chestnut-oak forest.

From the Visitor's Center, travel west on Rt 3 1.2 miles, turn left (south) on Rt 621 .7 miles to a roadcut in the saprolite of the Chopawamsic metavolcanic rocks. Continue on Rt 621 1.5 miles, turn left (southeast) on Rt 613, and stop to look at the chestnut-oak forest.

STOP 5. Spotsylvania quad. Granitic gneiss of the Ta River Metamorphic Suite.

Continuing on Rt 613, proceed 7.8 miles to Rt 627 at Goshen Church. Turn left and go 2.2 miles to the Ni River Bridge. Outcrops of the Ta River Metamorphic Suite occur about 100 yards along the bank upstream of the bridge.

STOP 6. Spotsylvania quad. Gneiss of the Po River Metamorphic Suite.

Continue northeast on Rt 627 2.3 miles, turn right (southeast) on Rt 628 2.7 miles, turn right (southwest) on Rt 208. Continue 3.1 miles to Spotsylvania. Proceed south on Rt 208 1.8 miles to the crossing of the Po River. Outcrops are on the east side of the road, north of the river. The rocks here are gneisses of the Po River Metamorphic Suite.

STOP 7. Salem Church quad. Metavolcanic rocks of the Chopawamsic Formation.

Continue south on Rt 208 1.9 miles to Snell, turn left (east) on Rt 606 5.3 miles to Interstate 95. Proceed north on I95 15.4 miles to Rt 17, just past the Rappahannock River Bridge. Proceed west on Rt 17 6.5 miles to Hartwood. Turn left (south) on Rt 752 2.8 miles to the tee, turn right .2 miles to the power line. Walk south along the power line to the ledge overlooking the river. Outcrops of the mafic Chopawamsic metavolcanics and granitoid intrusives are exposed on the cliff above the Rappahannock River. The intrusive rocks have been identified as trondjhemites based on their very low K-values (Pavlides, 1981; Pavlides et al., 1982). Follow the path on the left down to the river and proceed downstream to the second stream valley. Felsic metavolcanic rocks of the Chopawansic Formation with characteristic quartz eyes can be observed interbedded with mafic and volcaniclastic rocks and granitoid intrusives. At the second stream valley the Quantico Formation can be observed as basal quartzite and an overlying muscovite-biotite schist. Chestnut oak is abundant on the Chopawamsic Formation, even near the river, but decreases eastward on the Quantico Formation.

STOP 8. Quantico quad. Carbonaceous schists and slates of the Quantico Formation.

Return to Hartwood, turn right (east) on Rt 17, and return to I95. Proceed north 15 miles to Exit 49 - Quantico Marine Base. Turn left at the stop sign onto Russell Road. Go west .4 miles, park, and walk along the cloverleaf to the right to the outcrops of Quantico Formation.

Continue North on I95 to Washington, D.C.

REFERENCES

Bobyarchick, A. R., Pavlides, Louis, and Wier, Karen, 1981, Piedmont geology of the Ladysmith and Lake Anna East Quadrangles and vicinity, Virginia: U.S. Geological Survey Miscellaneous Investigations Map I-1282, scale 1:24,000.

Braun, E. L., 1950, Deciduous forests of eastern North America: Philadelphia, Blakestone Company, 596 p.

Brush, G. S., Lenk, C., and Smith, J., 1977, The natural forests of Maryland: an explanation of the vegetation map of Maryland: Maryland Power Plant Siting Program Report PPRP-21, 81 p.

Commonwealth of Virginia, 1963, Geologic map of Virginia: Division of Mineral Resources, Charlottesville, Virginia. Scale 1:500,000.

Gleason, H. A., 1926, The individualistic concept of the plant association: Bulletin of the Torrey Botanical Club, v. 53, p. 7-53.

Glover, L., and Tucker, R. D., 1979, Virginia Piedmont geology along the James River from Richmond to the Blue Ridge: Geological Society of America SE Section Meeting Field Guide 1-3, p. 1-14.

Hack, J. T., and Goodlett, J. C., 1960, Geomorphology and forest ecology of a mountain region in the central Appalachians: U.S. Geological Survey Professional Paper 347, 66 p.

Krohn, M. D., Milton, N. M., and Segal, D., 1981, Discrimination of a chestnut-oak forest unit for geologic mapping by means of a principal component enhancement of Landsat Multispectral Scanner data: Geophysical Research Letters 8(2):151-154.

Kruckeberg, A. R., 1984, California serpentines: flora, vegetation, geology, soils, and management problems: Berkeley, California, University of California Press, 180 p.

Kuchler, A. W., 1964, Potential natural vegetation of the conterminous United States: American Geographical Society Special Publication No. 36.

Milton, N. M., and Krohn, M. D., 1982, Chestnut-oak (Quercus prinus L.) distribution in the Virginia Piedmont as an aid to geologic mapping: Virginia Journal of Science, v. 33, p. 128.

Milton, N. M., Pohn, H. A., and Power, M. S., 1982, Vegetation distribution as an aid to geologic mapping in Pennsylvania: AAAS Annual Meeting, Washington, D. C., 3-8 January 1982, Proceedings, p. 140.

Pavlides, Louis, 1979, Piedmont geology of the Fredericksburg, Virginia area and vicinity: Geological Society of America, SE- Section Meeting Field Guide, 41 p.

Pavlides, Louis, 1980, Revised nomenclature and stratigraphic relationships of the Fredericksburg Complex and Quantico Formation of the Virginia Piedmont: U.S. Geological Survey Professional Paper 1146, 29 p., 1 pl., scale 1:96,000.

Pavlides, Louis, 1981, The central Virginia volcanic-plutonic belt: An island arc of Cambrian (?) age: U.S. Geological Survey Professional Paper 1231A, 44 p.

Pavlides, Louis, Gair, J. E., and Crawford, S. L., 1982, Central Virginia volcanic-plutonic belt as a host for massive sulfide deposits: Economic Geology, v. 77, p. 233-272.

Robinson, J. W., 1958, Phreatophytes: U.S. Geological Survey Water-Supply Paper 1432, 84 p.

Rune, O., 1953, Plant life on serpentines and related rocks in the north of Sweden: Acta Phytogeographica Suecica, v. 31, p. 1-139.

Seiders, M., and Mixon, R., 1981, Geologic map of the Occoquan Quadrangle and part of the Fort Belvoir Quadrangle, Prince William and Fairfax Counties, Virginia, U.S. Geological Survey Miscellaneous Investigations Map I-1175, scale 1:24,000.

Smith, J. W., Milici, R. C., and Greenburg, S. S., 1964, Geology and mineral resources of Fluvana County: Virginia Division Mineral Resources Bulletin 79, 62 p.

Whittaker, R. H., 1954, The vegetational response to serpentine soils, in R. H. Whittaker et al., The ecology of serpentine soils: A symposium: Ecology, v. 35, p. 275-288.

Wier, Karen, and Pavlides, Louis, 1985, Piedmont geology of the Spotsylvania quadrangle, Spotsylvania County, Virginia: U.S. Geological Survey Miscellaneous Investigations Map I-1568, scale 1:24,000.